

# Solution Synthesis of Metal Oxides for Electrochemical Energy Storage

## Applications

Xinhui Xia,<sup>a,b,‡</sup> Yongqi Zhang,<sup>a,‡</sup> Dongliang Chao,<sup>a</sup> Cao Guan,<sup>a</sup> Yijun Zhang,<sup>b</sup> Lu Li,<sup>b</sup> Xiang Ge,<sup>b</sup> Ignacio Mínguez Bacho,<sup>a</sup> Jiangping Tu,<sup>b,\*</sup> and Hong Jin Fan<sup>a,\*</sup>

<sup>a</sup> Division of Physics and Applied Physics, School of Physical and Mathematical Sciences, Nanyang Technological University, Singapore 637371, Singapore

<sup>b</sup> State Key Laboratory of Silicon Materials, Key Laboratory of Advanced Materials and Applications for Batteries of Zhejiang Province, and Department of Materials Science and Engineering, Zhejiang University, Hangzhou 310027, China

\* Address correspondence to fanhj@ntu.edu.sg (H.J. Fan), tujp@zju.edu.cn (J.P. Tu)

‡ These authors contributed equally to this work.

## Abstract

This article provides an overview of solution-based methods for the controllable synthesis of metal oxides and their applications for electrochemical energy storage. Typical solution synthesis strategies are summarized and the detailed chemical reactions are elaborated for several common nanostructured transition metal oxides and their composites. The merits and demerits of these synthesis methods and some important considerations are discussed in association with their electrochemical performance. We also propose the basic guideline for designing advanced nanostructure electrode materials, and the future research trend in the development of high power and energy density electrochemical energy storage devices.

Keywords: *solution growth methods, nanostructure electrodes, metal oxides, composite nanostructures, electrochemical energy storage*

## **1. Introduction**

Energy is the eternal pursuit of human kind and plays an important role in the development of human civilization and advancement of modern technology. Energy storage, an important intermediate step towards the subsequent versatile and efficient energy applications, has received great attention both in academy and industry. Among various energy storage systems, electrochemical energy storage (EES) devices (such as batteries and supercapacitors) have been extensively studied and considered to be one of the most promising green energy storage systems for the sustainable energy supply in near future, due to their high efficiency, versatility, and flexibility.

In the past decades, a dramatic expansion of EES research has been driven to meet the increasing demand of modern electronics, transportation and smart grid. Batteries and supercapacitors are two dominating types of EES devices, which consist of four parts: a positive electrode, a negative electrode, a separator, and an electrolyte. Noticeably, lithium ion batteries (LIBs) are the most important and widely used rechargeable batteries with advantages of high working voltage, high capacity and long cycling life. Meanwhile, supercapacitors have matured significantly over the last decade and emerged with the potential to facilitate major advances in energy storage due to their unique characteristics of high power density, long cycling life and fast recharge capability. Supercapacitors have an important role in complementing batteries in the energy storage field. EES is realized by electrochemical processes associated with electron and ion transports. During a discharge process, electrochemical reactions take place at the electrodes and the generated electrons flow through an external circuit to drive external loads. During the charge process, an external voltage is applied to store electrons at the electrodes by reversible electrochemical reactions. The performance of EES systems, both batteries and supercapacitors, is mainly determined by the electrode materials, which are the core parts and the key to high

performance. Advanced electrode materials play a decisive role in the efficient and versatile use of energy. Therefore, the development of EES techniques is largely attributed to the innovation and advance of electrode materials with tailored structure and high reactivity.

To date, various active materials have been studied for EES systems as anode or cathode materials including metal (Sn),<sup>1</sup> metal sulfides (NiS, CoS, etc.),<sup>2</sup> metal oxides (NiO, Co<sub>3</sub>O<sub>4</sub>, MnO<sub>2</sub>, CuO, etc.),<sup>3-7</sup> metal hydroxides (Ni(OH)<sub>2</sub>, Co(OH)<sub>2</sub>, etc.),<sup>1, 3, 5</sup> carbon materials (carbon nanotube, graphene, etc.),<sup>8, 9</sup> metal hydrides (AB<sub>5</sub> type),<sup>10</sup> metal carbides (TiC, TaC, etc.),<sup>3, 11</sup> metal nitrides (MoN, TiN, TaN, etc.),<sup>1, 3, 5, 12</sup> conducting polymers (polyaniline, polypyrrole, polythiophene, etc.),<sup>2, 13, 14</sup> sulphur,<sup>15, 16</sup> and silicon,<sup>17-19</sup> and so on. Among all these explored electrode materials, transition metal oxides are important classes of semiconductors with wide applications in EES systems due to their unique electrochemical reactivity. With the rapid development of materials design strategies and synthesis techniques, great progress has been achieved in fabrication of transition metal oxides with bespoke nanostructures and enhanced electrochemical performance. Nanostructured transition metal oxides have been proven to exhibit superior electrochemical performances to the bulk counterparts because of their novel properties associated with decreased size, unique shape, and defective nature. The nanoscale structure can effectively improve electrochemical reaction efficiency and utilization of active materials with improved energy and power densities. Up to now, lots of chemical and physical methodologies have been developed to prepare nanostructured transition metal oxides for EES applications. Compared to physical techniques, solution chemical synthesis method (or called “soft approach”) is a facile and alternative synthetic strategy for the preparation of advanced transition metal oxides with desirable morphology and improved performance. Solution-based synthesis methods are a big and rich family including hydrothermal (HT) synthesis method, solvothermal (ST) synthesis method, electro-deposition (ED) method, chemical bath deposition (CBD) method, electrophoretic deposition (EPD) method, sol-gel method, direct chemical precipitation (CP)

method, microwave synthesis (MS) method, and so on. The above solution-based synthetic methods do not need expensive equipment and high vacuum, and are usually easy to process and conducted under mild conditions with lower temperature. Different solution-based synthetic methods have their own advantages and disadvantages, and sometimes they can be complementary to each other or cooperate with each to fabricate advanced nanomaterials.

In this Featured Article, we spot the recent progress in solution-based synthetic methods for designing and fabricating nanostructured electrode materials of typical transition metal oxides (e.g., nickel oxide, cobalt oxide, iron oxide, copper oxide, manganese oxide, vanadium oxide, tungsten oxide, and their composites) for applications in LIBs and supercapacitors. We focus on the detailed solution synthesis details and their corresponding reaction mechanisms. Furthermore, we will address the structural and morphological advantages of solution-synthesized nanostructured transition metal oxides and their composites for EES applications. Finally, we summarize and compare the merits and demerits of different solution-based methods and propose general rules on how to design and fabricate high-performance electrode EES materials.

## **2. NiO and NiO-based composites**

Nickel oxide is a classic example of transition metal materials with wide applications in electrochromics, catalysis, chemical sensor and EES. It can be used as an anode material for LIBs or a cathode material for supercapacitors. Pure NiO is an insulator with a bulk band gap of  $\sim 3.4$  eV. It crystallizes in the rock-salt structure (cubic crystal structure, JCPDS 4-0835) with a lattice constant of 0.417 nm and a high-spin anti-ferromagnetic spin structure at low temperatures. Lots of NiO nanostructures (such as nanowires, nanoflakes, nanobowls and nanospheres) have been prepared by different solution-based synthesis methods and applied as active materials for EES with enhanced electrochemical performance.

### **2.1 Chemical bath deposition of NiO and NiO-based composites**

The CBD method was first proposed by Nagayama et al., who used this technique to prepare SiO<sub>2</sub> films on silicon wafers about 25 years ago.<sup>20</sup> The CBD method involves immersion of a substrate in an aqueous solution containing a precursor species. Then the desired oxide/hydroxide precipitates preferentially on the substrate surface and produces a conformal film. The CBD method is an advantageous technique due to its low cost, low temperature and also convenient for large-scale deposition, especially suitable for the preparation of uniform oxide film samples. This method usually needs strong chemical oxidant or reducing agent to drive reactions to take place. The flatness of the final sample is even related with the fluid mechanics of the reaction solution.

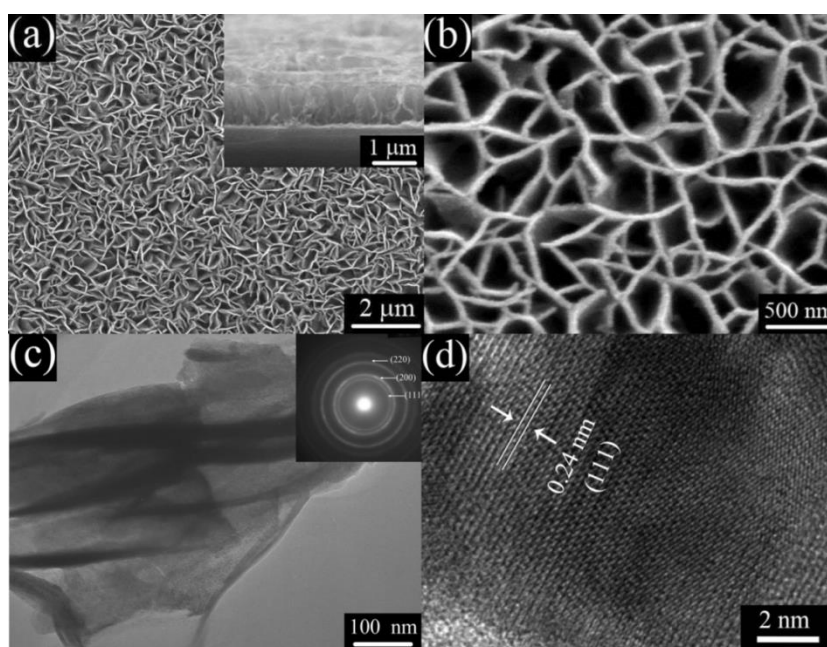


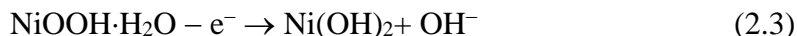
**Figure 1** Film of NiO nanoflakes obtained by chemical bath deposition. Reproduced with permission from Ref. 27.

Our group pioneered a facile modified CBD method for the synthesis of polycrystalline NiO nanoflake arrays and investigated their electrochromics, LIBs and supercapacitor performances.<sup>21-28</sup> The obtained NiO nanoflakes have diameters of 10–20 nm and grow vertically to the substrates. The nanoflakes are interconnected with each other forming a highly porous network with pore diameter of 30–300 nm (Figure 1). In our case, the electrolyte consists of nickel sulfate, ammonia and potassium persulfate. The precursor

reactions for the growth of NiO nanoflake arrays via CBD could be simply represented as follows:<sup>21, 22</sup>



During the annealing process:



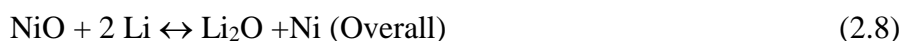
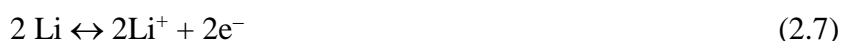
It is noteworthy that potassium persulfate here plays an important role in the formation of the NiO nanoflake arrays. Potassium persulfate acts as an oxidant to drive the whole reaction and facilitate the heterogeneous nucleation in the supersaturated solution. Without potassium persulfate, no NiO nanoflake arrays will be formed on the substrates. Other persulfates (such as  $\text{Na}_2\text{S}_2\text{O}_8$  and  $(\text{NH}_4)_2\text{S}_2\text{O}_8$ ) have similar functions. Impressively, the CBD-NiO nanoflakes can be formed on arbitrary substrates including ITO, FTO, Ti foil, graphite, carbon cloth, nickel foam, and so on. More importantly, this CBD process is very high efficiency, only needs several minutes to finish the whole deposition process.

Based on the above CBD method, we fabricated hierarchically porous NiO films by the combination of CBD method and polystyrene sphere template.<sup>27</sup> The obtained NiO films show a multilayer architecture with a substructure of NiO monolayer hollow-sphere array and a superstructure of porous net-like NiO nanoflakes. These hierarchically porous NiO films exhibit enhanced supercapacitor performances with higher capacitances ( $309 \text{ F g}^{-1}$  at  $1 \text{ A g}^{-1}$  and  $221 \text{ F g}^{-1}$  at  $40 \text{ A g}^{-1}$ ) than the dense counterparts ( $121 \text{ F g}^{-1}$  at  $1 \text{ A g}^{-1}$  and  $99 \text{ F g}^{-1}$  at  $40 \text{ A g}^{-1}$ ) and improved cycling stability. In addition, Yan et al.<sup>29</sup> prepared NiO hollow spheres powder samples by a similar CBD method and reported a capacitance of  $346 \text{ F g}^{-1}$  at  $1 \text{ A g}^{-1}$ . The reactions of NiO for supercapacitors are given as below:<sup>27</sup>



It is accepted that NiO is a p-type semiconductor whose conductivity is not good and kinetically unfavourable for high-rate capability. In order to further improve the pseudocapacitive performances of CBD-NiO nanoflake arrays, we adopted graphene to modify the conductivity of NiO to fabricate Graphene/NiO composite film by the combination of CBD and electrophoretic method, and improved capacitive performance was demonstrated in this composite film due to the conductivity modification by graphene.<sup>28</sup> In addition, Wu et al. modified the CBD-NiO nanoflakes by Ag nanoparticles, and verified that the introduction of Ag nanoparticles could effectively accelerate the electron transfer of the CBD-NiO nanoflakes leading to enhanced performance.<sup>30</sup> Meanwhile, the CBD-NiO nanoflakes are used to decorate other active material to form high-performance composite cathode materials for supercapacitors. We assembled the CBD-NiO nanoflake on porous Co<sub>3</sub>O<sub>4</sub> nanowire core to form Co<sub>3</sub>O<sub>4</sub>/NiO core/shell nanowire arrays, which exhibited noticeable supercapacitor performance with high specific capacitance of 853 F g<sup>-1</sup> at 2 A g<sup>-1</sup> after 6000 cycles owing to the unique porous core/shell nanowire array architecture.<sup>31</sup> Similar pseudocapacitive enhancement is also observed in the TiO<sub>2</sub>/CBD-NiO core/shell nanorod arrays reported by Wu et al..<sup>32</sup>

NiO is one of promising anodes of LIBs with a theoretic capacity of 718 mAh g<sup>-1</sup>. It has been proved that the electrochemical reaction mechanism of Li with transition metal oxides differs from the classical mechanisms, which are based either on reversible insertion/deinsertion of lithium into host structures or on lithium alloying reactions. The electrochemical reaction mechanism of Li with NiO in LIBs can be described as follows:<sup>4</sup>



Nevertheless, its practical application is restrained by the poor cycling stability resulting from the large specific volume change causing pulverization and deterioration of active materials during cycling. The above CBD-NiO nanoflake arrays are also applied as anode

materials for LIBs, but their LIBs performance, especially the cycling performance, is not satisfactory.<sup>24</sup> In order to improve their LIBs performance, our group used nanoporous and composite design strategies to deposit highly conductive layers (such as polyaniline, PEDOT, Ag, Co doping, and sputtered-Ni)<sup>23, 25, 26, 33</sup> on the surface of CBD-NiO nanoflake to form conductive composite arrays and enhanced LIBs performances were demonstrated in these systems. Meanwhile, Xia et al. reported a bio-template (lotus pollen grains) to prepare CBD-NiO/C composite nanoflake powder with high LIBs performance. These conductive layers can not only provide fast electron transportation path, but also act as a buffer layer to accommodate the strain caused by the lithium ion intercalation/deintercalation and alleviate the structure degradation caused by volume expansion during the cycling process. Expect for the outer decoration of conductive layers for CBD-NiO nanoflake, some other efforts have been directed at the search for hybrid materials such as ZnO/CBD-NiO,<sup>34</sup> and Fe<sub>2</sub>O<sub>3</sub>/CBD-NiO core/shell nanoarrays as anode for LIBs.<sup>35</sup> Some effective synergistic effects have been proven in these composite arrays such as enhanced mechanical stability and increased reaction surface area.

In addition to the above CBD method, there is another CBD method for the deposition of NiO, quite different from the former. Some researchers call it ammonia-evaporation method, but we believe that it still belongs to CBD.<sup>36</sup> In this CBD, the reaction solution is always very easy, just ammonia and nickel nitrate. This CBD reaction occurs at about 80–90 °C, and finally forming sandwich-like NiO triangular prism nanoarrays with side length of 500 nm after heat treatment (Figure 2).<sup>37, 38</sup> The involved reactions may be expressed as follows.<sup>36</sup>



After slow evaporation of ammonia, single-crystalline Ni(OH)<sub>2</sub> triangular prism nanoarrays precursors are formed. During annealing process:



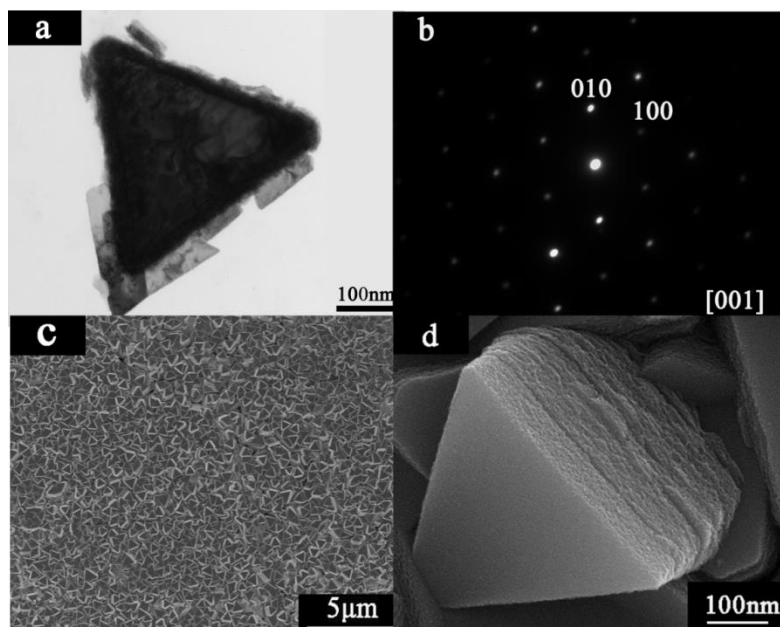


**Figure 2** (a) TEM image and (b) SAED pattern of chemical bath deposited NiO triangular prism. (c, d) SEM images of the film composed of NiO triangular prisms. Reproduced with permission from Ref. 38.

The NiO triangular prisms prepared by this CBD method have much bigger or larger size than those of the previous CBD method. It should be noticed that the quality of this NiO product is highly related with the position of substrates in the solution. The substrate should be 1–2 mm away from the bottom of reaction vessel. Otherwise, the film will not be uniform and homogeneous. Interestingly, the obtained NiO triangular prism is quasi-crystalline nature (Figure 2), and presents a capacity of  $400 \text{ mAhg}^{-1}$  after 50 cycles at 2 C for LIBs, and a specific capacitance of  $348 \text{ F g}^{-1}$  at  $2 \text{ A g}^{-1}$  after 4000 cycles for supercapacitors.<sup>40, 41</sup>

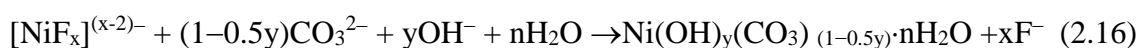
## 2.2 Hydrothermal synthesis and solvothermal synthesis of NiO and NiO-based composites

Hydrothermal synthesis is one of the most popular solution-based synthesis method and has been widely used for the synthesis of various transition metal oxides with specific size and morphology since the pioneering works from 1960s to 1980s. HT method is conducted in a sealed reaction container with the water as the reaction medium and the reaction

temperature is usually above 100 °C. A high pressure will self-develop and increase with the reaction temperature. The pressure in the autoclaves is also associated with other parameters such as the percentage fill of the vessel and any dissolved salts. It should be mentioned that the concept of HT has been extrapolated to non-aqueous systems, called solvothermal synthesis (ST), in which organic solvent is used as the reaction medium instead of water. HT/ST is easy to control and only needs simple reaction equipment such as oven and autoclaves.

To date, the HT+ST papers account for ~30 % in all the published papers of solution synthesis of NiO for EES applications. The HT/ST usually needs nickel sources and precipitants to work together to drive the whole reaction to take place. Nickel nitrate, nickel chloride and nickel acetate are the most used nickel sources. The most popular precipitants are urea [CO(NH<sub>2</sub>)<sub>2</sub>] and hexamethylenetetramine (HMT), respectively, because they have low hydrolysis temperature (<100 °C) and relatively controllable hydrolysis rate. The precipitants provide OH<sup>-</sup> or C<sub>2</sub>O<sub>4</sub><sup>2-</sup>, CO<sub>3</sub><sup>2-</sup> for the deposition of Ni-precursors [such as Ni(OH)<sub>2</sub>, Ni<sub>2</sub>(OH)<sub>2</sub>CO<sub>3</sub> and NiC<sub>2</sub>O<sub>4</sub>], which convert into NiO after annealing.

First, we introduce a typical and facile HT method for the synthesis of NiO nanoflake arrays. Previously, several research groups reported a similar HT method by using Ni(NO<sub>3</sub>)<sub>2</sub> or NiCl<sub>2</sub> as the nickel source, urea as the precipitant, NH<sub>4</sub>F as the growth promoter.<sup>39, 40</sup> The HT reactions can be illustrated as follows:

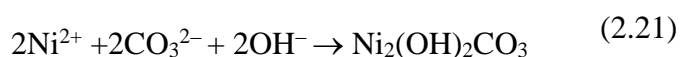
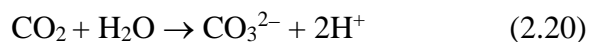


During annealing process:

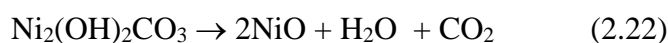


The final NiO samples are nanoflake arrays vertical to the substrates and flower-like nanoflake powder in the solution. The as-prepared NiO nanoflakes are single-crystalline nature.

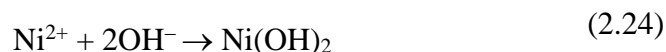
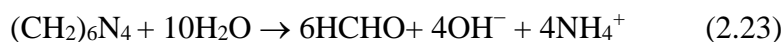
NH<sub>4</sub>F is acted as growth promoter to improve the growth density of nanoflakes and prompt the formation of basic nickel carbonate hydroxide precursor. Without NH<sub>4</sub>F, the load weight of NiO nanoflakes on the substrates will be much less, and the involved specific reactions are different, given as follows:<sup>41, 42</sup>



During the annealing process:



When the precipitant changes from urea to HMT,<sup>43</sup> the hydrolysis reaction will be



During the annealing process:



All the obtained NiO products by this HT method are nanoflakes or powders made up of nanoflakes. These nanoflake arrays show good LIBs performance with capacities of above 400 mAh g<sup>-1</sup> after 50 cycles at 0.3 A g<sup>-1</sup> and can deliver a capacitance of 300–500 F g<sup>-1</sup> at 2 A g<sup>-1</sup> after 3000 cycles as cathode materials of supercapacitors.<sup>39-41, 44</sup> In addition, several graphene/NiO, C/NiO, Ni/NiO composites have been reported via the above HT method to achieve enhanced electrochemical performance.<sup>42, 43, 45-47</sup>

Except for the above common precipitants, some other precipitants such as ammonia, NaOH, glycine, n-butylamine, N-methyl pyrrolidone, L-lysine, L-arginine, ethanolamine and butanol are also used to prepare NiO samples composed of nanoflakes.<sup>42, 46-55</sup> As for the organic precipitants, they have specific or even more complex reaction mechanisms, which

are not studied in detail in these papers. Among these NiO products, the powder samples are prone to exhibit sphere structures (Figure 3) due to the self-assembly of NiO nanoflakes. The electrochemical results reveal that the powder samples have inferior performance to film samples, both for supercapacitor and LIBs applications, due to the fact the powder active materials need to be mixed with carbon and polymer binders and compressed into pellets. This process risks negating the benefits associated with the reduced particle size and introduces supplementary, undesirable interfaces.

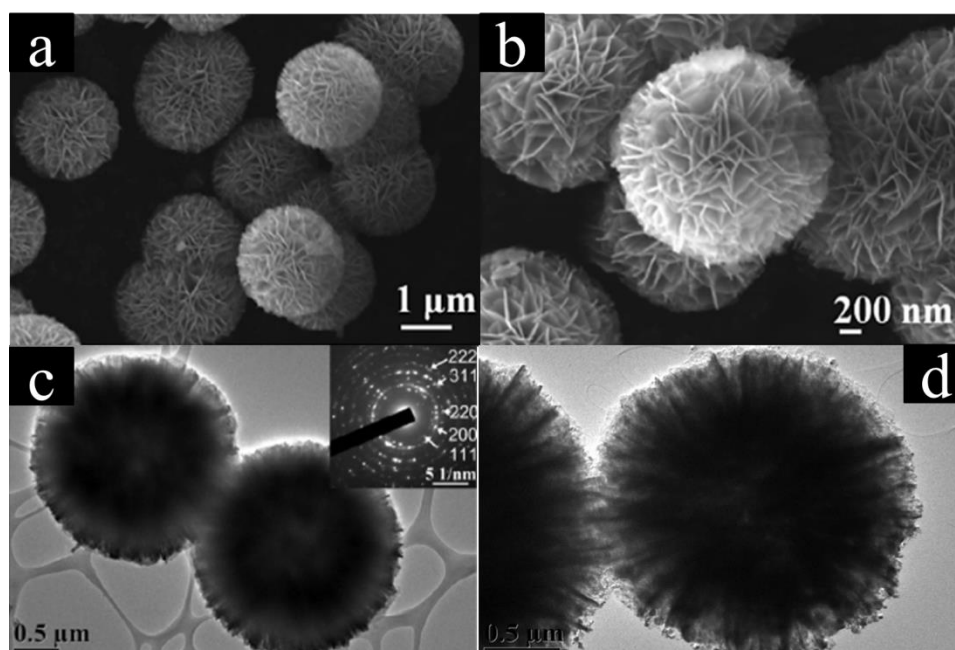
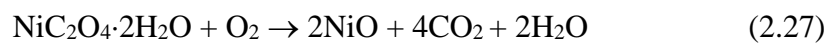
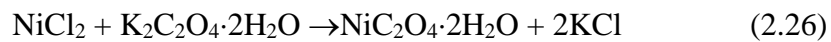


**Figure 3** NiO spheres composed of nanoflakes obtained by hydrothermal synthesis. Reproduced with permission from Ref. 51.

It is noticed that the morphology of NiO is highly related with that of precursors. If the precursors are hydroxides or oxyhydroxides, the final morphology of NiO will be nanoflakes. If the precursors are materials like oxalate which is prone to form nanowires, the final NiO products will keep the structure of nanowires. It is observed that the as-prepared NiO samples always show nanoflake structures or spheres composed of nanoflakes when the precursor is nickel hydroxide or oxyhydroxide. This phenomenon is mainly due to its typical crystal structure of hydroxide or oxyhydroxide precursor. It is well accepted that the brucite crystals ( $M(OH)_2$  or  $MOOH$ ,  $M=Mg, Ca, Ni, Co$ , and etc.) have a layered structure of the  $CdI_2$  type, which shows weak interaction between layers and the strong binding within the layered

planes.<sup>56, 57</sup> Neighboring layers are bound together by weak van der Waal forces. Therefore its (001) plane is stable, and the brucite crystal is prone to form two-dimensional nanoflakes. Then, these nanoflakes self-assemble with each other to form hollow spheres. The NiO preserves their morphology and show nanoflake structure. This phenomenon will change if the precursor is nickel oxalate. Su et al. used another precipitant ( $K_2C_2O_4$ ) to prepare mesoporous NiO nanowire by a modified HT method.<sup>58</sup> The specific reactions are shown as follows:<sup>58</sup>



The mesoporous NiO nanowires exhibit a capacitance of  $348 \text{ F g}^{-1}$  as electrodes in supercapacitors and a capacity of  $1280 \text{ mAh g}^{-1}$  after 100 cycles for LIBs.<sup>58</sup> It is reasonable that the precipitant can affect the morphology of final NiO samples. The specific mechanism is still not clear and speculated that the  $C_2O_4^{2-}$  plays an important role in the nanowire growth.

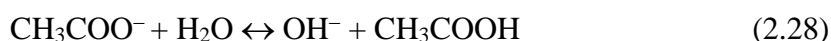
In view of the success of HT, scientific researchers extend the HT to the organic field, namely called solvothermal synthesis (ST). Nickel sources are dissolved in the organic solvent such as glycerol, ethylene glycol and ethanol to react and form NiO after annealing.<sup>59-</sup>  
<sup>62</sup> The organic solvent will decompose under high temperature and release precipitant ions to trigger reactions. To date, the detailed mechanisms of ST-NiO have not been studied well, and it is still hidden in the fog. Similarly, NiO nanoflake arrays and nanospheres composed of nanoflakes are obtained in the ST systems and show improved LIBs and supercapacitor performance.<sup>59-62</sup>

### 2.3 Electrochemical synthesis of NiO and NiO-based composites

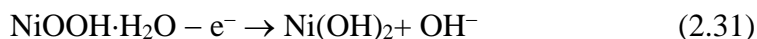
Among the existing solution synthetic approaches to film materials, electrochemical techniques show unique principles and flexibility in the control of the structure and morphology of samples. Generally, two kinds of electrochemical synthesis methods are adopted to prepare nanostructured transition metal oxides, namely ED and electrophoretic

deposition (EPD). ED is always involved with redox reactions related to electron transfer and phase change. ED is believed to be an ideal method for the fabrication of nanostructured films with various morphologies, because it occurs from the electrode surface and different morphologies of the materials can be obtained via the precise choice of deposition solution and conditions. ED provides the fabrication of films or coatings rather than powders, which is required for a number of applications in batteries, and supercapacitors. Meanwhile, EPD technique, another electrochemical synthesis method, is an economical and versatile processing technique with many advantages in the preparation of films from suspensions, such as high deposition rate and throughput, good uniformity and controlled thickness of the obtained films, and simplicity of scaling up.

According to the reaction mechanism, the ED is classified into two types: anodic ED and cathodic ED. Several ED-NiO nanostructures have been reported and applied for EES. Here, we introduce pioneering works of Wu et al. about the anodic ED method for the synthesis of NiO nanoflake arrays and composites in the mixed solution of NiSO<sub>4</sub>, Na<sub>2</sub>SO<sub>4</sub>, and CH<sub>3</sub>COONa. The involved reactions can be simply illustrated as follows:<sup>63</sup>



During the annealing process:



This anodic ED method can be applicable for lots of substrates such as nickel foam, stainless steel, FTO and ITO. The deposited NiO film has an interconnecting network is made up of flaky nickel oxides of 15–20 nm. Wu and his co-workers also used this anodic ED method to fabricate macroporous NiO bowl-like arrays, NiO/Ni(OH)<sub>2</sub> and NiO/C composites

and investigated their LIBs and supercapacitor performances.<sup>64-68</sup> The obtained NiO nanoflakes exhibit a very high capacity of  $\sim 990 \text{ mAh g}^{-1}$  at 15 C as anode of LIBs,<sup>64</sup> and a capacitance of  $\sim 170 \text{ F g}^{-1}$  at  $1 \text{ A g}^{-1}$  as cathode of supercapacitors.<sup>66</sup> The low supercapacitor performance is because that the samples are grown on flat stainless steel substrates, which is not an ideal substrate as good as nickel foam. The NiO bowl-like arrays show better supercapacitor performances than the unmodified ED counterparts.<sup>68</sup> Moreover, the modified composites NiO/Ni(OH)<sub>2</sub> and NiO/C show further improved supercapacitor performances with a capacitance over  $500 \text{ F g}^{-1}$ .<sup>65, 67</sup> Inspired by these works, Wu et al. prepared TiO<sub>2</sub>/NiO core/shell nanorod arrays (Figure 4) on carbon cloth and delivered a capacitance of  $611 \text{ F g}^{-1}$  at  $2 \text{ A g}^{-1}$ .<sup>32</sup>

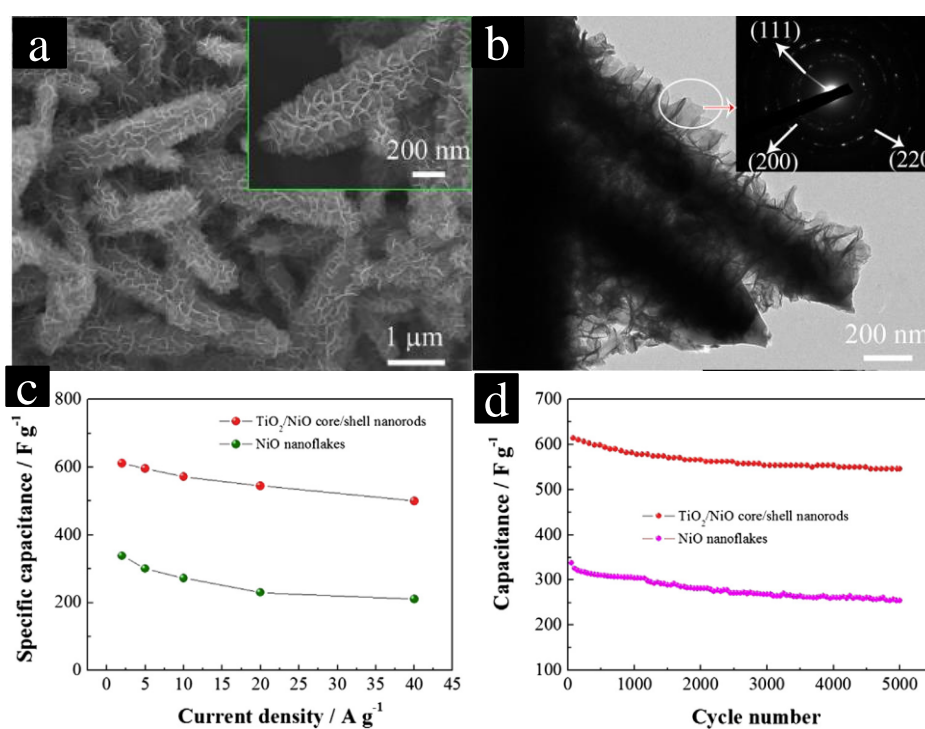
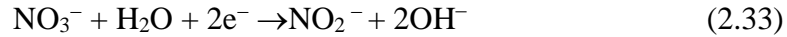


**Figure 4** (a, b) SEM-TEM images and (c, d) pseudocapacitive performances TiO<sub>2</sub>/NiO core/shell nanorod arrays on carbon cloth. The NiO nanoflakes are obtained by electro-deposition method. Reproduced with permission from Ref. 32.

As for the cathodic ED of NiO, the nickel source is usually Ni(NO<sub>3</sub>)<sub>2</sub> and the reactions are shown as follows:<sup>69</sup>



During the annealing process:



In this electrochemical reduction process, metallic Ni cannot form because the reaction potential of Ni<sup>2+</sup>/Ni is much more negative than that of NO<sup>3-</sup>/NO<sup>2-</sup>.<sup>57</sup> Yuan et al. prepared hierarchically ordered porous nickel oxide array film by the cathodic ED through monolayer polystyrene spheres template and reported a capacity of 518 mAh g<sup>-1</sup> at 1C for LIBs. It is noticed that the NiO directly prepared by cathodic ED usually shows a dense film structure, not a porous structure.<sup>69</sup> Some other NiO nanostructures and composites such as nanocorn, Ni/NiO core/shell and randomly porous NiO are fabricated by another cathodic ED, in which Ni nanostructures forms first and then are converted into NiO during annealing in air.<sup>70-72</sup> These NiO samples converted from Ni exhibit good high rate capability with a capacity of 436 mAh g<sup>-1</sup> at 20 C for LIBs as well as high capacitance above 1000 F g<sup>-1</sup> for supercapacitors.<sup>70-72</sup>

Meanwhile, Wu et al. developed a EDP method to prepare NiO films via Ni(OH)<sub>2</sub> sol in isopropyl alcohol solution.<sup>73, 74</sup> No redox reactions occur in the EDP process, just electrostatic effect to absorb the active material on the surface of substrates. The EDP-NiO films are composed of nanoparticles and exhibit a pseudocapacitive capacitance of ~180 F g<sup>-1</sup>.

## 2.4 Chemical precipitation synthesis of NiO and NiO-based composites

Chemical precipitation (CP) is an old and simple method, easy to process and especially suitable for large-scale synthesis of powder samples. CP occurs if the concentration of one solid is above the solubility limit in the host solid, due to rapid quenching or ion implantation, and the temperature is high enough that diffusion can lead to segregation into precipitates. Precipitation in solids is routinely used to synthesize large-scale micro/nano-size materials. CP is widely used to prepare nanoscale transition metal oxides, also reflected in the synthesis

of NiO for EES. Similar to HT method, the CP also needs nickel sources and precipitants, and the precipitation process usually occurs fast. The reaction rate is very fast, sometimes, the whole reaction only needs several minutes. The operation process of CP is conducted at room temperature and does not need high temperature. Nevertheless, it is difficult for CP to precisely control the morphology of metal oxides due to the fast precipitation. The CP papers account for ~20 % in all the published papers of solution synthesis of NiO for EES applications.

Compared to other solution synthesis methods, the reactions in the CP is much easier. The adopted precipitant is common reagent such ammonia, KOH and NaOH. The whole reactions can be shown as below:<sup>75-78</sup>



During the annealing process:



Lots of NiO nanostructures such as nanoplates, nanoparticles, nanospheres, nanoclusters have been prepared by the CP method and applied for EES.<sup>71, 75-83</sup> However, the pure nanosize CP-NiO samples do not show very good electrochemical performance, no matter in LIBs or supercapacitors. Hence, researchers combine other conductive scaffolds with CP-NiO to construct new NiO composites with enhanced EES performance. A series of composites (such as graphene/NiO, C/NiO, Ni/NiO) have been prepared by the co-chemical precipitation method,<sup>59, 71, 84-89</sup> and high capacitance (300-800 F g<sup>-1</sup>) and capacity (500-1000 mAh g<sup>-1</sup>) are demonstrated in these composite systems.

## 2.5 Sol-gel and Microwave synthesis of NiO and NiO-based composites

The name sol-gel derives from the fact that micro particles or molecules in a solution (sols) agglomerate and under controlled conditions eventually link together to form a coherent network (gel). There are two generic variations of the sol-gel technique. One is called the colloidal method, and the other is called the polymeric (or alkoxide) route. The differences

between the two stem from the types of starting materials (precursors) that are used. Both routes involve suspending or dissolving the precursor(s) in a suitable liquid, usually water for the colloidal route and alcohol for the polymeric route. The precursor is then activated by the addition of an acid (such as hydrochloric acid) or a base (such as potassium hydroxide). The activated precursors react together to form a network. The network grows and ages with time and temperature until it is the size of the container. At this point the viscosity of the liquid increases at an exponential rate until gelation occurs, that is, no more flow is observed. Many different industries could benefit from adopting sol-gel because of its versatility in fabricating a wide range of materials with different properties. Current examples are found in the construction, electronics, communications, automotive and EES.

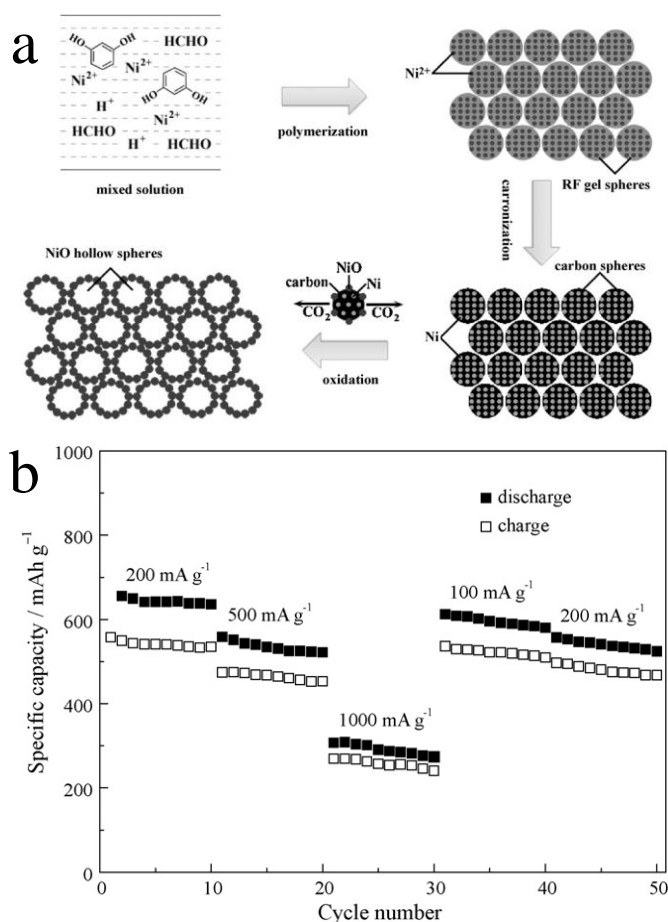


**Figure 5.** (a) Schematics of the sol-gel synthesis procedure of hollow NiO spheres. (b) Rate capability as the Li-ion battery electrode. Reproduced with permission from Ref. 90.

To date, there are only a few reports about the sol-gel method for the synthesis of NiO and NiO-based composites for EES applications. Previously, our group used  $\text{NiCl}_2$ ,  $\text{HCl}$  and

formaldehyde to form NiCl<sub>2</sub>/resorcinol-formaldehyde (RF) gel and finally obtained NiO hollow spheres after heat treatment (Figure 5).<sup>90</sup> This sol-gel process belongs to polymeric (or alkoxide) route. The as-prepared NiO hollow spheres present a high reversible LIBs capacity of 635 mAh g<sup>-1</sup> at 200 mA g<sup>-1</sup>. Kim et al. prepared NiO nanostructures with three distinct morphologies by a sol-gel method and their morphology-dependent supercapacitor properties were exploited.<sup>91</sup> They used Ni(NO<sub>3</sub>)<sub>2</sub>, Ni(CH<sub>3</sub>COO)<sub>2</sub>, hexamethylene tetramine and ammonia as the starting materials and utilized different control reagent to fabricate three NiO nanostructures (flower-like, slice-like and particle-like NiO). Their sol-gel method is a typical colloidal route. These NiO samples can deliver a capacitance of 480 F g<sup>-1</sup> at 0.5 A g<sup>-1</sup> for supercapacitors. Meanwhile, Liu et al. reported a NiO/NiCo<sub>2</sub>O<sub>4</sub>/Co<sub>3</sub>O<sub>4</sub> composite via a sol-gel method by using Ni(NO<sub>3</sub>)<sub>2</sub>, CoCl<sub>2</sub>, and propylene oxide. The composite shows a high specific capacitance (1717 F g<sup>-1</sup>) and enhanced rate capability.<sup>92</sup>

Microwave synthesis (MS) has become the method of choice for many chemists and biochemists for a multitude of reactions for one reason: it simply works better. Reactions that took hours, or even days, to complete can now be performed in minutes with better yields and cleaner chemistries. In many of the published examples, microwave heating has been shown to dramatically reduce reaction times, increase product yields and enhance product purities by reducing unwanted side reactions compared to conventional heating methods. The advantages of this enabling technology have, more recently, also been exploited in the context of multistep total synthesis of transition metal oxides. MS is suitable for large-scale synthesis of powder products.

According to the published papers about MS process of nanostructured NiO, notice the fact that the MS method can be regarded as a modified solution synthesis method built on the traditional CP method. First, a precipitation is formed by simply mixing precipitants (ammonia or sodium hydroxide) and nickel sources. Then transfer the precipitation into a microwave oven to go deep reaction to obtain NiO nanostructures such as nanospheres,

nanoflakes, nanoplates, nanoparticles.<sup>93-97</sup> These MS-NiO nanostructures show a capacity of 884 mAh g<sup>-1</sup> and a pseudocapacitance of (277–585 F g<sup>-1</sup>).<sup>93, 94, 96, 97</sup>

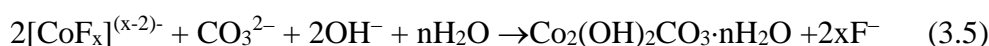
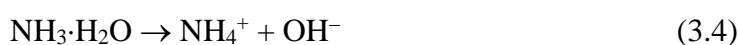
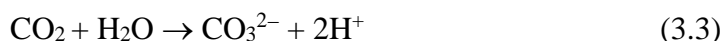
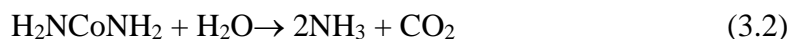
### 3. Cobalt oxides and cobalt oxides-based composites

Cobalt oxides (Co<sub>3</sub>O<sub>4</sub> and CoO) have attracted great attention for EES due to their excellent electrochemical reactivity and redox reversibility since the pioneering works of Tarason's group and Conway et al.<sup>3, 4</sup> Co<sub>3</sub>O<sub>4</sub> is a black antiferromagnetic solid with a band gap of ~2.0 V. As a mixed valence compound, its formula is sometimes written as Co<sup>II</sup>Co<sup>III</sup><sub>2</sub>O<sub>4</sub>, which adopts the normal spinel structure, with Co<sup>2+</sup> ions in tetrahedral interstices and Co<sup>3+</sup> ions in the octahedral interstices of the cubic close-packed lattice of oxide anions. The spinel Co<sub>3</sub>O<sub>4</sub> is a magnetic semiconductor with a lattice constant a=0.808 nm (JCPDS 42-1467). The other interesting cobalt oxide is CoO (cobalt monoxide), which has rock salt structure (NaCl structure, JCPDS 09-0402) consists of two interpenetrating fcc sublattices of Co<sup>2+</sup> and O<sup>2-</sup> with a lattice constant of 0.426 nm and a band gap of ~2.6 V. The CoO is not stable in the air and will be oxidized into the thermodynamically favoured form—Co<sub>3</sub>O<sub>4</sub>. In view of their high capacity (LIBs: the theoretical capacity of Co<sub>3</sub>O<sub>4</sub> and CoO is 890 mAh g<sup>-1</sup> and 718 mAh g<sup>-1</sup>, respectively) and capacitance (Supercapacitors: a theoretical capacitance of >2000 F g<sup>-1</sup>), the cobalt oxides (Co<sub>3</sub>O<sub>4</sub> and CoO) have been extensively studied as active materials for EES. Numerous nanostructured cobalt oxides (such as nanowires, nanoflakes, nanocage, nanorods, nanoparticles nanobowls and nanospheres) have been prepared by different solution-based synthesis methods and enhanced electrochemical performances have been demonstrated in these systems.

#### 3.1 Hydrothermal synthesis and solvothermal synthesis of cobalt oxides and cobalt oxides-based composites

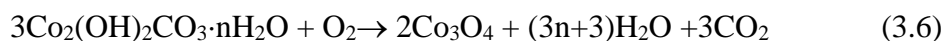
Among all the solution-based synthetic routes for the synthesis of cobalt oxides for EES, HT is the most popular solution synthesis method and the published HT papers account for

~40 % in all the published solution-based literature. Combined with our works, we introduce one of the most fascinating HT methods for the preparation of cobalt oxides (Co<sub>3</sub>O<sub>4</sub> and CoO) nanowire arrays and their composite materials. In our case, we used Co(NO<sub>3</sub>)<sub>2</sub> (can also be CoSO<sub>4</sub> or CoCl<sub>2</sub>), NH<sub>4</sub>F and urea as the starting materials and the whole reactions were conducted at 110–120 °C. The involved HT reactions can be illustrated as follows:<sup>31, 98-102</sup>

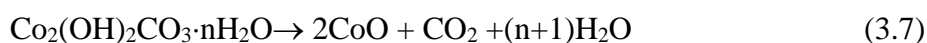


The Co<sub>3</sub>O<sub>4</sub> and CoO nanowires can be formed after heat treatment under different atmospheres: Co<sub>3</sub>O<sub>4</sub> in air and CoO in pure argon or nitrogen. If the argon is just normal, not high-purity, the final product will also be Co<sub>3</sub>O<sub>4</sub> nanowires. The different reactions in the annealing process are as follows:

During the annealing process for Co<sub>3</sub>O<sub>4</sub> nanowires:<sup>2, 31</sup>



During annealing process for CoO nanowires:<sup>100, 101</sup>



The cobalt oxides (Co<sub>3</sub>O<sub>4</sub> or CoO) nanowires show sharp tips and have an average diameter of ~80 nm, length up to around 5–25 μm (Figure 6). The length of nanowires could be easily controlled by the growth time. The as-prepared Co<sub>3</sub>O<sub>4</sub> or CoO nanowires consist of numerous interconnected nanoparticles and presents a rough appearance with a large quantity of mesoporous structure, which is ascribed to the successive release and loss of CO<sub>2</sub> and H<sub>2</sub>O during the thermal decomposition of Co<sub>2</sub>(OH)<sub>2</sub>CO<sub>3</sub> precursor,<sup>102-105</sup> which is single crystalline in nature.<sup>103</sup>

The above HT-cobalt oxides can be grown on almost all the substrates including ITO, FTO, glass slide, nickel foam, carbon cloth, Ti foil, nickel foil, copper foil and stainless steel and so on.<sup>2, 31, 98-101, 103, 106</sup> In the HT solution, the powder products can be collected and are some interesting cobalt oxides ( $\text{Co}_3\text{O}_4$  or  $\text{CoO}$ ) nanostructures (such as balls, spheres and hexapods) assembled by nanowires.<sup>107-110</sup> The  $\text{NH}_4\text{F}$  in the above HT method is acted as the growth promoter to improve the growth density of nanowires and prompt the formation of basic cobalt carbonate hydroxide precursor. Another problem to be noticed is that the reaction time also has great influence on the morphology of samples. When the time is less than 3 h, the products may not be nanowires, but nanoflakes. This special change is still under investigation.

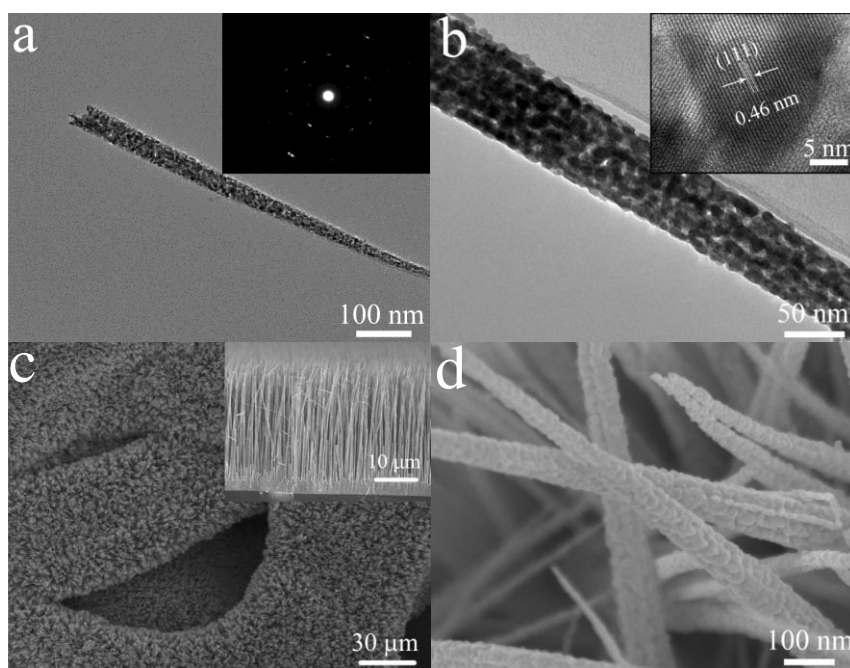
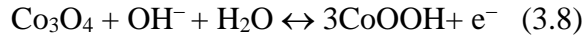
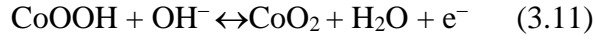


**Figure 6** Porous  $\text{Co}_3\text{O}_4$  nanowires by hydrothermal synthesis method. (a, b) TEM and HRTEM images of individual  $\text{Co}_3\text{O}_4$  nanowire; (c, d) SEM images of  $\text{Co}_3\text{O}_4$  nanowire array grown on nickel foam. Reproduced with permission from Ref. 103.

The as-prepared HT- $\text{Co}_3\text{O}_4$  and HT- $\text{CoO}$  nanowire arrays are well characterized as electrode materials for LIBs and supercapacitors. For supercapacitors application, the cobalt oxides ( $\text{Co}_3\text{O}_4$  and  $\text{CoO}$ ) undergo reversible redox reactions in the alkaline electrolyte. The reactions for  $\text{Co}_3\text{O}_4$  in supercapacitors are illustrated as follows:<sup>98, 106, 111-113</sup>



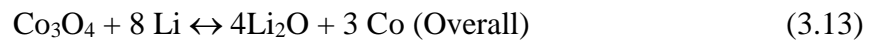
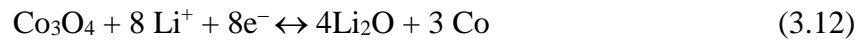
The electrochemical reactions for CoO are expressed as follows:<sup>31, 111, 114, 115</sup>



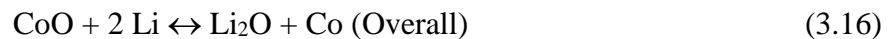
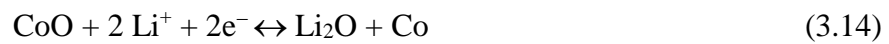
These cobalt oxides ( $\text{Co}_3\text{O}_4$  or  $\text{CoO}$ ) nanowire arrays exhibit noticeable pseudocapacitive performances with high capacitance of  $754 \text{ F g}^{-1}$  at  $2 \text{ A g}^{-1}$  and  $610 \text{ F g}^{-1}$  at  $40 \text{ A g}^{-1}$  as well as excellent cycling stability.<sup>100, 101, 103</sup> Generally, two redox peaks will be found in the CV curves of cobalt oxides ( $\text{Co}_3\text{O}_4$  or  $\text{CoO}$ ) nanowire array, namely,  $\text{CoOOH}$  and  $\text{CoO}_2$  will be formed at high oxidation potentials.  $\text{CoOOH}$  has been detected and confirmed, but  $\text{CoO}_2$ , sometimes, is considered as a virtual state, or not stable.

For LIBs application, the cobalt oxides ( $\text{Co}_3\text{O}_4$  and  $\text{CoO}$ ) can reversibly react with Li ion to store electrochemical energy and show promising applications as anode materials. The corresponding simplified reactions are expressed as follows:

Reactions for  $\text{Co}_3\text{O}_4$  with Li ion:<sup>116</sup>



Reactions for  $\text{CoO}$  with Li ion:<sup>4, 117</sup>



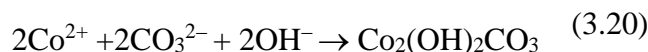
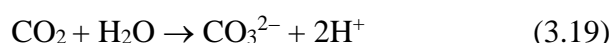
The as-prepared HT- $\text{Co}_3\text{O}_4$  and HT- $\text{CoO}$  nanowire arrays as anode of LIBs show high capacity more than  $800 \text{ mAh g}^{-1}$  ( $1167 \text{ mAh g}^{-1}$  at  $0.5\text{C}$  and  $903 \text{ mAh g}^{-1}$  at  $1 \text{ C}$ ).<sup>104, 105, 108,</sup>

<sup>110</sup> The enhanced EES performance is due to the unique one-dimensional (1D) architecture,

which provides fast diffusion paths for ions and facilitates the electron and ion transfer on the cobalt oxide/electrolyte interfaces. Moreover, the 1D nanowire array can accommodate the volume expansion and restrain the pulverization and deterioration of  $\text{Co}_3\text{O}_4/\text{CoO}$  during the repeated cycling process, resulting in enhanced cycling stability. Inspired by these interesting and fascinating results, new composites based on the HT- $\text{Co}_3\text{O}_4$  and HT-CoO nanowires have emerged and show noticeable and enhanced EES performance than the bare cobalt oxide nanowires. We developed several HT- $\text{Co}_3\text{O}_4$  and HT-CoO based core/shell nanowire arrays (e.g.,  $\text{Co}_3\text{O}_4/\text{C}$ ,  $\text{Co}_3\text{O}_4/\text{MnO}_2$ ,  $\text{Co}_3\text{O}_4/\text{NiO}$  and  $\text{Co}_3\text{O}_4/\text{Co}(\text{OH})_2$ ,  $\text{CoO}/\text{Ni}(\text{OH})_2$ ,  $\text{CoO}/\text{TiO}_2$ ,  $\text{Co}_3\text{O}_4/\text{Fe}_2\text{O}_3$ )<sup>8, 31, 56, 98, 100-102, 118</sup> and demonstrated their enhanced LIBs and supercapacitor performances with higher capacity and capacitances (even two times larger than the unmodified counterparts), and excellent cycling stability. Similar enhanced results have also been proven in other advanced composite nanowires such as Mo-decorated  $\text{Co}_3\text{O}_4$ ,  $\text{Co}_3\text{O}_4@\text{Pt}@\text{MnO}_2$ ,  $\text{Co}_3\text{O}_4@\text{NiCo}_2\text{O}_4$ ,  $\text{Co}_3\text{O}_4@\text{Ni}(\text{OH})_2$ ,  $\text{Co}_9\text{S}//\text{Co}_3\text{O}_4@\text{RuO}_2$  and  $\text{CoO}@\text{Polypyrrole}$ .<sup>114, 119-123</sup> The high capacity/capacitance and cycling stability in the core/shell systems are believed to benefit from the the unique architecture including the porous cobalt oxides core nanowire, nanostructured shell and ordered array configuration. (1) The highly porous system shortens the transportation/diffusion path for both electrons and ions, thus leading to faster kinetics and high-rate capability; (2) High surface area of the mesoporous nanowire arrays favors the efficient contact between active materials and electrolytes, providing more active sites for electrochemical reactions; (3) The porous core/shell nanowire array architecture possess favorably morphological stability, which helps to alleviate the structure damage caused by volume expansion during the cycling process. In short, these characteristics would lead to fast ion/electron transfer, sufficient contact between active materials and electrolyte, and enhanced flexibility, finally resulting in enhanced electrochemical performance. In addition, we found that the active material deposited on 3D porous substrates (such as nickel foam) shows better electrochemical performance than their

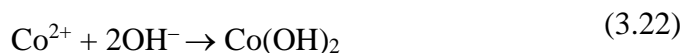
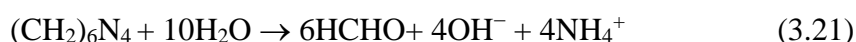
counterparts on the flat substrate, due to the fact that the 3D porous substrates provide higher active surface area and inner space for fast ion/electron transfer and higher energy conversion efficiency.

Notice that the cobalt oxides ( $\text{Co}_3\text{O}_4$  or  $\text{CoO}$ ) nanowires can also be prepared without  $\text{NH}_4\text{F}$ , but the obtained nanowires are much thinner and prone to be bending. The reactions of precursor are shown as follows:<sup>112, 124-127</sup>

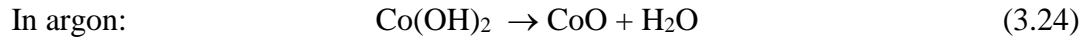
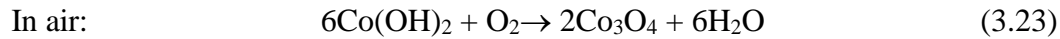


It is noteworthy that the chemical formula of  $\text{Co}_2(\text{OH})_2\text{CO}_3$  precursor is complex, sometimes it will contain the anions in the cobalt source (e. g.,  $\text{Cl}^-$ ,  $\text{SO}_4^-$  and  $\text{NO}_3^{2-}$ ). Lot of cobalt oxides nanostructures (e.g., nanorod, echinus-like, emongrass-like, chrysanthemum-like, nanosphere, nanowire, nanoflake, nanoplate, nanocube, nanonet) and composites ( $\text{Co}_3\text{O}_4/\text{graphene}$  and  $\text{Co}_3\text{O}_4/\text{carbon}$ ),<sup>107, 111, 124, 126-137</sup> have been fabricated by the HT method only with urea and cobalt sources, and showed high LIBs capacity of (700–100  $\text{mAh g}^{-1}$ ),<sup>107, 124, 130, 131</sup> and delivered large specific capacitances (500–1124  $\text{F g}^{-1}$ ) at high charge/discharge rate.<sup>111, 112, 125, 127-129</sup> Even so, researchers prefer the first HT method with  $\text{NH}_4\text{F}$  because the quality of the final cobalt oxides samples is much higher with better structural control and adhesion on the substrates and higher active materials load.

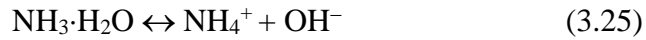
When the precipitant is hexamethylenetetramine (HMT), the reactions and precursor will be different, shown as follows.<sup>138, 139</sup>



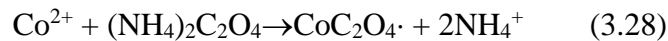
During the annealing process:



If the precipitant is ammonia or NaOH, the reactions of precursor are much easier as follow.<sup>133, 140-142</sup>



When the precipitant is oxalate,  $(\text{NH}_4)_2\text{C}_2\text{O}_4$ , the reactions of precursor are as follow.<sup>143</sup>



Meanwhile, some other organic precipitants (e.g., ethylene glycol, ethanol, L-arginine, polyethylene glycol, lysine) are also used for the preparation of nanostructured cobalt oxides (nanoparticle, nanoflake, nanowire, nanosphere),<sup>109, 117, 144-149</sup> and composites with graphene and carbon.<sup>109, 150</sup> The specific reactions associated with the hydrolysis of these organic precipitants, are still not clear and under investigation. Additionally, some HT reactions just utilize the hydrolysis of cobalt source such as  $\text{Co}(\text{NO}_3)_2$  at high temperature to form precursor.<sup>151, 152</sup> This HT is always used to prepare composite materials, particularly with graphene or carbon.

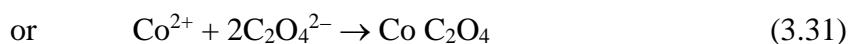
After analysing the HT-cobalt oxides papers, we found that the HT-cobalt oxides ( $\text{Co}_3\text{O}_4$  and  $\text{CoO}$ ) nanowire arrays are very popular with researches and can be easily fabricated in controllable manner, which could not be realized by other solution synthesis method. Moreover, the obtained porous HT-cobalt oxides ( $\text{Co}_3\text{O}_4$  and  $\text{CoO}$ ) nanowire arrays exhibit good EES performance with high capacitance/capacity. Additionally, they are good templates or scaffolds for constructing new high-performance core/shell nanoarrays or composites.

Nowadays, in order to further improve the EES performance, great efforts are focusing on the modification of HT-cobalt oxides ( $\text{Co}_3\text{O}_4$  and  $\text{CoO}$ ) nanowires by introducing graphene, metal, carbon nanotube and conducting polymers to get composite materials with new or improved functions. The introduction of conductive backbone or coating can improve the conductivity of the bare nanowires leading to enhanced electrochemical properties.

Solvothermal synthesis (ST) is the twin brother of HT. The literature of ST for the synthesis of cobalt oxides ( $\text{Co}_3\text{O}_4$  and  $\text{CoO}$ ) nanostructures is not as much as that of HT. Several cobalt oxides ( $\text{Co}_3\text{O}_4$  and  $\text{CoO}$ ) nanostructures (such as nanocapsules, nanosheets, nanospheres and nanoflower) have been obtained in the organic solvents including methanol, ethanol and ethylene glycol.<sup>153-159</sup> Detailed reactions have not been studied and shown in these papers. The EES performances of the ST-cobalt oxides are comparable to those prepared by HT.

### **3.2 Chemical precipitation synthesis of cobalt oxides and cobalt oxides-based composites**

The second-popular solution synthesis method of cobalt oxides ( $\text{Co}_3\text{O}_4$  and  $\text{CoO}$ ) is chemical precipitation (CP), which is regarded as the easiest chemical method for the fabrication of metal oxides. CP only need to mix the cobalt sources ( $\text{Co}(\text{NO}_3)_2$ ,  $\text{CoSO}_4$ ,  $\text{CoCl}_2$ , etc.) and precipitants (ammonia,  $\text{NaOH}$ ,  $\text{KOH}$ ,  $\text{Na}_2\text{CO}_3$ ,  $\text{K}_2\text{C}_2\text{O}_4$ , etc.) to produce precipitation under appropriate PH values. The involved reactions of precursors in CP are always very simple, expressed as follows.



Then the precursor converts into  $\text{Co}_3\text{O}_4$  or  $\text{CoO}$  after annealing in different atmospheres. The CP process is very easy to process and suitable for large-scale preparation. The CP

papers account for ~28 % in all the published solution-based papers of cobalt oxides for EES applications.

Common CP process is very fast and difficult to precisely control the morphology of metal oxides due to the fast precipitation. Though some unique nanostructured cobalt oxides ( $\text{Co}_3\text{O}_4$  and  $\text{CoO}$ ) have been realized by the CP, this controllable synthesis needs to be conducted with the help of some hard or soft templates (AAO, virus, carbon nanotube, surfactant, etc.).<sup>116, 160, 161</sup> Here, we first introduce a template-free method to fabricate cobalt oxide nanotubes developed by Lou's group.<sup>162</sup> Lou et al. used  $\text{Co}(\text{NO}_3)_2$  and ammonia as the starting materials to form needle-like  $\text{Co}_3\text{O}_4$  nanotubes in refluxed condition at 95–100 °C for 20 h. Firstly, a dense  $\beta\text{-Co}(\text{OH})_2$  nanowire will be formed according to the reaction:<sup>162</sup>



Then the  $\text{Co}(\text{OH})_2$  are oxidized into  $\text{Co}_3\text{O}_4$  by  $\text{O}_2$  in the solution:<sup>162</sup>

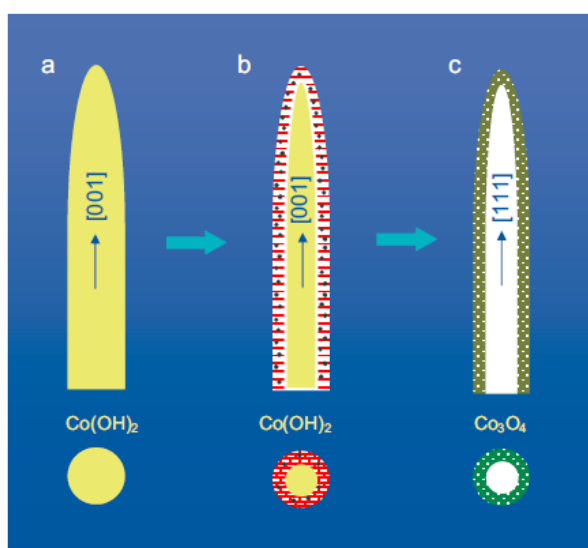
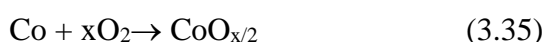
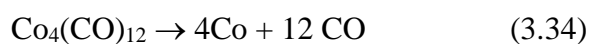


**Figure 7.** Schematic illustration of  $\text{Co}_3\text{O}_4$  needle-like nanotubes obtained by chemical precipitation method. (a) Single-crystalline  $\beta\text{-Co}(\text{OH})_2$  nanoneedles along [001] direction. (b)  $\text{Co}(\text{OH})_2$  with loose platelet-walls. (c)  $\text{Co}_3\text{O}_4$  needle-like nanotubes. Reproduced with permission from Ref. 162.

The as-prepared needle-like nanotubes are cylindrical and constructed from  $\text{Co}_3\text{O}_4$  building-blocks of less than 100 nm (Figure 7). As anode for LIBs, the needle-like  $\text{Co}_3\text{O}_4$

nanotubes deliver a capacity of 918 mAh g<sup>-1</sup>. The key point in this method is that the oxygen must be sufficient to drive the reaction. Therefore, the reaction is conducted in refluxed condition to add the amount of oxygen in the solution. The samples are powder form, and can be scale-up deposition.

As for the template-assisted CP of cobalt oxides, Kim' group.<sup>116, 163</sup> and Du et al.<sup>160</sup> adopted M13 virus and carbon nanotube as the sacrificial templates for the fabrication of Co<sub>3</sub>O<sub>4</sub> nanowire and nanotubes, respectively. The reactions are illustrated as below.<sup>160</sup>



The template-synthesized Co<sub>3</sub>O<sub>4</sub> nanowire and nanotubes show high capacity of 900–200 mAh g<sup>-1</sup> and good cycling stability for LIBs. These Co<sub>3</sub>O<sub>4</sub> products are high quality, but the template-CP is tedious, requiring multiple synthetic steps, caustic chemical treatments, and long curing times. Meanwhile, the scale-up has also proven difficult and is not cost-effective due to the destruction of (relatively) expensive templates.

Meanwhile, numerous nanostructured cobalt oxides (e.g., nanowire, nanocage, nanoflake, nanorod, nanobox) are fabricated by other research groups and applied as active materials for EES by different CP methods.<sup>108, 164-173</sup> As cathode materials for supercapacitors, these CP-cobalt oxides present capacitances of 200–800 F g<sup>-1</sup>, and the film samples show better performance. Furthermore, lots of cobalt oxides/graphene or cobalt oxides/carbon composites have been reported and showed enhanced EES performance than those pure materials due to the introduction of highly conductive carbon network.<sup>161, 174-179</sup> In recent years, this modification is mainly focused on graphene based composites, and the improvement is especially reflected in the improved cycling stability.

### 3.3 Electrochemical synthesis of cobalt oxides and cobalt oxides-based composites

Most of the published papers about ED of cobalt oxides for EES are based on a cathodic ED. The cathodic ED is mainly used for the synthesis of film samples, not powder form. This cathodic ED can be performed in a standard three-electrode glass cell, with the conductive substrate as the working electrode, saturated calomel electrode (SCE) as the reference electrode and a Pt foil as the counter-electrode. In this configuration, the cobalt source must be  $\text{Co}(\text{NO}_3)_2$ , while other cobalt sources are not applicable due to the unique reaction mechanism. The ED process is expressed as follows.<sup>57, 180-182</sup>



During the annealing process:<sup>183-188</sup>

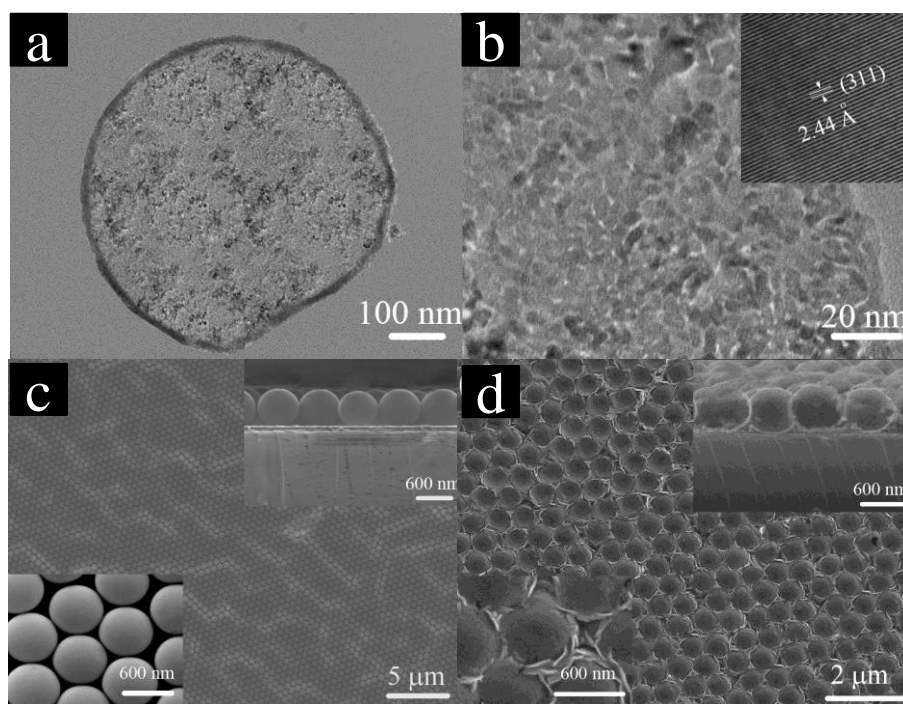
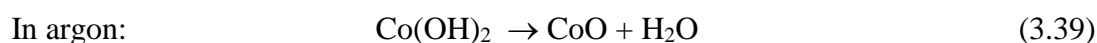
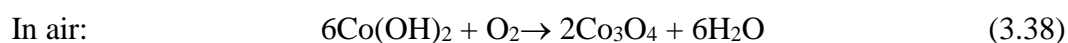


**Figure 8**  $\text{Co}_3\text{O}_4$  hollow sphere layers by electro-deposition on polystyrene sphere templates. TEM (a) and HRTEM (b) images of individual  $\text{Co}_3\text{O}_4$  hollow sphere. SEM images of (c) monolayer PS sphere template and (d)  $\text{Co}_3\text{O}_4$  monolayer hollow-sphere array. Reproduced with permission from Ref. 186.

Note that this ED process includes an electrochemical reaction and a precipitation reaction. In addition, metallic Co cannot form because the reaction potential of  $\text{Co}^{2+}/\text{Co}$  is much more negative than that of  $\text{NO}_3^-/\text{NO}_2^-$  during the electrochemical reduction process.<sup>57</sup> This ED is general, versatile and applicable to almost all conductive substrates. The thickness of the film is controlled by the reaction time and deposition current density. The as-electrodeposited precursor  $\text{Co}(\text{OH})_2$  film exhibits a porous structure consisting of randomly net-like arranged nanoflakes. This preferential growth is because that  $\text{Co}(\text{OH})_2$  crystal has a layered structure of the  $\text{CdI}_2$  type, which shows weak interaction between layers and strong binding within the layered planes, and finally forms 2D nanoflake. After heat treatment, the cobalt oxide keeps the morphology of  $\text{Co}(\text{OH})_2$  precursor and shows nanoflake arrays architecture.

The ED-cobalt oxides ( $\text{Co}_3\text{O}_4$  and  $\text{CoO}$ ) are evaluated as cathode for supercapacitor and exhibit capacitances of 200–400  $\text{F g}^{-1}$ . Our group prepared mesoporous  $\text{Co}_3\text{O}_4$  monolayer hollow-sphere array by the above ED via a polystyrene (PS) sphere colloidal monolayer template (Figure 8).<sup>186</sup> The  $\text{Co}_3\text{O}_4$  monolayer hollow-sphere array with mesoporous walls exhibits high pseudocapacitances of 358  $\text{F g}^{-1}$  at 2  $\text{A g}^{-1}$ , as well as excellent cycling stability for application as pseudocapacitors. This ED can be easily combined with other methods to fabricate cobalt oxide based composites. For example, Li et al. reported  $\text{Co}_3\text{O}_4/\text{Ni}(\text{OH})_2$  composite mesoporous nanosheet networks and showed improved capacitance of 1144  $\text{F g}^{-1}$ .<sup>189</sup> On the other hand, for LIBs application, the capacity of ED-cobalt oxides ( $\text{Co}_3\text{O}_4$  and  $\text{CoO}$ ) reaches to 500–900  $\text{mAh g}^{-1}$ .  $\text{Co}_3\text{O}_4/\text{TiO}_2$  and  $\text{Co}_3\text{O}_4/\text{graphene}$  composites are fabricated and also deliver enhanced capacities of about 1100  $\text{mAh g}^{-1}$ .<sup>182, 190</sup>

The other cathodic ED is to deposit metallic Co which is then oxidized into  $\text{CoO}_x$ :<sup>182, 191</sup>



In the metal based ED, the cobalt source is not limited to  $\text{Co}(\text{NO}_3)_2$ , other suitable sources can be  $\text{CoSO}_4$ ,  $\text{Co}(\text{NO}_3)_2$ ,  $\text{CoCl}_2$ , and  $\text{Co}(\text{CH}_3\text{COO})_2$ .

### 3.4 Sol-gel and microwave synthesis and chemical bath deposition of cobalt oxides and cobalt oxides-based composites

Sol-gel synthesis is a facile method for the fabrication of cobalt oxides and cobalt oxides-based composites. We take the work of Lin et al. for example for the illustration of reaction mechanism of cobalt oxides nanoparticles.<sup>192</sup>  $\text{CoCl}_2$ ,  $\text{NaOC}_2\text{H}_5$  and dehydrated EtOH are used as the starting materials and solvent, and the main reactions are expressed as follow.<sup>192</sup>

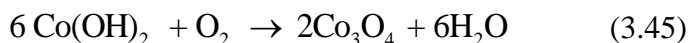


The above chemistry reactions lead to the formation of unique cobalt oxides via the hydrolysis and condensation of the cobalt alkoxide. The capacitance of the obtained cobalt oxides ( $\text{Co}_3\text{O}_4$  and  $\text{CoO}$ ) is not high, only  $\sim 175 \text{ F g}^{-1}$ . In addition, Liu et al. reported sol-gel  $\text{NiO/NiCo}_2\text{O}_4/\text{Co}_3\text{O}_4$  by using  $\text{CoCl}_2$  and propylene and exhibited a high specific capacitance of  $1717 \text{ F g}^{-1}$ .<sup>92</sup>

Several Cobalt oxides nanoparticles and composites with carbon nanotube have been reported via different sol-gel techniques for LIBs. Generally, these sol-gel methods belong to polymeric (or alkoxide) route with lots of organic solvents such as ethanol, isopropyl alcohol, cyclodextrin, citric acid, and polyvinyl pyrrolidone.<sup>193-197</sup> The specific sol-gel mechanism is different due to different solvents and starting materials. The sol-gel-cobalt oxide/CNT delivered much higher capacity than the pure ones, even two times larger.<sup>194</sup>

As for the microwave synthesis (MS) of cobalt oxides and cobalt oxides-based composites, it usually mix the cobalt sources ( $\text{CoSO}_4$ ,  $\text{Co}(\text{NO}_3)_2$ ,  $\text{CoCl}_2$ , and  $\text{Co}(\text{CH}_3\text{COO})_2$ ) and precipitants (ammonia, HMT, urea) together and then let the reactions take place under microwave oven. Cobalt oxide nanostructures (nanoparticles, nanorods, nanosheets and graphene composite) are fabricated and show a high capacity of  $931 \text{ mAh g}^{-1}$  and a capacitance of  $519 \text{ F g}^{-1}$ .<sup>198-206</sup>

In the following paragraphs, we focus on the CBD method for the synthesis of cobalt oxides and cobalt oxides-based composites. This CBD method was first proposed by Wu' group for the fabrication of free-standing  $\text{Co}_3\text{O}_4$  nanowire arrays in 2006. The specific reactions are illustrated as follows.<sup>207</sup>



The formation of the hollow CBD- $\text{Co}_3\text{O}_4$  nanowire arrays is proposed to the synergy between axial screw dislocation and Kirkendall effect.<sup>36, 56, 207</sup> These CBD- $\text{Co}_3\text{O}_4$  nanowire arrays can be formed on arbitrary substrates. It should be mentioned that oxygen is indispensable for preparing vertically aligned  $\text{Co}_3\text{O}_4$  nanowire arrays in this experiment. The oxygen in the solution helps to form  $\text{Co}(\text{OH})_2$  nanowire precursors. Without oxygen, only interconnected  $\text{Co}(\text{OH})_2$  nanowall films are formed on the substrate. The film quality is also related with the substrates position in the reaction solution. The substrates should be 2 mm away from the bottom of the vessel. Each nanowire is about 500 nm in diameter and about 15  $\mu\text{m}$  in length (Figure 9). The nanowires on Ti foil show a capacity of  $700 \text{ mAh g}^{-1}$  for LIBS,<sup>208</sup> and the sample on nickel foam exhibited a high capacitance of  $746 \text{ F g}^{-1}$ .<sup>209</sup>

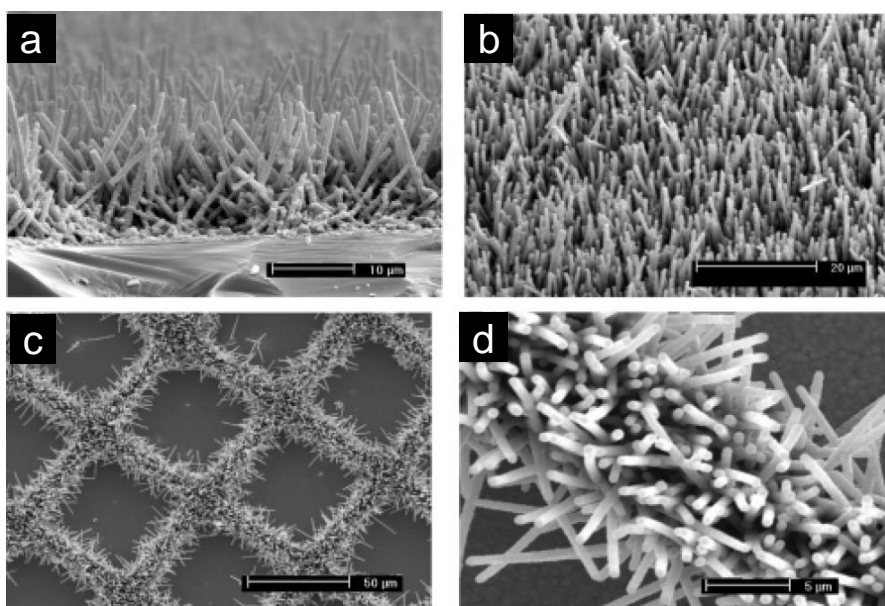


**Figure 9**  $\text{Co}_3\text{O}_4$  nanowire arrays by chemical bath deposition. Reproduced with permission from Ref. 207.

#### **4. Copper oxides and copper oxides-based composites**

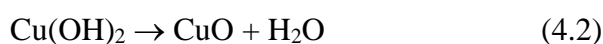
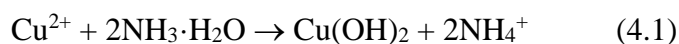
Copper oxides are one of the most attractive classes of transition metal oxides with widely applications in energy conversion devices (anode material for LIBs or cathode material for supercapacitors) and optoelectronic devices. Copper forms two oxides in accordance with its two valences: cuprous oxide ( $\text{Cu}_2\text{O}$ ) and cupric oxide ( $\text{CuO}$ ). Both are semiconductors with band gaps of 2.0 eV and 1.2 eV, respectively. Their band gaps make them good candidates for photovoltaic devices (e.g. solar cells and water splitting), catalysts, sensors and optoelectronic devices.<sup>210</sup>

$\text{Cu}_2\text{O}$  crystallizes in a simple cubic structure which can be considered as two sublattices, a facecentered cubic (fcc) sublattice of copper cations and a body-centered cubic (bcc) sublattice of oxygen anions (JCPDS 05-0667). The oxygen atoms occupy tetrahedral interstitial positions relative to the copper sublattice, so that oxygen is tetrahedrally coordinated by copper, whereas copper is linearly coordinated by two neighboring oxygens. These low coordination numbers are very unusual for metal oxides (only by two other substances,  $\text{Ag}_2\text{O}$  and  $\text{Pb}_2\text{O}$ , have the similar crystal structure). The other copper oxide,  $\text{CuO}$ , crystallizes with a monoclinic unit cell (JCPDS Card No. 41-0254), with a crystallographic point group of  $2/m$  or  $C_{2h}$ . Its space group of its unit cell is  $C_{2/c}$ . The theoretic capacity of  $\text{CuO}$  and  $\text{Cu}_2\text{O}$  as Li-ion battery anode is 670 and 374  $\text{mAh g}^{-1}$ , respectively. Various  $\text{CuO}$  and  $\text{Cu}_2\text{O}$  nanostructures have been prepared by different solution-based synthetic methods and applied as active materials for EES with enhanced electrochemical performances. We mainly focus on the mainstream solution-based synthesis methods of copper oxides for EES application.

##### **4.1 Chemical precipitation synthesis of Copper Oxide and Copper Oxides-based composites**

Among all the solution-based synthetic routes for the synthesis of copper oxides for EES, CP is the most popular solution synthesis method and the published CP papers account for ~50 % in all the published solution-based literature. Copper nitrate, copper chloride, copper sulfate and copper acetate are the most widely used copper sources. The adopted precipitants are common reagents such as ammonia and NaOH.<sup>211-214</sup> In the following section, we introduce some typical CP methods for the synthesis of hierarchical copper oxides with various morphologies.<sup>215</sup>

Previously, we fabricated various CuO nanostructures via a facile CP method by using CuSO<sub>4</sub> as the copper source and ammonia as the precipitant. The involved CP reactions can be illustrated as follows:<sup>215</sup>



The nanostructured CuO products are obtained after reacting for 12 h at 90 °C. In our case, the PH value has a great influence on the morphology of the CuO products because there is a competing reaction in the solution expressed as follows.<sup>215</sup>



Obviously, the Cu(OH)<sub>2</sub> could be dissolved due to the complex reaction for the existence of excess NH<sub>4</sub><sup>+</sup> and free NH<sub>3</sub> in the solution. There is no doubt that different pH value will lead to different concentrations of [Cu(NH<sub>3</sub>)<sub>4</sub>]<sup>2+</sup> and OH<sup>-</sup> in the solutions, and finally resulting in the formation of CuO with various morphologies such as leaf, shuttle, flower, dandelion, and caddice clew. These morphologies can be easily tailored by adjusting the pH value, indicating that the PH value is critical for the controllable growth of copper oxides in the CP method.

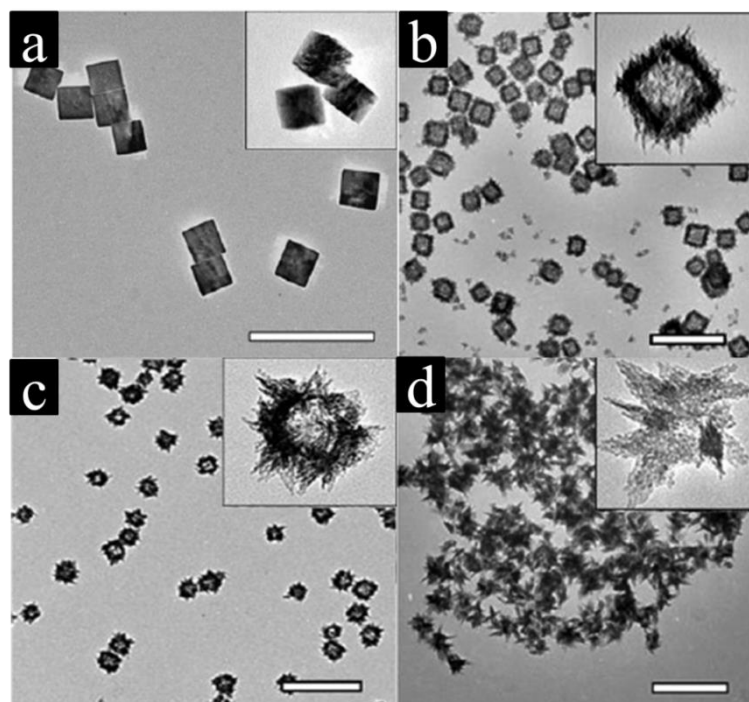
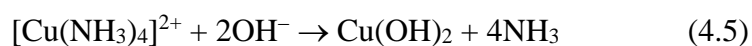
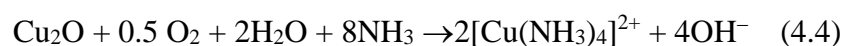


**Figure 10** Copper oxide colloidal nanoparticles by chemical precipitation method. (a) Cu<sub>2</sub>O nanocubes; (b) CuO hollow cubes; (c) hollow Spheres; (d) urchin-like particles. Reproduced with permission from Ref. 211.

The PH effect is also demonstrated in other works. Park et al. reported a similar morphology evolution by changing the PH value in the CP solution.<sup>211</sup> It is found that the Cu<sub>2</sub>O nanocubes could be converted to polycrystalline CuO hollow nanostructures through a sequential dissolution–precipitation process (Figure 10), by adding aqueous ammonia solutions in air. Increasing the pH of the solution leads to the formation of hollow cubes, hollow spheres, and urchin-like particles. The involved reactions are as follows.



The morphology of CP-copper oxides is also affected by other parameters such as the addition sequence of reagents. Tang's group found that the morphology of CP-CuO is also related with the order of addition of the reactive materials.<sup>216</sup> They reported CuO nanoribbons

and nanoflowers from the same reaction system by varying the order of addition of the reactive materials.

For LIBs application, the copper oxides (CuO and Cu<sub>2</sub>O) can reversibly react with Li ion to store electrochemical energy and the corresponding simplified reactions are expressed as follows:

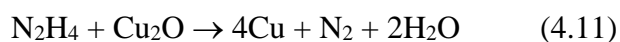
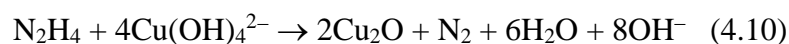
Reactions for CuO with Li ion:<sup>217, 218</sup>



As for Cu<sub>2</sub>O, only the eqn. (4.9) occurs for LIBs. It is observed that the LIBs performance of copper oxides is tightly associated with the morphology of samples. CuO samples with different morphologies show distinct electrochemical performances. Taking our work for example, compared to others CuO nanostructures, dandelion-like and caddice clew-like CuO prepared by our group exhibit reversible discharge capacities of 385 mAh g<sup>-1</sup> and 400 mAh g<sup>-1</sup> at 0.1 C, 340 mAh g<sup>-1</sup> and 374 mAh g<sup>-1</sup> at 0.5 C after 50 cycles, respectively.<sup>215</sup> The higher discharge capacities and better cycling performances are attributed to their larger surface area and porosity, leading to better contact between CuO and electrolyte and shorter diffusion length of lithium ions.

Inspired by the above works, we adopted a surfactant, cetyltrimethylammonium bromide (CTAB),<sup>219</sup> to modify the surface morphology of CuO spheres via a similar CP method. Ordered nano-needle arrays can be formed on the surface of the CuO spheres by the aid of CTAB. Each CuO sphere is about 2 μm in diameter and possesses a large number of nano-needles that are about 20–40 nm in width and more than 300 nm in length. The needle-like hierarchical structure can greatly increase the contact area between CuO and electrolyte, which provides more sites for Li<sup>+</sup> accommodation, shortens the diffusion length of Li<sup>+</sup> and enhances the reactivity of electrode reaction, especially at high rates. After 50 cycles, the reversible capacity of the prepared needle-like CuO can sustain a capacity of 441 mAh g<sup>-1</sup>.

Additionally, we used  $\text{N}_2\text{H}_4\cdot\text{H}_2\text{O}$  to replace ammonia to prepare  $\text{Cu}_2\text{O}/\text{Cu}$  core/shell nanosphere composites. The corresponding reactions are described as below.<sup>214</sup>



The core/shell  $\text{Cu}_2\text{O}/\text{Cu}$  exhibits weaker polarization, better cycling life and higher coulombic efficiency than the pure octahedral  $\text{Cu}_2\text{O}$  due to the conductivity modification by Cu. Meanwhile, in order to further improve the LIBs performance of CuO, we prepared CuO/MWCNT nanocomposite by the CP method with CTAB.<sup>218</sup> The MWCNTs are incorporated into the leaf-like CuO nanoplates and build up a network to connect the CuO nanoleaves. The as-prepared CuO/MWCNT exhibits superior reversible Li-ion storage, the capacity maintains  $627 \text{ mAh g}^{-1}$  after 50 cycles. The improved capability is ascribed to the MWCNT conductive network in the composite. Graphene/CuO composites are also realized in the above CP method and enhance electrochemical performance is proved.<sup>212, 220</sup> Similar enhancement was reported by Ko et al., who prepared CP-mesoporous CuO/CNTs with a capacity of  $600 \text{ mAh g}^{-1}$  at 5C (Figure 11).<sup>221</sup>

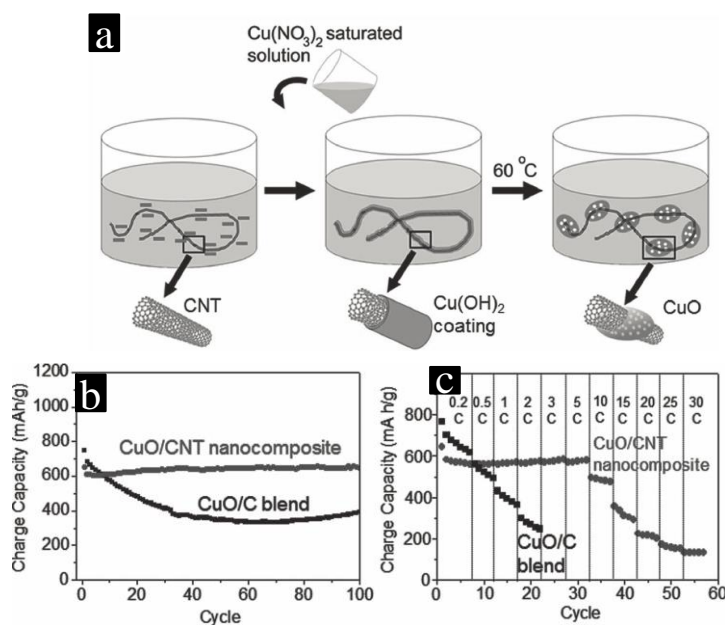
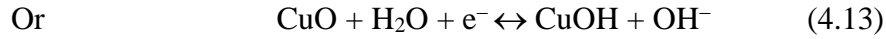
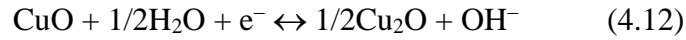


**Figure 11** (a) Preparation of the CuO/CNT composites by chemical precipitation. (b, c) cycling performances and rate capability of the CuO/CNT composites. Reproduced with permission from Ref. 221.

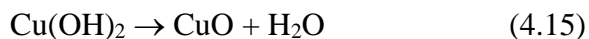
When CuO is applied for supercapacitors, the following redox reactions may be involved in the change between Cu(I) and Cu(II) species:<sup>213, 222, 223</sup>



But we have to point out that the copper oxides are not good active materials candidate for supercapacitors due to its poor electrochemical redox reactivity, and low discharge voltage in alkaline electrolyte, as compared to other metal oxides such as cobalt oxides and nickel oxides<sup>3</sup>. On the other hand, high-performance copper oxides based composites have attracted great attention, and great efforts are focusing on the modification of CP-copper oxides by introducing graphene,<sup>212, 220, 222</sup> metal<sup>214</sup>, and carbon nanotube<sup>213, 218, 221, 224</sup> by CP method to further improve the EES performance. The introduction of conductive backbone or coating can improve the conductivity of the bare copper oxides leading to enhanced electrochemical properties.

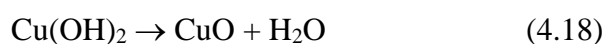
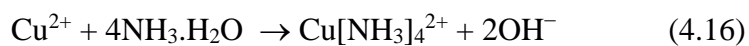
#### **4.2 Hydrothermal synthesis and solvothermal synthesis method of Copper Oxide and Copper Oxides-based composites**

HT and ST are facial solution-based ways to synthesize copper oxides. According to the published papers of HT/ST-copper oxides, one kind of copper sources is directly from the oxidization of Cu foil substrate.<sup>225-227</sup> The other kind of copper sources comes from copper salt, such as nitrate, copper sulfate and copper acetate.<sup>2, 228-230</sup> For the first kind source, we synthesized nanoflower-like CuO and CuO/Ni composite films directly on the copper foil in the mixed solution of NaOH and (NH<sub>4</sub>)<sub>2</sub>S<sub>2</sub>O<sub>8</sub>. The reactions occurred in this process can be summarized as follows:<sup>226, 231</sup>



The copper substrates are used not only as a source of copper but also as a support for the copper compound films. Note the fact that the pH value plays a vital role during the formation of the CuO film. When the reaction is carried out in acidic solution, no film is deposited on the copper surface. The copper will continuously be oxidized and dissolved, forming a blue solution. In pH range from 8 to 10, the copper foil loses its metallic luster, but there is still no perceptible solid deposit on it. When the molar ratio of  $[\text{NaOH}]/[(\text{NH}_4)_2\text{S}_2\text{O}_8]$  is  $>10$  and the concentration of NaOH is  $>1$  M, the above reaction leads to the deposition of a blue precursor film on the copper foil. At elevated temperature and high pH value, the  $\text{Cu}(\text{OH})_2$  can be easily converted into CuO. The formation of  $\text{Cu}(\text{OH})_2$  and CuO nanostructures on copper surfaces involves inorganic polymerization (polycondensation) reactions under alkaline and oxidative conditions. Particle morphology may vary depending on synthetic conditions. Even aging in aqueous solution may bring about significant dimensional, morphological, and structural changes. As a brief summary, the growth of fiber and scroll films of  $\text{Cu}(\text{OH})_2$  and copper oxides can be controlled by varying the concentration of NaOH and the reaction time if  $[\text{NaOH}]/[(\text{NH}_4)_2\text{S}_2\text{O}_8]$  is in the range of 10–40.<sup>231</sup> The obtained CuO/Ni composite film shows better LIBs performance than the pure CuO, and delivers a better capacity retention (96.3 %) than the pure CuO film (67.8 %).<sup>226</sup>

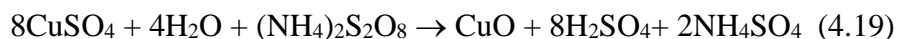
In addition, Zhang et al. synthesized gear-like CuO film directly on Cu substrate by ammonia. The formation mechanism from Cu to porous CuO nanoarrays can be interpreted as follows:<sup>227</sup>



In the above reaction process, the HT parameters (such as the reaction time, concentration of ammonia solution and reaction temperature) have great influence on the reaction rate and morphology of the final CuO film. The as-prepared gear-like CuO delivers a capacitance of

348 F g<sup>-1</sup> at 1 A g<sup>-1</sup>.<sup>227</sup> But the discharge voltage is negative (-0.3 V), indicating that the CuO is not a suitable pseudocapacitive material due to the poor working voltage window.

As for the second HT-copper oxides, Gund et al. fabricated nanosheet clusters of caddice clew, yarn ball and cabbage slash-like microstructures of copper oxides in the presence of different surfactants. The possible chemical reactions in the solution can be supposed as follows.<sup>230</sup>



These CuO microstructures show good surface properties like uniform surface morphology, good surface area and a uniform pore size distribution. The obtained CuO samples present a high specific capacitance of 535 F g<sup>-1</sup>. In addition, Gao et al. constructed complex CuO hollow micro/nanostructures with the use of CuSO<sub>4</sub>, ammonia and tyrosine.<sup>229</sup> These structures consist of CuO nanosheets, which self-organize into hollow micrometer-sized monoliths with a hierarchical architecture. The hierarchically hollow structures enhance mass transport in macroscales, promote the accessibility of the nanomaterials, and greatly facilitate dispersion, transportation, separation, and recycling of nanomaterials. The synthesized hierarchical CuO hollow micro/nanostructures exhibit a high discharge/charge capacity of 560 mAh g<sup>-1</sup> for LIBs.<sup>229</sup>

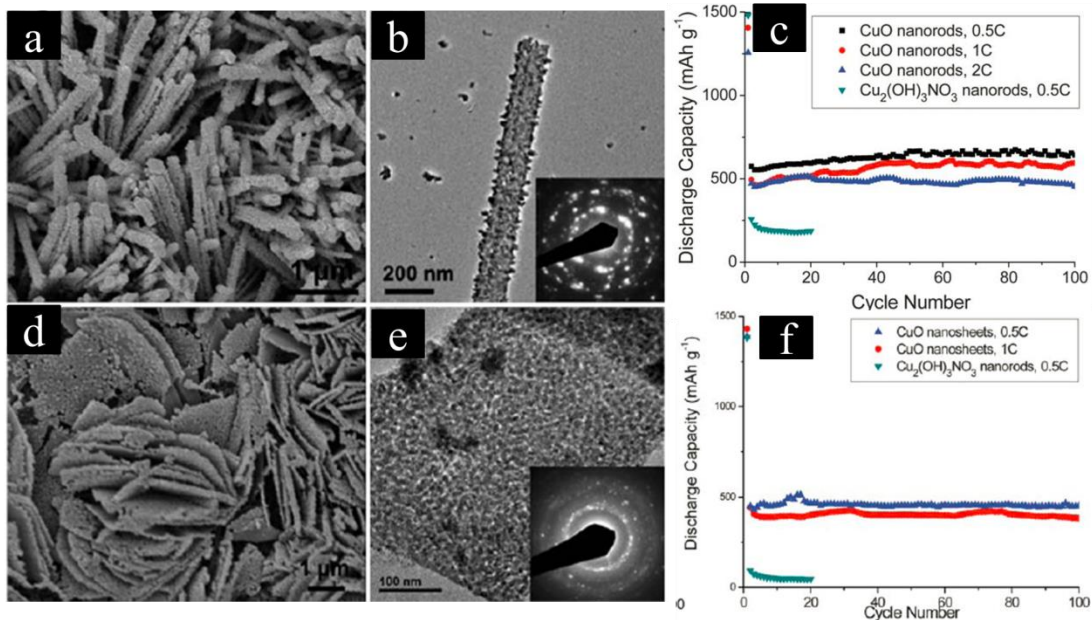
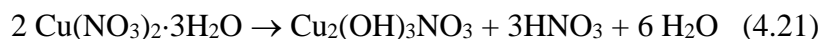
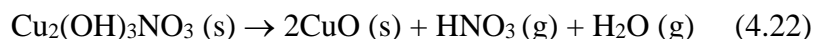


**Figure 12** (a, b) SEM-TEM images and (c) cycling stability of CuO nanorods obtained by hydrothermal synthesis; (d, e) SEM-TEM images and (f) cycling stability of CuO nanosheets obtained by hydrothermal synthesis. Reproduced with permission from Ref. 225.

In the following section, we introduce an important ST work of Lou's group for the synthesis of ST-copper oxides nanostructures including nanorodrods and nanosheets (Figure 12).<sup>225</sup> They developed a facile ST method with  $\text{Cu}(\text{NO}_3)_2$  source and 2-proponal or ethanol solvent, and the possible main reactions are expressed as follow:



During the annealing process:



The morphology of  $\text{Cu}_2(\text{OH})_3\text{NO}_3$  nanostructures can be readily controlled by using different solvents, in which precursor supersaturation for nucleation and crystal growth is determined by solvent polarity and solubility. In the above method, notice that the precise control of precursor concentration and supersaturation plays a prime role in the synthesis of  $\text{Cu}_2(\text{OH})_3\text{NO}_3$  nanostructures and the degree of supersaturation directly determines the crystal growth mode. Generally both the concentration and supersaturation of the precursor for the formation of low-dimensional  $\text{Cu}_2(\text{OH})_3\text{NO}_3$  nanostructures must be kept at a relatively low level to avoid overwhelming isotropic growth or even homogeneous nucleation

in the solution. The above chemistry reactions lead to the formation of unique copper oxides, nanorods (in 2-propanol) and nanosheets (in ethanol). The unique nanostructural copper oxide films show excellent electrochemical performance as demonstrated by high capacities of 450–650 mAh g<sup>-1</sup> at 0.5–2 C and almost 100% capacity retention over 100 cycles after the second cycle.<sup>225</sup>

### 4.3 Electrochemical synthesis of Copper Oxide and Copper Oxides-based composites

Most of the published papers on ED of copper oxides for EES are based on a cathodic ED. Similar to the ED used for other metal oxides, the cathodic ED is mainly used for the synthesis of copper oxide film samples, not powder form. This cathodic ED can be conducted in either or standard three-electrode or two-electrode glass cell. Copper sulfate or copper acetate is used as the copper source and the final ED-copper oxide is Cu<sub>2</sub>O, not CuO. Cu<sub>2</sub>O is electrodeposited by reactions given as follows:<sup>214, 232</sup>



The electrolyte of the above ED reaction is alkaline. If the PH is low, the competing reaction of Cu<sup>2+</sup> to metallic copper will occur:<sup>233</sup>

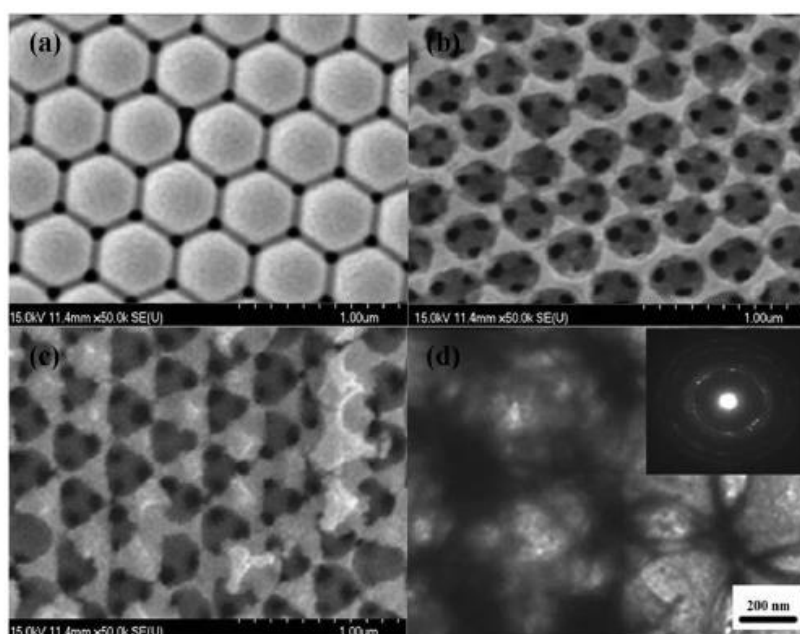


**Figure 13** 3D porous composite nanostructures obtained by electrode-deposition on polystyrene opals template. (a) Polystyrene opals template, (b) Ni inverse opals structure after

first deposition, (c) Cu<sub>2</sub>O/Ni structure after second deposition, and (d) TEM image of the Cu<sub>2</sub>O/Ni structure. Reproduced with permission from Ref. 236.

Our group reported highly ordered porous Cu<sub>2</sub>O film via the above ED on copper foil through a self-assembled polystyrene sphere template. Compared with the dense Cu<sub>2</sub>O film, the ordered porous Cu<sub>2</sub>O film exhibits an improved electrochemical cycling stability. The capacity of the porous Cu<sub>2</sub>O film can maintain a capacity 336 mAh g<sup>-1</sup> and 213 mAh g<sup>-1</sup> after 50 cycles at the rate of 0.1 C and 5 C, respectively.<sup>234</sup> Flexible ED-CNTs/Cu<sub>2</sub>O hybrid electrodes synthesized by Ajayan et al. exhibit superior electrochemical performance compared with pure CNTs.<sup>235</sup> Deng et al. synthesized the three-dimensionally ordered macroporous Cu<sub>2</sub>O/Ni inverse opal electrodes for electrochemical supercapacitors by the similar method. The calculated capacitance of the as-prepared 3D Cu<sub>2</sub>O/Ni electrode is 502 F g<sup>-1</sup> (Figure 13).<sup>236</sup> The improved electrochemical performances due to their porous structure film, which provides not only the direct contact of active material/current collector but also the sufficient contact of active material/electrolyte. Enhanced EES performances are also demonstrated in some other ED-Cu<sub>2</sub>O/CNT and Cu<sub>2</sub>O/Ni composites systems.<sup>235, 236</sup>

## 5. MnO<sub>2</sub> and MnO<sub>2</sub>-based composites

Though manganese oxides have several different forms and phases (such as MnO<sub>2</sub>, Mn<sub>2</sub>O<sub>3</sub>, MnO and Mn<sub>3</sub>O<sub>4</sub>), MnO<sub>2</sub> is the one of the most fascinating manganese oxides for EES applications due to its high capacity/capacitance, earth abundance, low cost and environmental friendliness. It is well known that MnO<sub>2</sub> can exist in different structural forms (e.g.,  $\alpha$  (JCPDS 44-0141),  $\beta$  (JCPDS 24-0735),  $\gamma$  (JCPDS 14-0644),  $\delta$  (JCPDS 80-1098),  $\epsilon$  (JCPDS 30-0820),  $\lambda$  (JCPDS 44-0992) type), when the basic structural unit ([MnO<sub>6</sub>] octahedron) is linked in different ways. The difference in the above polymorphs lies in the arrangement of the Mn<sup>4+</sup> within the octahedral sites. Based on the different [MnO<sub>6</sub>] links, MnO<sub>2</sub> can be divided into three categories: the chain-like tunnel structure such as  $\alpha$ ,  $\beta$  and  $\gamma$

type; the sheet or layered structure such as  $\delta$ -MnO<sub>2</sub>, and the 3D structure such as  $\lambda$ -MnO<sub>2</sub>. MnO<sub>2</sub> usually crystallizes in the rutile crystal structure with three-coordinate oxide and octahedral metal centres. The band gap of MnO<sub>2</sub> is 0.26–0.7 eV depending on different polymorphs ( $\beta$ -MnO<sub>2</sub> is ~0.26 eV and  $\gamma$ -MnO<sub>2</sub> is ~0.6 eV).

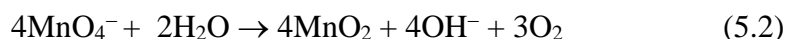
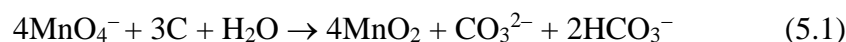
MnO<sub>2</sub> have been extensively studied as active materials in EES systems since last century. The widely known example is the electrolytic manganese dioxides (EMD), which are the current commercial cathode materials for high-energy alkaline primary battery, which is not the focus of this review and will not be discussed here. Meanwhile, in recent years, great efforts are devoted to fabricating MnO<sub>2</sub>-based high-performance EES devices such as LIBs and supercapacitors. In particular, the MnO<sub>2</sub> is considered as the most promising metal oxide electrode materials for supercapacitors owing to its high working voltage (near 2 V in aqueous system), low cost, high capacitance (theoretical capacitance of ~1370 F g<sup>-1</sup>) and easy-processing.<sup>237</sup> So far, the published papers about MnO<sub>2</sub> and MnO<sub>2</sub>-based composites for supercapacitors are more than 350. This number even surpasses cobalt oxides and nickel oxides in terms of their combined supercapacitor research. The electrochemical properties of MnO<sub>2</sub> are significantly affected by their phases and morphologies. A great many MnO<sub>2</sub>-based nanostructures have been reported and fabricated by different solution-based synthesis methods, and enhanced electrochemical performances have been demonstrated in these systems with promising practical applications. In this section, we will introduce some typical solution-based synthetic methods (hydrothermal synthesis, chemical precipitation and electro-deposition methods) for MnO<sub>2</sub> and MnO<sub>2</sub>-based composites and focus on the specific reaction mechanisms as well as their EES performances.

## 5.1 Hydrothermal synthesis of MnO<sub>2</sub> and MnO<sub>2</sub>-based composites

HT is one of the three most popular solution-based methods (hydrothermal synthesis, chemical precipitation and electro-deposition methods) for the synthesis of MnO<sub>2</sub> and MnO<sub>2</sub>-based composites for EES. According to the reaction mechanisms and reagents, basically, there are about three kinds of HT methods for the fabrication of MnO<sub>2</sub> and MnO<sub>2</sub>-based composites for EES. Herein, we introduce these three HT methods of MnO<sub>2</sub> in detail in the following paragraphs.

### **5.1.1 HT reactions with oxidant (KMnO<sub>4</sub>) and reducing agent (such as C, Cu and ethanol)**

The first kind of HT method of MnO<sub>2</sub> involves the chemical reactions between oxidant (KMnO<sub>4</sub>) and reducing agent (such as C, Cu, ethanol and polyethylene glycol).<sup>6, 238-246</sup> Previously, our group adopted this facile HT method to fabricate self-supported Co<sub>3</sub>O<sub>4</sub>/MnO<sub>2</sub> core/shell nanowire arrays on Ti foil.<sup>98</sup> In our case, we used the amorphous carbon as the reducing agent and the reactions are expressed as follows.<sup>241, 242, 244</sup>



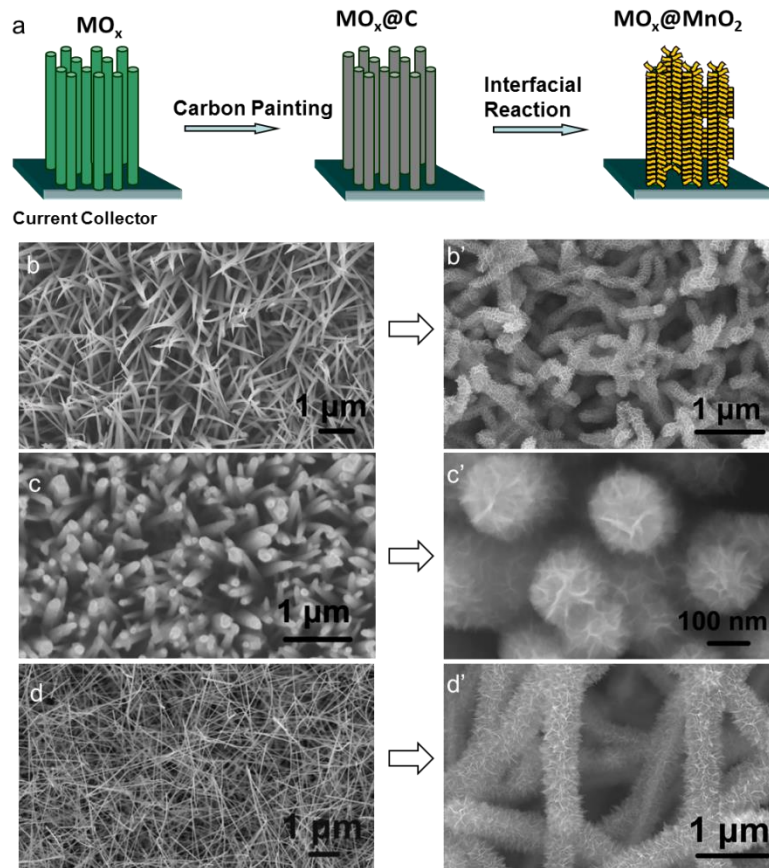
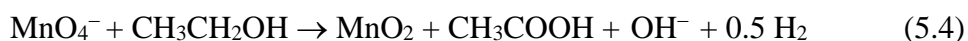
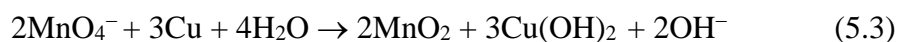


**Figure 14.** MnO<sub>2</sub> nanosheets by hydrothermal synthesis via the chemical reaction between KMnO<sub>4</sub> with carbon. (a) Schematics of the fabrication procedure for the MnO<sub>2</sub> nanosheet branches on various metal oxide core nanowires. (b) Co<sub>3</sub>O<sub>4</sub> nanowire array, (c) ZnO nanowires, and (d) SnO<sub>2</sub> nanowires. SEM images in the right column show the corresponding nanowire arrays with MnO<sub>2</sub> nanomembrane branches. Reproduced with permission from Ref. 98.

For the above reactions, when the KMnO<sub>4</sub> solution is mixed with the carbon source at room temperature before the hydrothermal processing, the nanocrystalline MnO<sub>2</sub> will be formed on the surface of the carbon source due to the slow redox process according to eqn. (5.1).<sup>241</sup> When the solution is further treated in the hydrothermal reaction, the nanoflaky MnO<sub>2</sub> grows from the preformed nanocrystalline due to the decomposition of KMnO<sub>4</sub> in water according to eqn. (5.2), where MnO<sub>2</sub> nanoflakes will be formed. Except for the amorphous carbon, the carbon source can also be CNT, graphene, carbon cloth and so on. The reaction in eqn. (5.1) will promote the reaction in eqn. (5.2) to take place. This main problem in this HT method is that it will consume the carbon source and hard to precisely

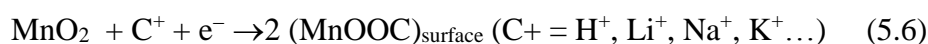
control the morphology of MnO<sub>2</sub>/carbon. In view of these characteristics, MnO<sub>2</sub> hollow nanostructures can be formed when the HT reaction occurs deeply and sacrifice the carbon template. The key point in this HT is to use a reducing agent to trigger the reaction. If the reducing agent is Cu or ethanol, the reactions in eqn. (5.1) will be different as shown as below.<sup>238, 246</sup>



The obtained HT-MnO<sub>2</sub> shows nanoflake structure. In our experiment, the MnO<sub>2</sub> nanoflake are well decorated on the surface of Co<sub>3</sub>O<sub>4</sub> nanowire core forming core/shell nanowire arrays (Figure 14), which exhibit excellent supercapacitor performance with high capacitance of 480 F g<sup>-1</sup> at 2.67 A g<sup>-1</sup>, good cycle life with 2.7 % capacitance loss after 5000 cycles and remarkable rate capability.<sup>98</sup> It is reported that the pseudocapacitive (Faradic) reactions occurring on the surface and in the bulk of the electrode are the major charge storage mechanisms for manganese oxides. The surface Faradaic reaction involves the surface adsorption of electrolyte cations on the manganese oxide, illustrated as follows.<sup>98, 237, 242</sup>



The bulk Faradaic reaction relies on the intercalation or deintercalation of electrolyte cations in the bulk of the manganese oxide:<sup>98, 237</sup>



In our work, the redox process is mainly governed by the insertion and deinsertion of Li<sup>+</sup> and from the electrolyte into the porous nanostructured MnO<sub>2</sub> matrix. In addition, hierarchical TiO<sub>2</sub> nanobelts@MnO<sub>2</sub> ultrathin nanoflakes core/shell arrays were reported by the same HT method and showed a specific capacitance of 557 F g<sup>-1</sup> as cathode for supercapacitors.<sup>240</sup> Some other MnO<sub>2</sub> nanostructures (such as nanosphere, hollow sphere, and tubular nanostructure) have also been fabricated by this HT method and applied as electrode materials for EES.<sup>238, 242-244</sup> However, the above as-prepare pure MnO<sub>2</sub> nanostructures show a

capacitance lower than 400 F g<sup>-1</sup> due to the poor conductivity of MnO<sub>2</sub>.<sup>242-244, 246</sup> To effectively utilize MnO<sub>2</sub> materials, MnO<sub>2</sub> composites with carbon (e.g., MnO<sub>2</sub>/C nanosphere, MnO<sub>2</sub>/CNT, MnO<sub>2</sub>/Graphene) are constructed and exhibit improved electrochemical performances than the pure counterparts.<sup>241, 245, 247</sup> On the other hand, the MnO<sub>2</sub> is a potential active material (either cathode or anode) for LIBs. The theoretical capacity of MnO<sub>2</sub> as LIBs anode is ~1232 mAh g<sup>-1</sup>, and the reactions are described as follows.<sup>241, 245, 248</sup>



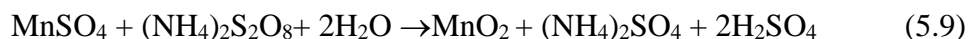
As anode for LIBs, the carbon/MnO<sub>2</sub> nano-urchins exhibit a reversible capacity of 628 mAh g<sup>-1</sup>.<sup>245</sup> The nanoflakey MnO<sub>2</sub>/CNT nanocomposite electrode exhibits a large reversible capacity of 801 mA h g<sup>-1</sup>.<sup>241</sup> Moreover, Gu et al. prepared branched nanorods of MnO<sub>2</sub>/Fe<sub>2</sub>O<sub>3</sub> by the above HT method and presented a reversible specific capacity of 1028 mAh g<sup>-1</sup> at 1000 mA g<sup>-1</sup> up to 200 cycles, much higher than the MnO<sub>2</sub> alone.<sup>6</sup> The improved electrochemical performance is due to the synergistic effect such as enhanced stability, better conductivity and strain accommodation.

### **5.1.2 HT reactions with high-valence oxidant (KMnO<sub>4</sub> or persulfate) and low-valence manganese sources such as MnSO<sub>4</sub> or MnCl<sub>2</sub>**

The reaction between KMnO<sub>4</sub> and MnSO<sub>4</sub> is given as below.<sup>249-252</sup>



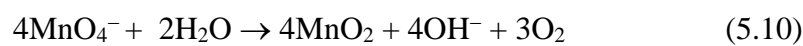
It is believed that this HT method is especially suitable for the preparation of composite materials with carbon because the first HT method needs to consume reducing agent such as carbon source and this will not happen here. During the reaction, the MnSO<sub>4</sub> will preferentially react with KMnO<sub>4</sub> to form nanoflake MnO<sub>2</sub>. Of course, the concentration ratio between MnSO<sub>4</sub> and KMnO<sub>4</sub> should be controlled. Hence, the carbon backbone is always kept and served as a support for the deposition of MnO<sub>2</sub>. Moreover, the morphology of the MnO<sub>2</sub> can be tuned by the hydrothermal time. When the oxidant is persulfate such as K<sub>2</sub>S<sub>2</sub>O<sub>8</sub> or (NH<sub>4</sub>)<sub>2</sub>S<sub>2</sub>O<sub>8</sub>, the specific reactions are shown as below.<sup>253-256</sup>



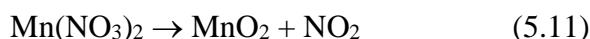
Lots of  $\text{MnO}_2$  nanostructures including nanoflakes, nanorods, nanospheres have been obtained by this HT reaction and showed a capacitance of 168–455  $\text{F g}^{-1}$  for supercapacitor application.<sup>249, 250, 256-259</sup> Meanwhile, other composites (e.g.,  $\text{MnO}_2/\text{graphene}$ ,  $\text{MnO}_2/\text{CNT}$ ,  $\text{MnO}_2/\text{ZnO}$ ,  $\text{MnO}_2/\text{PPy}$ ,  $\text{MnO}_2/\text{PANI}$ ) are reported and present enhanced capacitances of 516–873  $\text{F g}^{-1}$  attributed to the combination with conductive layers.<sup>251-253, 260, 261</sup> It should be mentioned that this HT reaction will not do harm to other conductive scaffold and favourable for construction of  $\text{MnO}_2$  based composite materials. Furthermore, this HT is applicable to co-synthesize conducting polymers with  $\text{MnO}_2$  because the  $\text{KMnO}_4$  or persulfate is also common oxidant for the chemical polymerization of conducting polymers.

### 5.1.3 Direct hydrolysis of $\text{KMnO}_4$ or $\text{Mn}(\text{NO}_3)_2$

The direct hydrolysis of  $\text{KMnO}_4$  is the most facile and popular HT method for the preparation of  $\text{MnO}_2$  and  $\text{MnO}_2$ -based composites illustrated as follows.<sup>262, 263</sup>



The above HT reaction is very easy to control and process. It only needs to control the concentration of  $\text{KMnO}_4$  and HT time. The problem in this HT is that the  $\text{KMnO}_4$  may also react with other active materials leading to the formation of side products. In addition to the normal nanoflakes or nanosheets,<sup>247, 264</sup> by the aid of some templates or surfactants,  $\text{MnO}_2$  nanospheres, nanourchins or nanorods and composites with, metal, carbon, conducting polymers, and metal oxides, are also fabricated and applied for LIBs and supercapacitors.<sup>146, 227, 262, 264-271</sup> The as-prepared  $\text{MnO}_2$  nanostructures show a capacitance range of 200–528  $\text{F g}^{-1}$  and a capacity range of 213–983  $\text{mAh g}^{-1}$ . The electrochemical performance of composites is superior to the bare counterparts. On the other hand, the  $\text{Mn}(\text{NO}_3)_2$  is another manganese source for the direct hydrolysis to prepare  $\text{MnO}_2$  nanorods (Figure 15), expressed as below.<sup>272</sup>



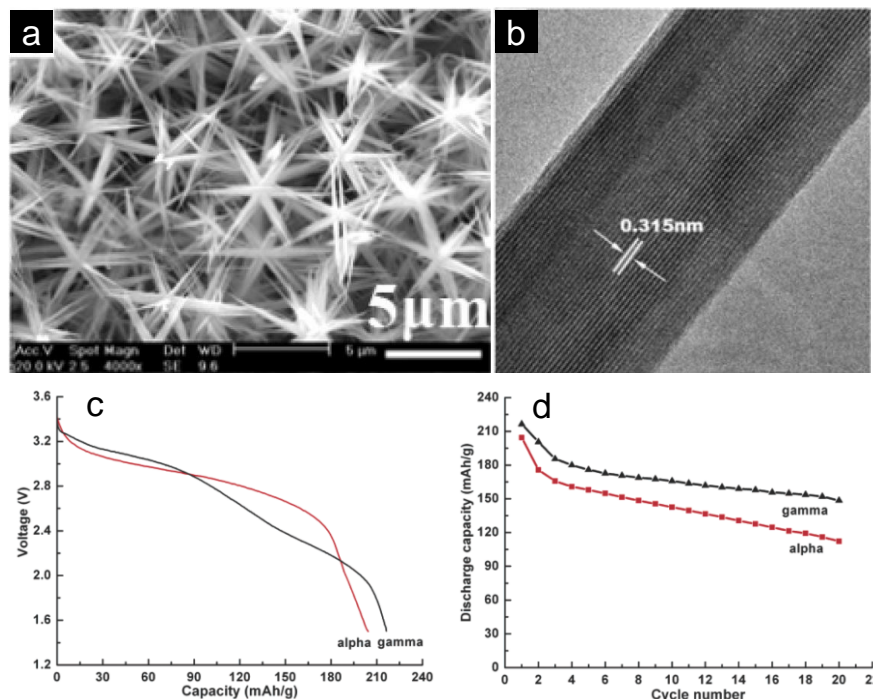


**Figure 15** (a, b) SEM and TEM images of MnO<sub>2</sub> nanorods hydrothermal synthesized from Mn(NO<sub>3</sub>)<sub>2</sub> precursor. (c) Discharge curves and (d) first 20 cycles of  $\alpha$ - and  $\gamma$ -MnO<sub>2</sub> phase nanostructures in the laboratory Li-MnO<sub>2</sub> cells. Reproduced with permission from Ref. 272.

But this method is not usual, and the side product NO<sub>2</sub> is toxic. The obtained MnO<sub>2</sub> nanorods are applied as the cathode for LIBs. The  $\alpha$ -MnO<sub>2</sub> nanostructures shows a flat plateau between 3.0 and 2.5 V, and the discharge capacity is 204 mAh g<sup>-1</sup> to an end voltage of 1.5 V. For  $\gamma$ -MnO<sub>2</sub> nanorods, the open-circuit potential was 3.43 V, and the discharge capacity exceeds 210 mAh g<sup>-1</sup> indicating that a desirable amount of lithium inserted (in Li<sub>x</sub>MnO<sub>2</sub>,  $x \approx 0.70$ ).<sup>272</sup> The reactions are expressed as follows.<sup>272</sup>



## 5.2 Chemical deposition of MnO<sub>2</sub> and MnO<sub>2</sub>-based composites

To date, the CP-MnO<sub>2</sub> papers account for ~37 % in all the published literature about solution-based synthesis of MnO<sub>2</sub> for EES. The reactions in CP are almost the same as those of HT, but the CP is not conducted in sealed vessel, and usually does not need high reaction temperature. The manganese sources are KMnO<sub>4</sub>, MnCl<sub>2</sub>, MnSO<sub>4</sub>, Mn(NO<sub>3</sub>)<sub>2</sub> and

Mn(CH<sub>3</sub>COO)<sub>2</sub>. Similar to HT, the CP-MnO<sub>2</sub> can also be classified into three kinds according to different reaction mechanisms. We will introduce different CP types of MnO<sub>2</sub> by taking some typical examples in the following and describe the corresponding mechanisms as well as EES performances.

### 5.2.1 CP reactions between oxidant (KMnO<sub>4</sub>) and reducing agent (such as C, Cu, N<sub>2</sub>H<sub>4</sub> and ethanol)

Lang et al. reported a facile CP method for the fabrication of nanoporous gold/MnO<sub>2</sub> hybrid electrodes by using KMnO<sub>4</sub> and N<sub>2</sub>H<sub>4</sub> in alkaline electrolyte (Figure 16).<sup>273</sup> But they used the N<sub>2</sub>H<sub>4</sub> gas as the reducing agent. The N<sub>2</sub>H<sub>4</sub> gas is very active and the possible reactions are as follows.<sup>273</sup>

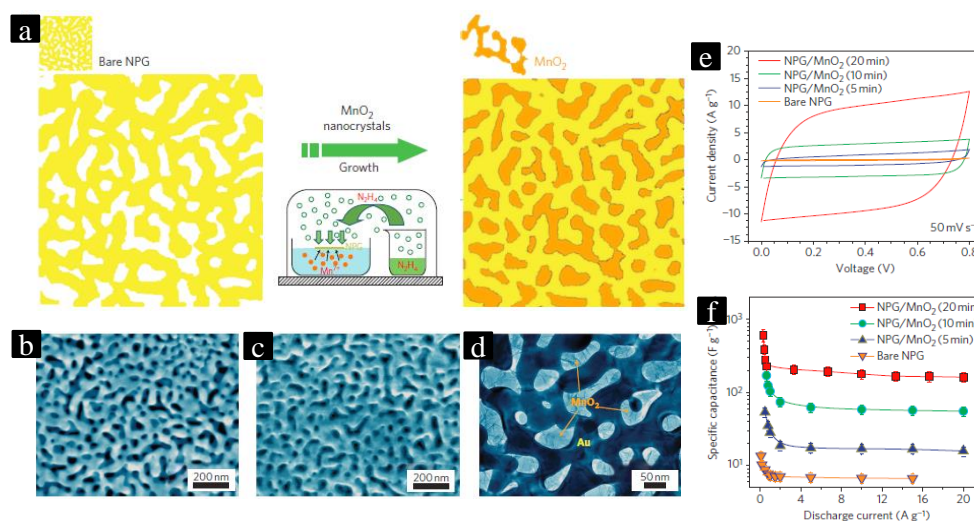
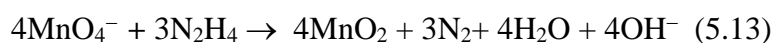


**Figure 16** (a) Schematics of the nanoporous Au/MnO<sub>2</sub> hybrid materials by chemical precipitation of MnO<sub>2</sub> on surfaces of porous Au template. (b-d) SEM images, (e) CV curves and (f) rate capability of nanoporous Au/MnO<sub>2</sub> hybrid materials. Reproduced with permission from Ref. 273.

The as-fabricated nanoporous gold/MnO<sub>2</sub> hybrid electrodes show nanoporous structure and enhanced conductivity, resulting in a specific capacitance of the constituent MnO<sub>2</sub> (~1145 F g<sup>-1</sup>). Although MnO<sub>2</sub> has intrinsically low conductivity that limits its charge/discharge rate, the charge-transfer-reaction pseudocapacitance of the nanoporous gold/MnO<sub>2</sub> electrode can be enhanced by the fast ion diffusion in the three-dimensional nanoporous architecture and

highly electrical conductivity of the nanoporous gold skeleton as well as the epitaxial metal/oxide interfaces.

In the meantime, several  $\text{MnO}_2$  nanostructures (nanorods and nanosheets) and composites (e.g.,  $\text{MnO}_2/\text{CNT}$ ,  $\text{PANI}/\text{C}/\text{MnO}_2$ ,  $\text{MnO}_2/\text{graphene}$ ,  $\text{TiO}_2/\text{C}/\text{MnO}_2$ ) have been reported via this CP reactions between carbon sources with  $\text{KMnO}_4$  and applied for EES.<sup>274-285</sup> The involved reactions are the same as that of the eqn. (5.1) above. Though the CP- $\text{MnO}_2$  has the same reaction mechanism with that of HT, the CP reaction is conducted under mild condition and lower temperature, and the samples are all powder forms, not film. In other words, the CP is suitable for large-scale fabrication of  $\text{MnO}_2$  and composites. Notice that the reactions between carbon sources and  $\text{KMnO}_4$  are easier to control than that proposed by Lang et al. using  $\text{N}_2\text{H}_4$  gas,<sup>273</sup> and more environmental friendliness. Additionally,  $\text{Cu}/\text{MnO}_2$  superstructures and  $\text{MnO}_2$  nanosheet/graphene flake composites are prepared by using Cu or ethanol as the reducing agent according to similar reaction of eqn. (5.3) and (5.4).<sup>286, 287</sup> Comparing the bare  $\text{MnO}_2$  and their composites, it is found that the  $\text{MnO}_2$ -based composites show much higher capacitance and better cycling stability and high-rate capability due to the ion/electron transfer modification by introduction of conductive layers including graphene, CNT and conducting polymers. The  $\text{PANI}/\text{C}/\text{MnO}_2$  shows a capacitance of  $695 \text{ F g}^{-1}$ , about two times larger than the pure  $\text{MnO}_2$ .<sup>275</sup> As cathode for LIBs, the  $\text{MnO}_2$  on the GS affords an unprecedented high capacity of  $230 \text{ mAh g}^{-1}$  after 150 cycles,  $\sim 30 \%$  higher than the bare  $\text{MnO}_2$ .<sup>284</sup>

### **5.2.2 CP reactions between oxidant ( $\text{KMnO}_4$ , persulfate or $\text{H}_2\text{O}_2$ ) and manganese sources such as $\text{MnSO}_4$ , $\text{MnCl}_2$ or $\text{Mn}(\text{CH}_3\text{COO})_2$ .**

The CP- $\text{MnO}_2$  prepared by reactions between ( $\text{KMnO}_4$ , persulfate or  $\text{H}_2\text{O}_2$ ) and manganese sources (such as  $\text{MnSO}_4$ ,  $\text{MnCl}_2$  or  $\text{Mn}(\text{CH}_3\text{COO})_2$ ) is quite popular. This reaction is easy to control and more suitable for preparation of composites without sacrificing the needed conductive backbone. Peng et al. reported ultrathin 2D  $\text{MnO}_2/\text{graphene}$  hybrid nanostructures

via the above method by using  $\text{H}_2\text{O}_2$  and  $\text{MnCl}_2$  as the starting materials.<sup>288</sup> The CP reactions are given as below.<sup>288</sup>



The whole reaction is very fast and exothermic. The  $\text{MnO}_2$  is homogeneously grown on the graphene nanosheets and the obtained  $\text{MnO}_2$ /graphene nanosheets based planar supercapacitors demonstrate the impressive electrochemical performance with a high specific capacitance of  $267 \text{ F g}^{-1}$ , and excellent rate capability and cycling performance with capacitance retention of 92 % after 7000 charge/discharge cycles.<sup>288</sup>

The most widely used oxidant and reducing agent is  $\text{KMnO}_4$  and  $\text{MnSO}_4$ , respectively. The involved reaction is the same as that shown in eqn. (5.8). Manganese source is not limited in  $\text{MnSO}_4$ , can also be  $\text{MnCl}_2$  or  $\text{Mn}(\text{CH}_3\text{COO})_2$ . The other common oxidant is  $\text{K}_2\text{S}_2\text{O}_8$  or  $(\text{NH}_4)_2\text{S}_2\text{O}_8$ , like the reaction in eqn. (5.9). Based on these reactions, lots of  $\text{MnO}_2$  nanostructures (e.g., nanorods, mesoporous  $\text{MnO}_2$ , clew-like, hollow urchin) and  $\text{MnO}_2$ -based composites (such as  $\text{MnO}_2$  nanospheres/C/PEDOT-PST,  $\text{MnO}_2$ /graphene,  $\text{MnO}_2$ /CNT,  $\text{MnO}_2$ /graphene/CNT,  $\text{MnO}_2$ /RGO,  $\text{Co}_3\text{O}_4$ /Pt/ $\text{MnO}_2$ ,  $\text{SnO}_2$ / $\text{MnO}_2$ , PANI/ $\text{MnO}_2$ ) have been reported and used as active materials for EES.<sup>121, 289-304</sup> It is observed that this CP- $\text{MnO}_2$  is help for fabrication of composites, and the CP process is not complex. When they are applied for EES, like other modification research, the composites with conductive backbone show much higher capacitance and capacity, and better rate capability and cycling performances.

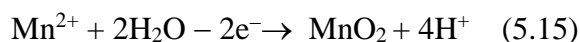
### 5.2.3 CP reaction by direct hydrolysis of $\text{KMnO}_4$

The direct hydrolysis of  $\text{KMnO}_4$  is another popular CP for the synthesis of  $\text{MnO}_2$  electrode materials for EES. The reaction is shown in eqn. (5.10). Bao et al. prepared flexible  $\text{Zn}_2\text{SnO}_4$ / $\text{MnO}_2$  core/shell hybrid composites by the direct hydrolysis of  $\text{KMnO}_4$ .<sup>305</sup> The  $\text{MnO}_2$  resulting from hydrolysis of  $\text{KMnO}_4$  is uniformly coated on the surface of  $\text{Zn}_2\text{SnO}_4$  nanorod with a diameter of  $\sim 80 \text{ nm}$ . This CP- $\text{MnO}_2$  shows a specific capacitance of  $642 \text{ F/g}$  at a current density of  $1 \text{ A g}^{-1}$  in  $1 \text{ M Na}_2\text{SO}$  aqueous solution as cathode for supercapacitors.

This CP-MnO<sub>2</sub> is also widely adopted to prepared enhanced porous-structured MnO<sub>2</sub> composites for EES applications and improved electrochemical performances have been demonstrated in these systems such as MnO<sub>2</sub> nanowires/CoAl, Fe<sub>2</sub>O<sub>3</sub>/MnO<sub>2</sub> core/shell nanowire, MnO<sub>2</sub>/carbon, MnO<sub>2</sub>/polypyrrole, graphene/MnO<sub>2</sub>, MnO<sub>2</sub>/PEDOT/graphene, and graphene/ MnO<sub>2</sub>.<sup>262, 263, 306-314</sup> For this CP method, one point to be noticed is the concentration of KMnO<sub>4</sub>, which will affect the morphology of the final samples.

### 5.3 Electrochemical synthesis of MnO<sub>2</sub> and MnO<sub>2</sub>-based composites

Electro-deposition is always used to prepare MnO<sub>2</sub> film which can be easily combined with other conductive substrates or scaffold to form high-performance composites for EES. Up to now, most of the ED-MnO<sub>2</sub> nanostructures and composites are prepared by anodic ED with Mn(CH<sub>3</sub>COO)<sub>2</sub> or MnSO<sub>4</sub> as the starting material. The support electrolyte is Na<sub>2</sub>SO<sub>4</sub>. The anodic ED reactions are proposed as follows.<sup>315-317</sup>



The ED can be conducted in either two-electrode or three-electrode system. The substrates have a significant effect in this anodic ED. If the substrate is nickel foam or copper, the metal will dissolve at high potential. This phenomenon will not happen in carbon-based substrates.

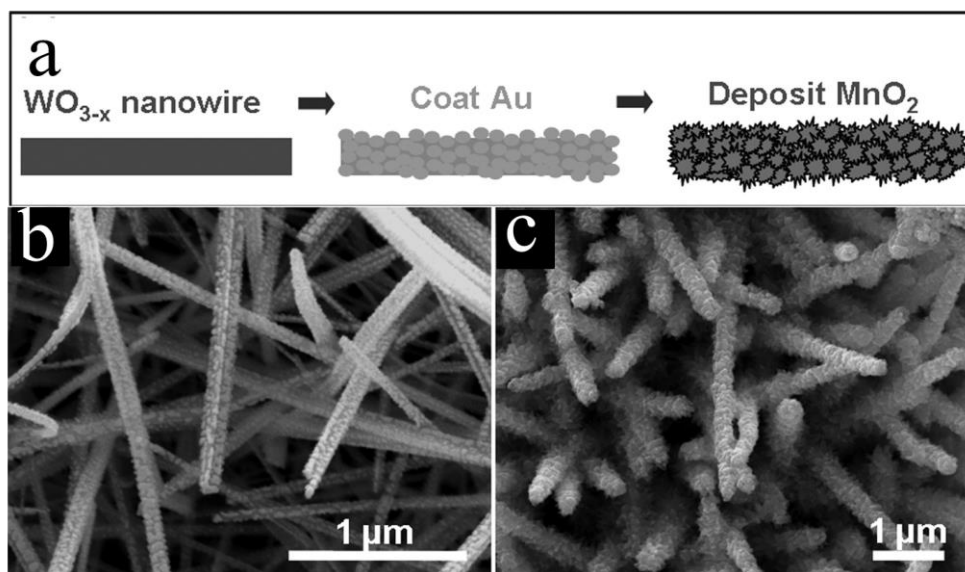
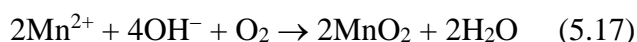


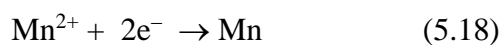
**Figure 17** (a) Schematics of the fabrication process for  $\text{WO}_{3-x}@\text{Au}@\text{MnO}_2$  composite nanowires. The  $\text{MnO}_2$  outer shell is by electro-deposition. SEM images of (b)  $\text{WO}_{3-x}@\text{Au}$  nanowires, and (c)  $\text{WO}_{3-x}@\text{Au}@\text{MnO}_2$  nanowires on carbon cloth. Reproduced with permission from Ref. 316.

Previously, Lu et al. reported a  $\text{WO}_{3-x}@\text{Au}@\text{MnO}_2$  core/shell nanowires on carbon cloth by the above anodic ED and showed a capacitance of  $588 \text{ F g}^{-1}$  (Figure 17).<sup>316</sup> The ED- $\text{MnO}_2$  layer exhibits highly electrochemical reactivity leading to enhanced supercapacitor performance for the composite nanowires. Based on the anodic ED method, numerous  $\text{MnO}_2$  nanostructured electrodes (e.g., nanorod, nanosheet, nanowire, nanotube) and composites ( $\text{MnO}_2/\text{Pt}$ ,  $\text{MnO}_2/\text{Metal}$ ,  $\text{MnO}_2/\text{PEDOT-PST}$ ,  $\text{MnO}_2$  nanosheet,  $\text{MnO}_2$  nanorod,  $\text{MnO}_2/\text{Au}$ ,  $\text{MnO}_2/\text{PEDOT}$ ,  $\text{MnO}_2/\text{CNT}$ ,  $\text{MnO}_2$  nanopillars,  $\text{MnO}_2/\text{graphene hydrogel}$ , mesoporous  $\text{MnO}_2$ ,  $\text{MnO}_2/\text{TiN}$ ,  $\text{MnO}_2/\text{PPY}$ ,  $\text{IrO}_2/\text{MnO}_2$ ,  $\text{MnO}_2/\text{RuO}_2$ , etc.) have been fabricated for EES applications.<sup>315, 317-349</sup> The morphology of  $\text{MnO}_2$  in the composites is related to the deposition time and deposition current density. The anodic ED- $\text{MnO}_2$  can deliver a high capacitance up to  $1222 \text{ F g}^{-1}$  at  $5 \text{ A g}^{-1}$ ,<sup>329</sup> and superior cycling life and rate capability are proven in the composites with metal and graphene.<sup>315-317, 338, 339</sup> As anode of LIBs, the mesoporous  $\text{MnO}_2$  nanosheet arrays exhibit a reversible capacity as high as  $1690 \text{ mAh g}^{-1}$  after 100 cycles.<sup>335</sup>

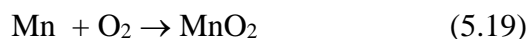
The cathodic ED- $\text{MnO}_2$  mainly comes from two routes: (1) direct cathodic ED of  $\text{MnO}_2$  in  $\text{Mn}(\text{NO}_3)_2$  electrolyte and (2) conversion from metal Mn electrodeposited from an electrolyte containing a  $\text{Mn}^{2+}$  ion or  $\text{KMnO}_4$ . First, we introduce the work of Li and co-workers, who used the above two kind of cathodic ED for the construction of mesoporous  $\text{MnO}_2/\text{carbon aerogel}$  and  $\text{ZnO}/\text{MnO}_2$  composites, respectively.<sup>350, 351</sup> The reactions in  $\text{Mn}(\text{NO}_3)_2$  electrolyte are expressed as follows.<sup>350</sup>



The above mesoporous MnO<sub>2</sub>/carbon aerogel composites show a high specific capacitance of 515.5 F g<sup>-1</sup>. Meanwhile, they developed another cathodic ED using Mn(CH<sub>3</sub>COO)<sub>2</sub> electrolyte, expressed as below.<sup>351</sup>

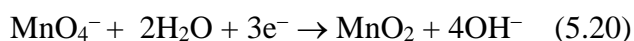


During the annealing process:



These prepared single-crystal ZnO nanorod/amorphous and nanoporous MnO<sub>2</sub> shell composites have been employed as supercapacitor electrodes and give a high specific capacitance of 405 F g<sup>-1</sup>. Similar cathodic ED-MnO<sub>2</sub> is also reported by other groups.<sup>352, 353</sup>

There is third kind of cathodic ED of MnO<sub>2</sub>, which is realized by reduction of KMnO<sub>4</sub>, shown as follows.<sup>307, 354, 355</sup>



MnO<sub>2</sub>/CNT, Fe<sub>2</sub>O<sub>3</sub>/MnO<sub>2</sub> and amorphous MnO<sub>2</sub> films are prepared by this cathodic ED and high capacitances of 463–838 F g<sup>-1</sup> are verified in the composite systems.<sup>307, 354, 355</sup>

In a nutshell, the anodic ED is most popular ED method for synthesis of MnO<sub>2</sub> and its deposition process is very easy to control. The MnO<sub>2</sub> of anodic ED exhibits the best EES performances among the ED-MnO<sub>2</sub> samples.

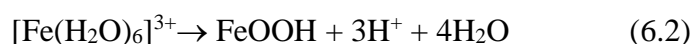
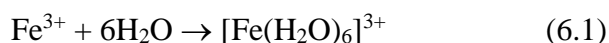
## 6. Iron oxides and iron oxides-based composites

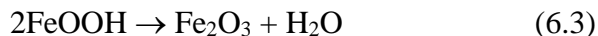
Iron is the fourth most common element in the earth's crust (6.3 % by weight) and is usually oxidized into three kinds of oxides (Fe<sub>2</sub>O<sub>3</sub>, Fe<sub>3</sub>O<sub>4</sub>, and FeO), which are promising active materials for applications in photo-catalysis, EES and photo-electrochemical water splitting. Hematite Fe<sub>2</sub>O<sub>3</sub> is the most thermodynamically stable form of iron oxide under ambient conditions and as such, it is also the most common form of crystalline iron oxide. The Fe<sub>2</sub>O<sub>3</sub> have different polymorphs including α-Fe<sub>2</sub>O<sub>3</sub> (rhombohedral structure, JCPDS 80-2377), β-Fe<sub>2</sub>O<sub>3</sub> (orthorhombic structure, JCPDS 08-0093) and γ-Fe<sub>2</sub>O<sub>3</sub> (cubic structure,

JCPDS 89-5892) depending on the structure of  $\text{Fe}(\text{O})_6$  octahedra. The arrangement of cations produces pairs of  $\text{Fe}(\text{O})_6$  octahedra. Each octahedron shares edges with three neighboring  $\text{Fe}(\text{O})_6$  octahedra in the same plane and one face with an octahedron in an adjacent plane. Different combination of  $\text{Fe}(\text{O})_6$  octahedra will form different  $\text{Fe}_2\text{O}_3$  polymorphs.<sup>356</sup> The band gap of  $\text{Fe}_2\text{O}_3$  is about 1.9–2.2 eV depending on different polymorphs. Another important iron oxide is  $\text{Fe}_3\text{O}_4$ , whose crystal structure is similar to that of  $\text{Co}_3\text{O}_4$ .  $\text{Fe}_3\text{O}_4$  has a face-centred cubic unit cell (JCPDS 65-3107).  $\text{Fe}_3\text{O}_4$  differs from most other iron oxides in that it contains both divalent and trivalent iron. Its structure consists of octahedral and mixed tetrahedral/octahedral layers. Its band gap is  $\sim 0.1$  eV.  $\text{FeO}$  has a defective NaCl structure and a band gap of  $\sim 2.4$  eV. It consists of two interpenetrating face centred cubic structures of  $\text{Fe}^{\text{II}}$  and  $\text{O}^{2-}$  (JCPDS 43-1312).  $\text{FeO}$  is not stable in air and prone to be oxidized into  $\text{Fe}_3\text{O}_4$  or  $\text{Fe}_2\text{O}_3$ . Over the past decades, numerous iron oxides and composites have been prepared by solution-based methods and applied as electrode materials for EES. In this section, we mainly focus on the HT, ST, CP and ED methods for the synthesis of iron oxides and corresponding electrochemical performances.

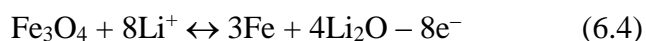
## **6.1 Hydrothermal synthesis and solvothermal synthesis method of iron oxide and iron oxides-based composites**

To date, the HT+ST papers account for  $\sim 32$  % in all the published papers of solution synthesis of iron oxides for EES applications.  $\text{FeCl}_3$ ,  $\text{FeSO}_4$  and  $\text{Fe}(\text{NO}_3)_3$  are the most widely used iron sources. The solvent includes water, ethanol and ethylene glycol.<sup>357-362</sup> As one of strong acid weak alkali salts, iron salt is very easy to hydrolyze into ferric hydroxide precipitation in water at high temperature. Then, ferric hydroxide precipitation decomposes into ferric oxide and water. The reactions are as following:<sup>35</sup>





In order to accelerate the deposition process, some precipitants (such as urea,<sup>363, 364</sup> sodium hydroxide<sup>357, 358, 364</sup> and sodium acetate<sup>365, 366</sup>) are also used to promote the HT process. They could yield OH<sup>-</sup> during the hydrolysis in the solution and consume the H<sup>+</sup> in eqn. (6.2) to accelerate the reaction. Previously, we prepared porous Fe<sub>3</sub>O<sub>4</sub>/C core/shell nanorods by the above HT reactions and demonstrated a high capacity of 762 mAh g<sup>-1</sup> for LIBs application.<sup>358</sup> Additionally, Zhang et al. reported an interesting carbon coated Fe<sub>3</sub>O<sub>4</sub> nanospindles by using FeCl<sub>3</sub> and NaH<sub>2</sub>PO<sub>4</sub>.<sup>367</sup> The main reactions are similar to those above. But the NaH<sub>2</sub>PO<sub>4</sub> is important for controlling the morphology of the samples. The hydrolysis of NaH<sub>2</sub>PO<sub>4</sub> produces OH<sup>-</sup> as a precipitating agent. It controls the nucleation as well as growth of small iron oxide particles and finally forming Fe<sub>3</sub>O<sub>4</sub> nanospindles (Figure 18). The obtained Fe<sub>3</sub>O<sub>4</sub>/C nanospindles show a high reversible capacity of 745 mAh g<sup>-1</sup>. Meanwhile, we adopted FeCl<sub>3</sub> and Na<sub>2</sub>SO<sub>4</sub> as the starting materials to fabricate Fe<sub>2</sub>O<sub>3</sub> nanorod array on carbon cloth.<sup>35</sup> The Na<sub>2</sub>SO<sub>4</sub> is believed to be favorable for the formation of rods. The specific mechanism is still not clear.<sup>35</sup> Some other iron oxides nanostructures (such as nanorods, nanoparticles and spheroids) and iron oxides-based composites (e.g., Fe<sub>3</sub>O<sub>4</sub>/C, Fe<sub>3</sub>O<sub>4</sub>/graphene) have been reported by similar HT reactions.<sup>357, 366, 368-370</sup> The iron oxides grown on the carbon backbone show much better EES performance than the pure counterparts. As anode of LIBs, the ferric oxides (Fe<sub>3</sub>O<sub>4</sub> and Fe<sub>2</sub>O<sub>3</sub>) can reversibly react with Li ion to store electrochemical energy and the corresponding simplified reactions are expressed as follows:<sup>314, 371</sup>



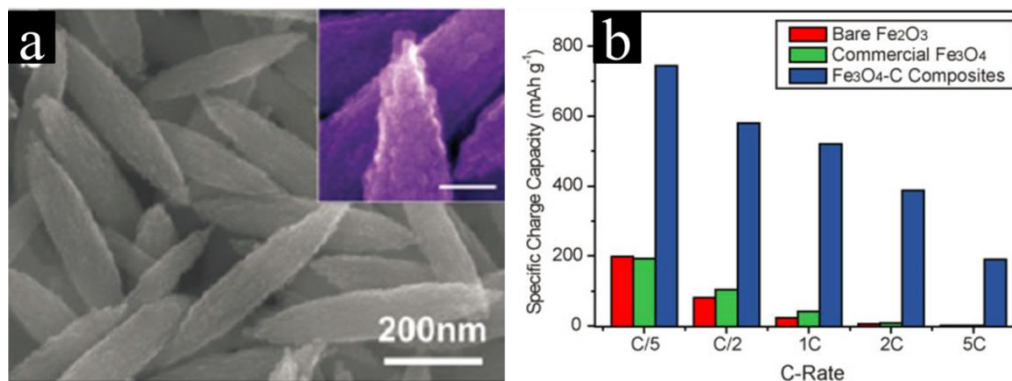
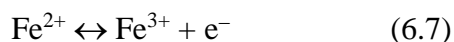
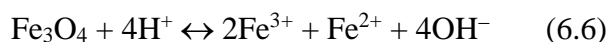


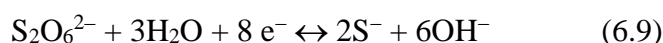
**Figure 18** (a) SEM images of hydrothermal synthesized Fe<sub>3</sub>O<sub>4</sub> spindles with additional carbon coating. (b) Rate capability of the HT-Fe<sub>3</sub>O<sub>4</sub>/C spindles electrode compared to bare Fe<sub>2</sub>O<sub>3</sub> without carbon, and commercial Fe<sub>3</sub>O<sub>4</sub> powders. Reproduced with permission from Ref. 367.

The iron oxides and composites are also investigated as cathode materials for supercapacitors. The Fe<sub>3</sub>O<sub>4</sub>/reduced graphene oxide delivers a capacitance of 480 F g<sup>-1</sup>. As for the supercapacitor electrode, the capacitance mechanism of ferric oxides in aqueous electrolytes is still not clear yet. The possible reactions are given as follows.

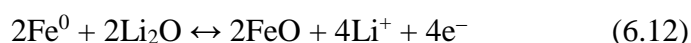
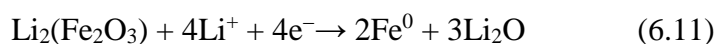
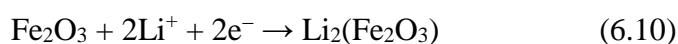
In alkaline electrolyte such as KOH solution<sup>372</sup>



If the electrolyte is Na<sub>2</sub>SO<sub>3</sub> solution<sup>370, 373</sup>

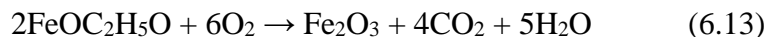


As the electrolyte is lithium perchlorate (LiClO<sub>4</sub>) in ethylene carbonate (EC)/dimethyl carbonate (DMC) (in a volume ratio of 1:1):<sup>374</sup>



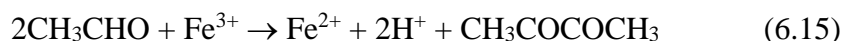
It is noteworthy that the solvent has great influence on the morphology of the final products, especially in organic solvents. Therefore, solvothermal synthesis (ST) is developed

for the synthesis of iron oxides and composites. Zeng et al. reported flower-like  $\alpha$ -Fe<sub>2</sub>O<sub>3</sub> by using ethanol as solvent and proposed that the tentative solvothermal precursor could be a composition of FeOC<sub>2</sub>H<sub>5</sub>O, <sup>362, 375</sup> which converts into iron oxides after annealing. During the annealing process in air:<sup>375</sup>

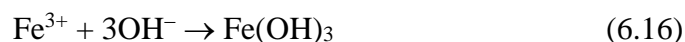


In addition, they conducted a series of other investigations to further understand the effect of ethanol in the process. It is believed that ethanol may play important roles in at least three aspects: (i) acting as the solvent; (ii) acting as starting material to form the iron alkoxide precursor; and (iii) providing water molecules in the system by etherification. They also found that the rate of reaction has a strong impact on the morphology of products.

Ethylene glycol (EG) is another common solvent to synthesize ferric oxides in ST method<sup>363, 365, 366, 368</sup>. As a kind of reducing agent, EG is always used to synthesize Fe<sub>3</sub>O<sub>4</sub> in most cases. Our group synthesized hierarchical hollow-structured single-crystalline magnetite (Fe<sub>3</sub>O<sub>4</sub>) microspheres as LIBs anode.<sup>365</sup> In our case, the solution is a mixture of ferric chloride, EG, polyvinylpyrrolidone (PVA) and NaAc, which is used as iron source, solvent and reducing agent, surfactant and precipitant, respectively. The possible reactions are shown as follows:<sup>365</sup>



Meanwhile, NaAc hydrolyze to offer OH<sup>-</sup> in the ST system.<sup>365</sup>



The as-prepared hierarchical hollow-structured Fe<sub>3</sub>O<sub>4</sub> shows a high specific capacity and excellent cycle performance (851 mAh g<sup>-1</sup> at 1 C and 750 mAh g<sup>-1</sup> at 3 C up to 50 cycles).<sup>365</sup> However, the poor intrinsic electrical conductivity of iron oxides hinders its practical applications for EES. There are different approaches to overcome these problems. One

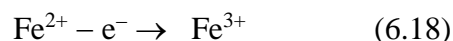
solution is to fabricate iron oxide nanostructures. Other strategies are to confine the iron oxide nanostructures with carbon to form a composite with the carbon host matrix. Fe<sub>3</sub>O<sub>4</sub>/C core/shell structure<sup>358, 364, 367</sup>, ferric/graphene<sup>363, 368</sup> or CNTs composites<sup>357, 373, 374</sup> are synthesized to improve the conductivity of the integrate electrode.

## 6.2 Electrochemical synthesis of iron oxides and iron oxides-based composites

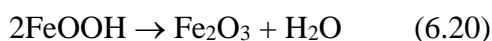
The electro-deposition (ED) methods for iron oxides and their composites are also classified into two types: cathodic ED and anodic ED. So far, there are three typical ED reactions for the fabrication of iron oxides nanostructures for EES applications. The obtained products are films, not powders. These three ED reactions have their own merits and demerits and will be discussed in detail in this section.

### 6.2.1 Anodic ED with Fe(NH<sub>4</sub>)<sub>2</sub>(SO<sub>4</sub>)<sub>2</sub> or FeSO<sub>4</sub>

The first ED developed for iron oxides and their composites is based on the anodic reaction of Fe(NH<sub>4</sub>)<sub>2</sub>(SO<sub>4</sub>)<sub>2</sub>. The precursor formation relies on the oxidation of Fe<sup>2+</sup> to Fe<sup>3+</sup>, which further reacts with the available OH<sup>-</sup> from a slightly alkaline electrolyte to form insoluble FeOOH. In this reaction, a brown deposit can be observed at the beginning of anodic deposition, indicating the formation of FeOOH. The specific reactions are illustrated as follows.<sup>376</sup>



During the annealing process in air atmosphere:<sup>376</sup>



During the annealing process in H<sub>2</sub> atmosphere:

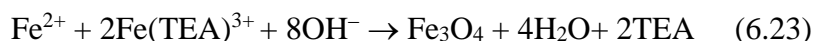
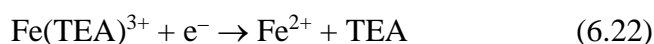


The as-prepared iron oxides always show a highly porous structure composed of nanosheets. Wu et al. prepared Fe<sub>2</sub>O<sub>3</sub> nanosheets arrays by the above method and showed a

capacitance of 146 F g<sup>-1</sup>.<sup>376</sup> FeSO<sub>4</sub> is also used as the iron source to prepare iron oxides nanostructures via the same reaction mechanism. A big problem in this anodic ED is that the iron source Fe(NH<sub>4</sub>)<sub>2</sub>(SO<sub>4</sub>)<sub>2</sub> or FeSO<sub>4</sub> is not stable and will be easily oxidized by the O<sub>2</sub> in the electrolyte. So it is necessary to put some pure iron powder in the electrolyte to stabilize the iron source. Several iron oxides-based composites (such as Fe<sub>2</sub>O<sub>3</sub>/carbon fibre, Fe<sub>2</sub>O<sub>3</sub>/MnO<sub>2</sub> and TiO<sub>2</sub>/Fe<sub>2</sub>O<sub>3</sub>) have been fabricated for EES via the above anodic ED by the aid of other templates including AAO, TiO<sub>2</sub> nanotube, and carbon fibre.<sup>307, 377, 378</sup> As cathode material of supercapacitors, the Fe<sub>2</sub>O<sub>3</sub>/MnO<sub>2</sub> presents a maximum specific capacitance of 838 F g<sup>-1</sup>.<sup>307</sup> For LIBs application, the Fe<sub>2</sub>O<sub>3</sub>/carbon fibre and TiO<sub>2</sub>/Fe<sub>2</sub>O<sub>3</sub> exhibit a capacity of 970 mAh g<sup>-1</sup> and 1190 mAh g<sup>-1</sup>, respectively, much higher than the bare Fe<sub>2</sub>O<sub>3</sub> (680 mAh g<sup>-1</sup>).<sup>377, 378</sup>

### 6.2.2 Cathodic ED with Fe<sub>2</sub>(SO<sub>4</sub>)<sub>3</sub> and tri-ethanolamine (TEA) in alkaline electrolyte

In order to find a more stable and feasible ED for iron oxides, researchers have developed another facile cathodic ED using Fe<sub>2</sub>(SO<sub>4</sub>)<sub>3</sub> and tri-ethanolamine (TEA) as the starting materials. But this cathodic ED is usually adopted to fabricate Fe<sub>3</sub>O<sub>4</sub> film. Previously, we prepared a 3D porous nano-Ni/Fe<sub>3</sub>O<sub>4</sub> composite film by the cathodic ED.<sup>379</sup> The reactions are expressed as follows.<sup>379, 380</sup>



The electrolyte here is very stable and the deposition process is easy to control. The Fe<sub>3</sub>O<sub>4</sub> nanoflakes are grown on the 3D Ni backbone forming a highly porous integrated electrode. The resultant 3D porous nano-Ni/Fe<sub>3</sub>O<sub>4</sub> composite film shows a high capacity of 951 mAh g<sup>-1</sup> as well as enhanced rate capability. In addition, Tarascon's group used the same method to prepare Fe<sub>3</sub>O<sub>4</sub>-based Cu nano-architected electrodes for LIBs with superior high-rate capability.<sup>381</sup> Similar Fe<sub>3</sub>O<sub>4</sub>/Cu core/shell nanorod arrays are reported by Duan et al. and deliver a capacity of 1003 mAh g<sup>-1</sup>.<sup>382</sup>

### 6.2.3 Anodization of Fe foil.

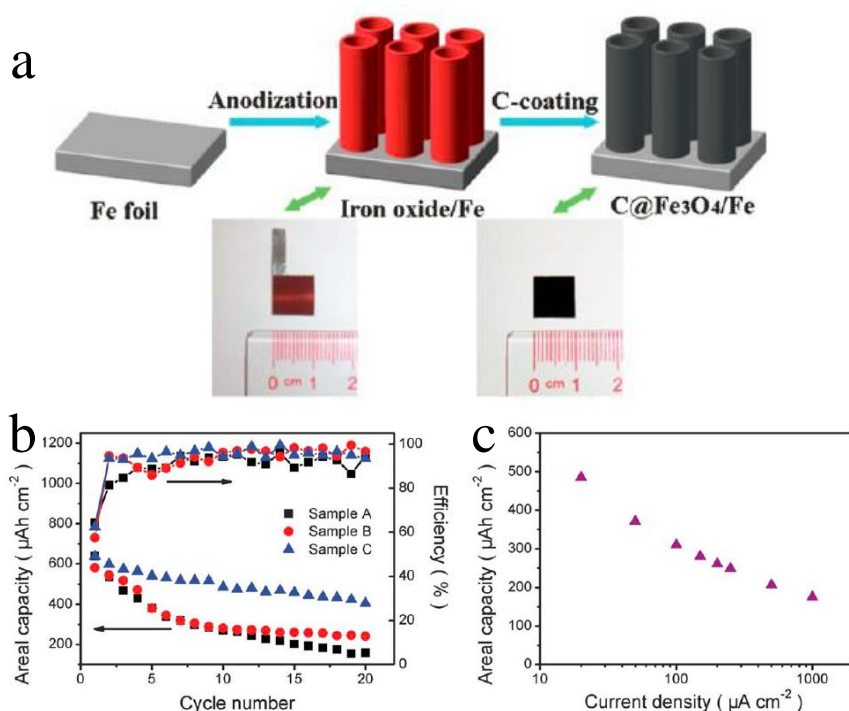


**Figure 19** (a) Schematics of the synthesis of the C@Fe<sub>3</sub>O<sub>4</sub> composite electrode. (b, c) Li-ion battery cycling life and rate capability of C@Fe<sub>3</sub>O<sub>4</sub> composite electrode. Reproduced with permission from Ref.383.

The third ED of iron oxides is anodization of iron foils. This method originates from the well-known anodization of Ti foils towards TiO<sub>2</sub> nanotubes. The electrolyte is ammonium fluoride in an aqueous ethylene glycol solution. The working voltage is about 50 V. Xie et al. reported such an anodization method to fabricate Fe<sub>3</sub>O<sub>4</sub>/C nanotube arrays (Figure 19).<sup>383</sup> The involved precursor reactions are simply expressed as below.<sup>383</sup>



The Fe<sub>3</sub>O<sub>4</sub> in the Fe<sub>3</sub>O<sub>4</sub>/C nanotube arrays is formed by the reduction of Fe<sub>2</sub>O<sub>3</sub> via carbon. The NH<sub>4</sub>F can accelerate the anodization reaction. The as-fabricated Fe<sub>3</sub>O<sub>4</sub>/C nanotubes grow vertically on the substrates and have average pore diameter of 100 nm. The Fe<sub>3</sub>O<sub>4</sub>/C nanotubes exhibit high capacity (1020 mAh cm<sup>-2</sup> at 20 mA cm<sup>-2</sup>) and high rate capability

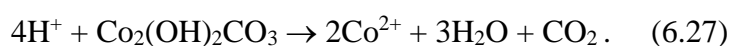
(176 mAh cm<sup>-2</sup> at 1000 mA cm<sup>-2</sup>). It is noteworthy that it is difficult to calculate the true load mass of active materials obtained by this method because the active materials directly come from the Fe foil.

### 6.3 Chemical precipitation of iron oxides and iron oxides-based composites

Generally, CP-Fe<sub>2</sub>O<sub>3</sub> or CP-Fe<sub>3</sub>O<sub>4</sub> is prepared by directly mixing iron sources (e.g., FeCl<sub>2</sub>, FeCl<sub>3</sub>, Fe(NH<sub>4</sub>)<sub>2</sub>(SO<sub>4</sub>)<sub>2</sub>, MnSO<sub>4</sub>, Fe(NO<sub>3</sub>)<sub>3</sub>) with precipitants (e.g., NaOH, ammonia, Na<sub>2</sub>CO<sub>3</sub>, CH<sub>3</sub>COONa). The iron sources usually react with the OH<sup>-</sup> or CO<sub>3</sub><sup>2-</sup> to form precursor, which converts into iron oxides after heat treatment. Meanwhile, there is a special CP based on hydrolysis of iron sources. We have investigated the hydrolysis reaction and prepared some high-performance iron oxides-based electrode materials for LIBs, including TiO<sub>2</sub> nanotube, 3D graphene foam and Co<sub>3</sub>O<sub>4</sub> supported iron oxides.<sup>324, 384-386</sup> Herein, we take the TiO<sub>2</sub>/Fe<sub>2</sub>O<sub>3</sub> core/shell nanoarrays as an example (Figure 20a) for discussion of the reaction process.<sup>324</sup> The FeCl<sub>3</sub> is unstable in the electrolyte and will hydrolyze into H<sup>+</sup> ions,



When there exists a sacrificial template, Co<sub>2</sub>(OH)<sub>2</sub>CO<sub>3</sub> in this case, it will react with the above H<sup>+</sup> and this reaction accelerates the hydrolysis reaction according to<sup>324</sup>



During the annealing process, 2FeOOH → Fe<sub>2</sub>O<sub>3</sub>+H<sub>2</sub>O . (6.28)

The FeOOH product of hydrolysis can change into Fe<sub>2</sub>O<sub>3</sub> after annealing in an air or oxygen ambient according to Eq. (6.28). The key point in this method is the sacrificial template to drive the hydrolysis reaction. The sacrificial template can be also metal oxides (such as ZnO, Al<sub>2</sub>O<sub>3</sub>) or metal hydroxides [Ni(OH)<sub>2</sub> or Co(OH)<sub>2</sub>]. Using a similar method, we also obtained 3D GF-supported Fe<sub>3</sub>O<sub>4</sub> nanoparticles with a homogeneous coverage, thanks to the uniform coating of ZnO by ALD (see Figure 20b).

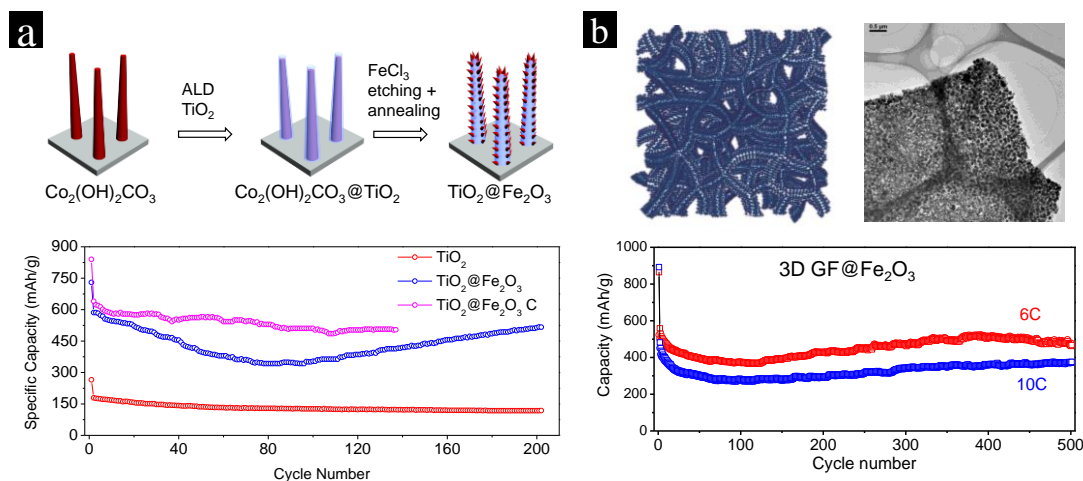
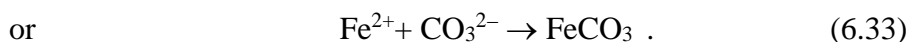
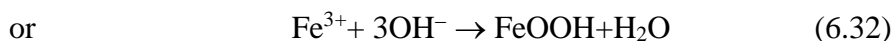


**Figure 20** Fe<sub>2</sub>O<sub>3</sub> nanostructures obtained by chemical precipitation for the Li-ion battery anode materials. (a) Co<sub>2</sub>(OH)<sub>2</sub>CO<sub>3</sub> nanowires as the sacrificial template and ALD TiO<sub>2</sub> as the support for the final Fe<sub>2</sub>O<sub>3</sub> nanoparticles. The battery cycling life is shown below. Reproduced with permission from Ref. 324. (b) 3D graphene foam supported ALD ZnO as the sacrificial template for chemical precipitation reaction. Reproduced with permission from Ref. 385.

Similar result is reported by other authors. Wang et al. reported a typical CP method for the synthesis of Fe<sub>2</sub>O<sub>3</sub> nanorods by using FeSO<sub>4</sub> and CH<sub>3</sub>COONa as the starting materials. The CH<sub>3</sub>COONa is used as a source of hydroxide ions during the hydrolysis of iron salts to form FeOOH. The reactions are given as follow.<sup>387</sup>



In addition to above hydrolysis, other CP reactions in basic solutions are much easier, for example,<sup>388-392</sup>



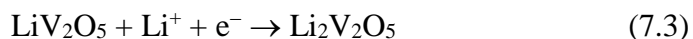
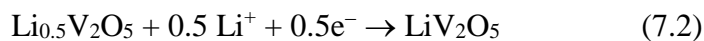
Then, the precursor converts into Fe<sub>2</sub>O<sub>3</sub> or Fe<sub>3</sub>O<sub>4</sub> after annealing in different atmosphere. Nonetheless, CP method based on a sacrificial template provides better control in nano

morphology. A direct CP reaction with basic solution may be too fast and result in unwanted agglomerations.

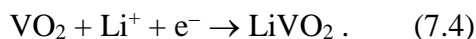
The as-prepared CP-iron oxides are powders, not films. In order to have good EES performance, often the CP-Fe<sub>2</sub>O<sub>3</sub> or CP-Fe<sub>3</sub>O<sub>4</sub> will need further surface engineering or form composites with conductive host. For example, the Fe<sub>3</sub>O<sub>4</sub>/carbon nanotube composites can deliver a high discharge capacity of 656 mAh g<sup>-1</sup> and stable cyclic retention.<sup>388</sup> The TiO<sub>2</sub>/Fe<sub>2</sub>O<sub>3</sub> core/shell nanoarrays, after a further step of carbon coating, exhibit a high reversible capacity of 840 mAh g<sup>-1</sup> and evidently improved cycle stability (Figure 20a). With a homogeneous hybridization with 3D chemical-vapor-deposited graphene foam, the Fe<sub>3</sub>O<sub>4</sub> nanoparticles LIB anode demonstrates an ultra-fast charging and discharging with a rate of 60 C within 500 cycles (Figure 20b).

## 7. Vanadium oxides and vanadium oxides-based composites

Vanadium oxides are typical multi-functional materials and have attracted strong interest over the past years for their unique electrical, optical, electrochemical properties. Two kinds of vanadium oxides, vanadium pentoxide (V<sub>2</sub>O<sub>5</sub>) and vanadium dioxide (VO<sub>2</sub>), are considered as promising active cathode materials for EES due to their high capacity/capacitance, high working voltage and excellent cycling stability. The V<sub>2</sub>O<sub>5</sub> has an orthorhombic structure (JCPDS 41-1426) with lattice parameters  $a = 3.563 \text{ \AA}$ ,  $b = 11.510 \text{ \AA}$ ,  $c = 4.369 \text{ \AA}$ . The building block is a deformed VO<sub>6</sub> octahedron. The shortest V-O bond length corresponds to a double vanadyl bond ( $V-O_1 = 1.585 \text{ \AA}$ ). The V<sub>2</sub>O<sub>5</sub> has a layered structure with an easy cleavage plane (perpendicular to the c-axis) and a band gap of ~2.8 eV. The theoretical capacity of V<sub>2</sub>O<sub>5</sub> is ~294 mAh g<sup>-1</sup> between 4.0 and 2.0 V (vs. Li<sup>+</sup>/Li), which is higher than those of LiCoO<sub>2</sub> (140 mAh g<sup>-1</sup>), LiMn<sub>2</sub>O<sub>4</sub> (148 mAh g<sup>-1</sup>) and LiFePO<sub>4</sub> (170 mAh g<sup>-1</sup>). The electrochemical reactions between V<sub>2</sub>O<sub>5</sub> and Li ion between 4.0 and 2.0 V (vs. Li<sup>+</sup>/Li) are expressed as follows:<sup>49, 393-395</sup>



Another important vanadium oxide is VO<sub>2</sub>, which is a typical binary compound with different polymorphs. The polymorphic varieties in this system include tetragonal rutile-type VO<sub>2</sub> (R), monoclinic VO<sub>2</sub> (M), and at least three metastable phases named as VO<sub>2</sub> (B), VO<sub>2</sub>(A) and VO<sub>2</sub> (C). VO<sub>2</sub> can adopt different structures according to different synthesis methods. Generally speaking, the structures of the four VO<sub>2</sub> polymorphs, VO<sub>2</sub> (R), VO<sub>2</sub> (M), VO<sub>2</sub> (B), and VO<sub>2</sub> (A), are based on an oxygen bcc lattice with vanadium in the octahedral sites, the oxygen octahedra being more or less regular. They can be separated in two groups, depending on the mutual orientation of the fourfold axis of the oxygen octahedra. The oxygen octahedra can be aligned either along two perpendicular directions, as it is the case in the rutile structure. The band gap of VO<sub>2</sub> is 0.5–0.7 eV depending on different polymorphs. The theoretical capacity of VO<sub>2</sub> is ~340 mAh g<sup>-1</sup> between 4.0 and 1.5 V (vs. Li<sup>+</sup>/Li). The reaction can be written as<sup>396, 397</sup>



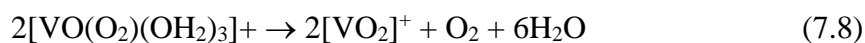
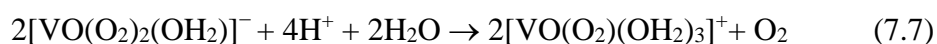
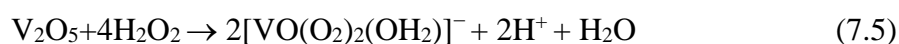
In this section, we will briefly introduce some typical solution-based synthesis methods (mainly hydrothermal, solvothermal, electrodeposition and sol-gel) for the synthesis of vanadium oxides and composites for EES applications.

### **7.1 Hydrothermal synthesis and solvothermal synthesis of vanadium oxides and vanadium oxides-based composites**

The HT and ST methods are popular with materials researchers and have been widely used for the fabrication of vanadium oxides and composites. Generally, there are two common types of HT routes for the synthesis of V<sub>2</sub>O<sub>5</sub> for EES. One HT method is to use the metavanadate (NaVO<sub>3</sub> or NH<sub>4</sub>VO<sub>3</sub>) and HCl as the starting materials and utilize the

hydrolysis of ammonium metavanadate in the acid solution to form vanadium oxides after heat treatment.<sup>115, 313, 394, 398-402</sup> The other HT method is to utilize V<sub>2</sub>O<sub>5</sub> sols precursor resulting from the reactions between commercial V<sub>2</sub>O<sub>5</sub> powder and H<sub>2</sub>O<sub>2</sub>, and finally obtain V<sub>2</sub>O<sub>5</sub> nanostructures after hydrothermal synthesis and annealing.<sup>395, 403-405</sup> Carbon sources (such as graphene, carbon nanotube and sucrose) and V<sub>2</sub>O<sub>5</sub> are usually used as the starting materials to prepare HT-VO<sub>2</sub> and their composites.<sup>406, 407</sup>

First, we introduce the sol-based HT method for the synthesis of porous structured V<sub>2</sub>O<sub>5</sub> for EES. Typically, the commercial powder V<sub>2</sub>O<sub>5</sub> reacts with the H<sub>2</sub>O<sub>2</sub> (30 wt. %) in deionized water and forms yellow slurry bubbled vigorously (note that this reaction is exothermic). Several parallel or sequential chemical reactions occur in the HT due to the decomposition of excess H<sub>2</sub>O<sub>2</sub>, expressed as follows.<sup>395, 403, 408</sup>



During the annealing process:



This sol-based HT route is very facile but needs to control the amount of H<sub>2</sub>O<sub>2</sub>. In this method, the peroxovanadates plays an important role in the formation of nanostructured V<sub>2</sub>O<sub>5</sub> and composites such as nanobelt, 3D porous architecture V<sub>2</sub>O<sub>5</sub> and V<sub>2</sub>O<sub>5</sub>/graphene.<sup>395, 404, 405</sup> Yan' group reported a 3D porous architecture V<sub>2</sub>O<sub>5</sub> composed of nanosheets and showed a high specific capacitance of 451 F g<sup>-1</sup> in a neutral aqueous Na<sub>2</sub>SO<sub>4</sub> electrolyte for supercapacitors application (Figure 21).<sup>395</sup> In addition, the V<sub>2</sub>O<sub>5</sub> nanobelt shows a high reversible specific capacities of 163 mAh g<sup>-1</sup> at 6.8 C.<sup>405</sup> All the above HT vanadium oxides are power materials, not films.

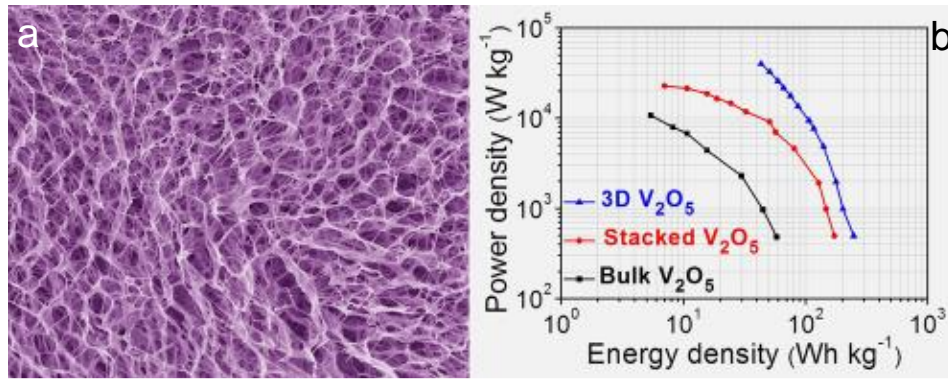
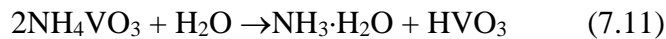
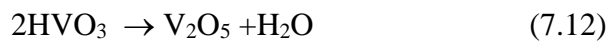


**Figure 21** (a) SEM image and (b) Ragone plot of hydrothermal-synthesized  $V_2O_5$  porous film composed of nanosheets. Reproduced with permission from Ref. 395.

The other HT of  $V_2O_5$  is associated with the hydrolysis of metavanadate. For example:

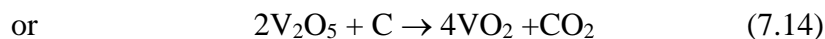
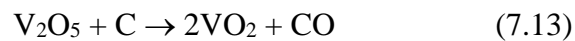


During the annealing process:



The metavanadate based HT method have been used for fabrication of  $V_2O_5$  nanomaterials (tarfruit-like, nanowire), and composites (e.g.,  $V_2O_5$ /graphene,  $V_2O_5$ /CNT,  $V_2O_5$ /PPY,  $V_2O_5$ /SnO<sub>2</sub>) by the aid of some surfactants and copolymers.<sup>115, 313, 394, 398-402</sup> These  $V_2O_5$  composites exhibit a high capacitance up to 500 F g<sup>-1</sup> and a capacity of 200 mAh g<sup>-1</sup> at high working current of 1000 mA g<sup>-1</sup>.

The HT-VO<sub>2</sub> nanostructures could be prepared by a reduction reaction between  $V_2O_5$  and carbon sources such as graphene and sucrose, simply expressed as below.<sup>406, 407</sup>



VO<sub>2</sub>/graphene nanoribbon and nanobelts reported by Yan's group and Yang et al. exhibit a capacity of 160–300 mAh g<sup>-1</sup>.<sup>406, 407</sup> The nanobelt and nanoribbon is very thin and favourable for fast ion/ electron transfer. The introduction of graphene improves the conductivity of composite leading to enhanced properties and cycling stability.

In parallel with HT, solvothermal synthesis (ST) of vanadium oxides are also extensively studied to construct vanadium oxides nanostructures including rod-like, nanosphere, urchin-like and hollow microflower.<sup>40, 393, 396, 397, 409-411</sup> The vanadium sources of ST are different from those for HT. Most of the vanadium sources are vanadium based organic solvents, such as vanadium oxytripropoxide,<sup>409</sup> and vanadium isopropoxide.<sup>412</sup> Usually, the solvents are ethylene glycol, ethanol or N-methylpyrrolidone. The specific reactions are still not fully clear and need further investigation. The ST-vanadium oxides nanostructures could deliver a higher specific capacitance of 537 F g<sup>-1</sup> at a current density of 1 A g<sup>-1</sup> in neutral aqueous electrolytes.<sup>409</sup> The ST-V<sub>2</sub>O<sub>5</sub> hollow microflowers exhibit a remarkable reversible capacity of 211 mAh g<sup>-1</sup> and good cycling stabilities and excellent rate capabilities.<sup>393</sup>

## **7.2 Sol-gel synthesis and electrochemical synthesis of vanadium oxides and vanadium oxides-based composites**

Here we focus on the sol-gel and electro-deposition methods of vanadium oxides and composites for EES. According to formation mechanism of sols, there are three basic kinds of sol-gel for the synthesis of vanadium oxides for EES. The first kind of sol-gel sol is the same as that of the sol-based HT methods. The vanadium bulks or commercial V<sub>2</sub>O<sub>5</sub> powders are dissolved in H<sub>2</sub>O<sub>2</sub> to form sol containing [VO<sub>2</sub>]<sup>+</sup>.<sup>413, 414</sup> The second type is to use vanadium oxy tripropoxide, which hydrolyses to form V<sub>2</sub>O<sub>5</sub> sol.<sup>415, 416</sup> The last one is to obtain HVO<sub>3</sub> sol by ion exchange method using NaVO<sub>3</sub> as the starting material.<sup>417</sup> Several nanoscale sol-gel-vanadium oxides (such as nanoporous V<sub>2</sub>O<sub>5</sub>, nanoparticle and nanotube),<sup>413, 415, 418</sup> and composites (V<sub>2</sub>O<sub>5</sub>/graphene and V<sub>2</sub>O<sub>5</sub>/CNT),<sup>414, 416-419</sup> have been fabricated and delivered a high LIBs capacity of >200 mAh g<sup>-1</sup>, and a pseudocapacitance of 200–316 F g<sup>-1</sup>. But the nanosized morphologies of sol-gel-vanadium oxides are often prepared via other hard or soft templates.

In addition to the sol-gel method, electro-deposition synthesis is another facile way to the fabrication of vanadium oxides and composites, mainly for film samples. We note that the ED-V<sub>2</sub>O<sub>5</sub> is often prepared by anodic ED method with the VOSO<sub>4</sub> as the vanadium source and Na<sub>2</sub>SO<sub>4</sub> as the supporting electrolyte. The plausible involved reactions may be as follows:



Nanoporous ED-V<sub>2</sub>O<sub>5</sub> films and composites films (e. g., V<sub>2</sub>O<sub>5</sub>/CNT, V<sub>2</sub>O<sub>5</sub>/TiO<sub>2</sub>, V<sub>2</sub>O<sub>5</sub>/graphene, V<sub>2</sub>O<sub>5</sub>/PANI),<sup>420-424</sup> have been synthesized by the above ED method and applied as cathodes for LIBs and supercapacitors. The ED-V<sub>2</sub>O<sub>5</sub>/graphene cathode delivered a discharge capacity of 208 mAh g<sup>-1</sup> during the 100th cycle.<sup>420</sup> The aligned mixed V<sub>2</sub>O<sub>5</sub>-TiO<sub>2</sub> nanotube arrays exhibit a capacitance of 220 F g<sup>-1</sup>.<sup>425</sup>

In addition, it is found that the chemical precipitation and microwave synthesis of vanadium oxides and composites for EES are not the research focus and the corresponding papers are quite few, so we do not introduce them here.

## 8. Tungsten oxides and tungsten oxides-based composites

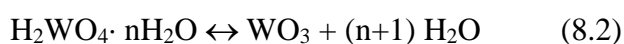
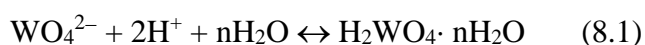
Tungsten oxide (WO<sub>3</sub>), also known as tungsten trioxide, has attracted extensive attention because of its distinctive physical and chemical properties, making it suitable for applications in electrochromic devices, photo-catalysis, gas sensing and EES.<sup>2, 179, 405, 426-433</sup> The simplest crystal structure of WO<sub>3</sub> is referred to the “ideal” cubic type and described as the three-dimensional networks of corner-sharing WO<sub>6</sub> octahedra. However, cubic WO<sub>3</sub> is seldom observed experimentally. The common WO<sub>3</sub> displays a little distorted structures compared with cubicWO<sub>3</sub>, classified into following five forms: tetragonal (α-WO<sub>3</sub>), orthorhombic (β-WO<sub>3</sub>), monoclinic I (γ-WO<sub>3</sub>), triclinic (δ-WO<sub>3</sub>), monoclinic II (ε-WO<sub>3</sub>) and hexagonal (h-WO<sub>3</sub>). The different phases of WO<sub>3</sub> depend on different synthesis methods and ambient

temperature. The  $\gamma$ -WO<sub>3</sub> (JCPDS 72-1465) and h-WO<sub>3</sub> (JCPDS 85-2459) are the most stable phases at room temperature. The band gap of WO<sub>3</sub> is ~ 2.7 eV. WO<sub>3</sub> is stable in the acid solution and will dissolve in the alkaline electrolyte.

In the past decades, the research of WO<sub>3</sub> mainly focused on the field of electrochromics and photocatalysis. Over recent years, scientific researchers have found that WO<sub>3</sub> is also an active material for EES as the new findings deepened our knowledge of electrochromics, which is an electrochemical process associated with ion/electron transfer in nature. Compared to other metal oxides, the published literature of WO<sub>3</sub> is still not much, but a growing number of papers are dedicated to the solution-based synthetic methods for the synthesis of WO<sub>3</sub> and its composites for EES.

### 8.1 Hydrothermal synthesis of tungsten oxides and tungsten oxides-based composites

To date, most of the nanostructured WO<sub>3</sub> for EES have been fabricated by HT method, which is classified into two types according to different mechanism and tungsten sources: Na<sub>2</sub>WO<sub>4</sub> and metal W. For the first one, the HT-WO<sub>3</sub> uses Na<sub>2</sub>WO<sub>4</sub> and HC as the starting materials and the WO<sub>3</sub> precipitation from a in a concentrated acid solution containing tungsten ion. The reactions are described as follows.<sup>179, 434</sup>



Different WO<sub>3</sub> nanostructures and composites such as nanoflake, nanowire, nanoplate, nanoflowers WO<sub>3</sub>/SnO<sub>2</sub> and WO<sub>3</sub>/graphene have been prepared by this HT method and applied as active materials for EES.<sup>435-439</sup> It is noteworthy that the WO<sub>3</sub> nanowires can be formed with the help of (NH<sub>4</sub>)<sub>2</sub>SO<sub>4</sub> and each nanowire is a hexagonal single crystal and their long axes are oriented toward the [0001] direction. in the presence of an appropriate amount of ammonium sulfate in the solution, WO<sub>3</sub> primary particles aggregate along the [0001] direction of the h-WO<sub>3</sub> unit cell via self-assembly, because sulfate ions preferentially adsorb on the faces parallel to the c-axis of the WO<sub>3</sub> nanocrystal and thus 1D single crystal

nanowires are finally formed.<sup>179, 435</sup> These WO<sub>3</sub> based nanostructures show quite good electrochemical performances. The ordered WO<sub>3</sub> nanowire arrays on carbon cloth exhibit a high specific capacitance of 521 F g<sup>-1</sup> at 1 A g<sup>-1</sup> (Figure 22).<sup>435</sup> The WO<sub>3</sub>/graphene nanocomposite electrode delivers a reversible lithium storage capacity of 656 mAh g<sup>-1</sup> after 100 cycle at 100 mA g<sup>-1</sup> and an enhanced cyclability compared with the bare WO<sub>3</sub> nanowires electrode.<sup>439</sup> The obtained capacitance and capacity are comparable to those of other metal oxides.<sup>3, 4, 440</sup>

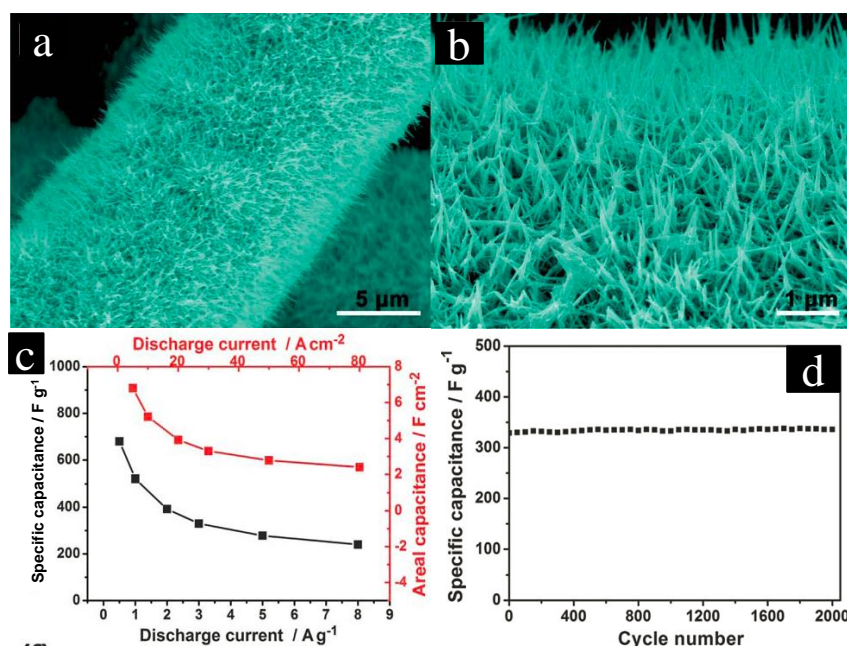
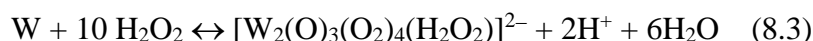


**Figure 22** (a, b) SEM images of the hydrothermal synthesized WO<sub>3</sub> nanowire arrays on the carbon cloth. (c) Pseudocapacitive rate capability and (d) cycling life of the WO<sub>3</sub> nanowire array electrode. Reproduced with permission from Ref. 435.

The other HT can be called sol-based HT method, which first prepares WO<sub>3</sub> sols by reacting metal W with H<sub>2</sub>O<sub>2</sub>. Then the WO<sub>3</sub> sols are treated in HT condition to form WO<sub>3</sub> nanomaterials. The possible reactions about is very complex, may be as below.<sup>441-443</sup>

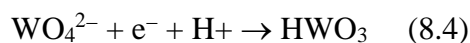


The hexagonal WO<sub>3</sub> nanostructures are fabricated by the sol-based HT and show a discharge capacity of 215 mAh g<sup>-1</sup>.<sup>442, 443</sup> The first HT method is much easier than the second one, which is tedious and difficult for the preparation of sols.

## 8.2 Other solution-based synthesis of tungsten oxides and tungsten oxides-based composites

Though lots of papers about  $\text{WO}_3$  have been reported for electrochromic and catalytic applications, there are only a few papers about  $\text{WO}_3$  prepared by other solution-based methods (such as sol-gel, electro-deposition and microwave synthesis) for EES. Therefore, we will introduce them together in this section.

Zou et al. reported a  $\text{WO}_3$ /Polyaniline composite prepared by a cathodic electro-deposition method and a specific capacitance of  $168 \text{ F g}^{-1}$ .<sup>444</sup> The W sources are usually tungstic acid or tungstate such as  $\text{Na}_2\text{WO}_4$ . The formed precursor in the ED is  $\text{HWO}_3$  with blue color with reactions shown as below.



The precursor  $\text{HWO}_3$  will change into amorphous  $\text{WO}_3$  after dehydrogenation under anodic potential. The reaction mechanism of Sol-gel  $\text{WO}_3$  is similar to that of above sol-based HT, but the W source is not limited in metal W, can also be other tungstate.  $\text{V}_2\text{O}_5$ - $\text{WO}_3$  and  $\text{RuO}$ - $\text{WO}_3$  composites have been fabricated and showed enhance LIBs and supercapacitor performances due to the synergistic effect between  $\text{V}_2\text{O}_5$ ,  $\text{RuO}$  and  $\text{WO}_3$ .<sup>445, 446</sup> Additionally, a crystalline tungsten oxide mixtures,  $\text{WO}_3$ - $\text{WO}_3 \cdot 0.5\text{H}_2\text{O}$  is prepared by a microwave synthesis for supercapacitor with a capacitance of  $290 \text{ F g}^{-1}$ .<sup>447</sup>

## 9. Conclusions and perspectives

Electrochemical energy storage devices and systems are playing an important role in developing a secure and green energy future of human society. The performance of EES systems, both lithium ion batteries and supercapacitors, is mainly determined by the electrode materials. Among the electrode materials studied so far, metal oxides based electrodes can provide high energy density with Faradic reaction, thus have drawn much attention for next-generation high-performance EES devices. In the past decades, the nanoscale metal oxides

and their composites have elicited much interest due to their distinctive structural features and intriguing properties. Generally, compared to bulk materials, nanostructured metal oxides can provide many merits, including enlarged electrode/electrolyte contact area for reactions, short ion diffusion distance and better charge transfer kinetics.

<b>Methods</b>	<b>Applicable objects</b>	<b>Merits</b>	<b>Demerits</b>
Electro-deposition (ED)	Nanostructured films	Easy control in morphology, Relatively fast	Unsuitable for large-scale production
Chemical precipitation (CP)	Powders, colloidal nanostructures	Fast deposition, Large-scale production	Difficult in morphology control
Microwave synthesis (MS)	Powders, colloidal nanostructures	Much faster than CP, Large-scale production	Difficult in morphology control
Sol-gel	Nanostructured film and powders	Large-scale production	Unwanted dense film without using template, so difficult in producing porous films
Hydrothermal and solvothermal synthesis (HT, ST)	Nanostructured film and powders	Easy control in morphology, Large-scale production	High temperature, Slow growth
Chemical bath deposition (CBD)	Nanostructured film and powders	Easy control in morphology, Large-scale production, Faster than HT and ST	Limited to a few metal oxides

**Table 1** Merits and demerits of different solution-based methods

To date, a wide range of solution-based synthesis methods have been developed to prepare high-quality metal oxides and metal oxide-based composites for EES applications. Each method has its own advantages and disadvantages (**Table 1**). These solution-based synthesis

methods usually can be combined smartly to construct non-conventional nanostructures with tailored morphologies and functions. ED is usually used to prepare film samples and the deposition process is easy to control, but ED is not favorable for large-scale production. In contrast to ED, CP is suitable for fabrication of powder products and easy for large-scale deposition, but the morphology of samples is difficult to precisely control due to the fast CP reaction. MS can be considered a special CP method, which is conducted in microwave oven. Its reaction rate is much faster than the common CP. Similar to CP, sol-gel is also a method for large-scale production, but sol-gel is not limited in powder products and can be extended to prepare film samples. However, the sol-gel-film always shows a dense and flat morphology without other porous templates. EPD is only used for the preparation of films, while it usually needs organic solvents and high working voltage above 50 V. HT and ST can be for both powder and film samples, but they need high reaction temperature and the reactions are required to be conducted in sealed vessels.

After analysing the published literature, notice the fact that heavy research is focused on metal oxides based composites with CNT, graphene, porous metal, conducting polymers. These modifications are aiming at improving the ion/electron transportation characteristic of metal oxides and obtaining high energy and power densities. It is well accepted that the EES systems involve electrochemical process with charge transfer and ion diffusion. Unfortunately, most of the active electrode materials (e.g., NiO, MnO<sub>2</sub>, Co<sub>3</sub>O<sub>4</sub> and Fe<sub>2</sub>O<sub>3</sub>) are p-type semiconductors whose electric conductivity is too low to support fast electron transport required by high rates. Therefore, great efforts are dedicated to ameliorating the electrochemical activity and kinetic feature of metal oxides by designing composite materials with other highly conductive layers or scaffolds.

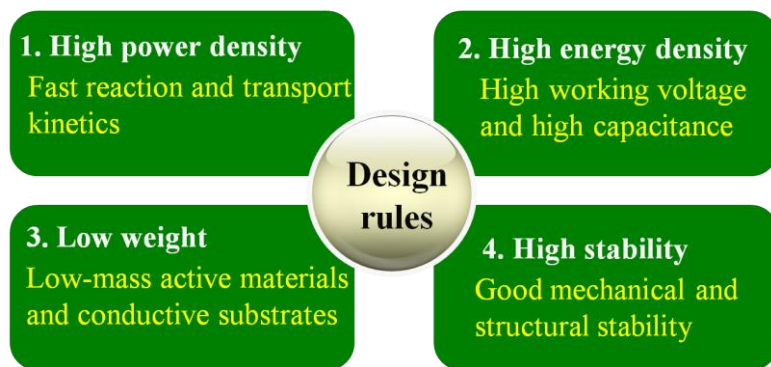


**Figure 23** Proposed basic rules for designing high-performance electrodes for supercapacitors.

In view of such context, it becomes necessary to think about this question: What are the general principles or guidelines for designing advanced electrode materials? Of course, the rules for supercapacitors and LIBs are kind of different due to their different electrochemical reactions. In the following, we propose the basic rules for designing high-performance electrodes of supercapacitors (see also Figure 23),<sup>3, 5, 448</sup> which can be summarized as four and elaborated as follows.

Rule 1: High power density. This is the most important rule and the prerequisite for high-performance supercapacitors. Supercapacitors are unique because of their high power density, fast recharge capability and long cycle life. The power density is controlled by the kinetic feature of the electrodes, which is tightly related to the transport characteristics of ions and electrons in electrodes and at the electrode/electrolyte interfaces.<sup>448</sup> Therefore, electrodes with porous nanostructures and good conductivity are highly desirable, especially the combination of these two is indispensable for high power density. Porous nanostructures are favorable for fast ion/electron transfer and facilitate the sufficient contact between electrolyte and active materials leading to fast reaction kinetics. As for the conductivity issue, the active materials with high conductivity will show low polarization and accelerate reaction kinetics. In this regard, researchers generally adopt conductive scaffolds or conductive coatings to improve the conductivity of the whole electrode to obtain faster reaction kinetics and enhanced performances.

Rule 2: High capacitance and high working voltage. The energy density ( $E$ ) of a supercapacitor is governed by the equation:  $E = \frac{1}{2}CV^2$  (where  $C$  and  $V$  represent the capacitance of the electrode and the potential across the electrode, respectively).<sup>3, 448</sup> In this context, an effective way to boost energy density is to develop electrode materials with high capacitance and high working voltage. To achieve high capacitances, firstly, we have to select active materials with high capacitances. Previous research about active materials of supercapacitors is heavily focused on pure carbon materials, but their specific capacitances are not high enough and encumber the energy density. Then the scientific community shifts its attention to pseudocapacitive materials (such as metal oxides/hydroxides, metal sulfides and conducting polymers),<sup>5, 7, 237</sup> whose specific capacitances are several times larger than carbon materials. Nevertheless, most of pseudocapacitive materials are p-type semiconductors whose conductivity is low and not kinetically favorable for fast electron transfer in high-rate capability. Fortunately, it is found that the two design strategies for high power density in Rule 1 are also applicable for improving capacitance. The porous nanostructure design (porous construction of pseudocapacitive materials) and conductivity modification (combination between pseudocapacitive materials and highly conductive backbones) can effectively improve the utilization of active materials resulting in higher capacitance. As for the working voltage, it depends on several factors including the intrinsic electrochemical reactions of active materials, electrolyte species and macroscopic structure of supercapacitors. Generally, asymmetric supercapacitors exhibit higher working voltage than the symmetric ones.

Rule 3: Lighter the better. The mass unit of energy density and power density is Wh/kg and W/kg, respectively. This means that the energy density and power density will be much higher if the weight of the electrode is low. In commercial supercapacitors, the conductive substrates are metal foams or foils (such as nickel foam or aluminum foil) that do not contribute to the capacitance, but just as a support for active materials. Their weight will

account for a large portion in the device and decrease the overall energy density and power density. Fortunately, benefiting from the advancement of superlight graphene/graphite technologies,<sup>8, 270</sup> three-dimensional (3D) porous graphene or graphite foams have attracted great attention and become promising new light-weight substrates with high conductivity and chemical stability.<sup>449</sup>

Rule 4: High structural stability. A supercapacitor requires a long cycling life more than  $10^4$  times, so the electrode materials must have strong mechanical and structural stability to reach high cycling life. It has been demonstrated that nanoarrays grown directly on substrates possess good mechanical and structural stability during cycling compared to powders. Particularly, a core/shell nanowire array not only has the merits of porous structure, but also possesses good strain accommodation during cycles resulting in high cycling life.<sup>101, 450</sup>

Based on the rules above, the ideal electrode materials for supercapacitors should be highly porous, conductive, light, highly active and stable. Most of the rules are also applicable for LIBs except the Rule 1. It is noteworthy that the energy density of LIBs is the core characteristics, not the power density. Any design strategy should not sacrifice the energy density of LIBs. Last but not least, experimental and theoretical fundamental studies on ion/electron transport behavior at the surface and cross-electrode under device working conditions can be of also great help in both electrode design and device configuration.

### **Acknowledgements**

H. J. Fan thanks the financial support by SERC Public Sector Research Funding (Grant number 1121202012), Agency for Science, Technology, and Research (A\*STAR) and MOE AcRF Tier 1 (RG 66/11). Support from the Energy Research Institute @NTU (ERI@N) is also great appreciated. J. P. Tu thanks the financial supported by the National Science and Technology Support Program (2012BAK30B04-05) and Key Science and Technology Innovation Team of Zhejiang Province (2010R50013).

## Notes and References

1. J. M. Tarascon and M. Armand, *Nature*, 2001, **414**, 359-367.
2. X. Xia, D. Chao, X. Qi, Q. Xiong, Y. Zhang, J. Tu, H. Zhang and H. J. Fan, *Nano Lett.*, 2013, **13**, 4562-4568.
3. J. R. Miller and P. Simon, *Science*, 2008, **321**, 651-652.
4. P. Poizot, S. Laruelle, S. Grugeon, L. Dupont and J. M. Tarascon, *Nature*, 2000, **407**, 496-499.
5. G. P. Wang, L. Zhang and J. J. Zhang, *Chem. Soc. Rev.*, 2012, **41**, 797-828.
6. Q. Zhang, E. Uchaker, S. L. Candelaria and G. Cao, *Chem. Soc. Rev.*, 2013, **42**, 3127-3171.
7. Y. Zhang, H. Feng, X. B. Wu, L. Z. Wang, A. Q. Zhang, T. C. Xia, H. C. Dong, X. F. Li and L. S. Zhang, *Int. J. Hydrogen. Energ.*, 2009, **34**, 4889-4899.
8. C. H. Xu, B. H. Xu, Y. Gu, Z. G. Xiong, J. Sun and X. S. Zhao, *Energy Environ. Sci.*, 2013, **6**, 1388-1414.
9. E. Frackowiak and F. Beguin, *Carbon*, 2001, **39**, 937-950.
10. B. Sakintuna, F. Lamari-Darkrim and M. Hirscher, *Int. J. Hydrogen. Energ.*, 2007, **32**, 1121-1140.
11. R. Dash, J. Chmiola, G. Yushin, Y. Gogotsi, G. Laudisio, J. Singer, J. Fischer and S. Kucheyev, *Carbon*, 2006, **44**, 2489-2497.
12. D. Choi, G. E. Blomgren and P. N. Kumta, *Adv. Mater.*, 2006, **18**, 1178-1182.
13. A. S. Arico, P. Bruce, B. Scrosati, J. M. Tarascon and W. Van Schalkwijk, *Nat. Mater.*, 2005, **4**, 366-377.
14. C. W. Cheng and H. J. Fan, *Nano Today*, 2012, **7**, 327-343.
15. X. L. Ji, K. T. Lee and L. F. Nazar, *Nat. Mater.*, 2009, **8**, 500-506.
16. J. Hassoun and B. Scrosati, *Angew. Chem. Int. Edit.*, 2010, **49**, 2371-2374.
17. C. K. Chan, H. L. Peng, G. Liu, K. McIlwrath, X. F. Zhang, R. A. Huggins and Y. Cui, *Nat. Nanotech.*, 2008, **3**, 31-35.
18. L. F. Cui, Y. Yang, C. M. Hsu and Y. Cui, *Nano Lett.*, 2009, **9**, 3370-3374.
19. L. F. Cui, R. Ruffo, C. K. Chan, H. L. Peng and Y. Cui, *Nano Lett.*, 2009, **9**, 491-495.
20. H. Nagayama, H. Honda and H. Kawahara, *J. Electrochem. Soc.*, 1988, **135**, 2013-2016.
21. X. H. Xia, J. P. Tu, J. Zhang, X. L. Wang, W. K. Zhang and H. Huang, *Electrochim. Acta*, 2008, **53**, 5721-5724.
22. X. H. Xia, J. P. Tu, J. Zhang, X. L. Wang, W. K. Zhang and H. Huang, *Sol. Energ. Mat. Sol. C.*, 2008, **92**, 628-633.
23. X. H. Huang, J. P. Tu, X. H. Xia, X. L. Wang, J. Y. Xiang and L. Zhang, *J. Power Sources*, 2010, **195**, 1207-1210.
24. X. H. Huang, J. P. Tu, X. H. Xia, X. L. Wang, J. Y. Xiang, L. Zhang and Y. Zhou, *J. Power Sources*, 2009, **188**, 588-591.
25. X. H. Huang, J. P. Tu, Z. Y. Zeng, J. Y. Xiang and X. B. Zhao, *J. Electrochem. Soc.*, 2008, **155**, A438-A441.
26. X. H. Huang, J. P. Tu, X. H. Xia, X. L. Wang and J. Y. Xiang, *Electrochem. Commun.*, 2008, **10**, 1288-1290.
27. X. H. Xia, J. P. Tu, X. L. Wang, C. D. Gu and X. B. Zhao, *J. Mater. Chem.*, 2011, **21**, 671-679.
28. X. H. Xia, J. P. Tu, Y. J. Mai, R. Chen, X. L. Wang, C. D. Gu and X. B. Zhao, *Chem-eur. J.*, 2011, **17**, 10898-10905.
29. X. Y. Yan, X. L. Tong, J. Wang, C. W. Gong, M. G. Zhang and L. P. Liang, *Mater. Lett.*, 2013, **95**, 1-4.
30. J. B. Wu, Z. G. Li and Y. Lin, *Electrochim. Acta*, 2011, **56**, 2116-2121.
31. X. H. Xia, J. P. Tu, Y. Q. Zhang, X. L. Wang, C. D. Gu, X. B. Zhao and H. J. Fan, *ACS Nano*, 2012, **6**, 5531-5538.
32. J. B. Wu, R. Q. Guo, X. H. Huang and Y. Lin, *J. Power Sources*, 2013, **243**, 317-322.
33. Y. J. Mai, X. H. Xia, R. Chen, C. D. Gu, X. L. Wang and J. P. Tu, *Electrochim. Acta*, 2012, **67**, 73-78.

34. J. Fang, Y. F. Yuan, L. K. Wang, H. L. Ni, H. L. Zhu, J. S. Gui, J. L. Yang, Y. B. Chen and S. Y. Guo, *Mater. Lett.*, 2013, **111**, 1-4.
35. Q. Q. Xiong, J. P. Tu, X. H. Xia, X. Y. Zhao, C. D. Gu and X. L. Wang, *Nanoscale*, 2013, **5**, 7906-7912.
36. Y. G. Li, B. Tan and Y. Y. Wu, *Chem. Mater.*, 2008, **20**, 2602-2602.
37. Y. Q. Zhang, X. H. Xia, J. P. Tu, Y. J. Mai, S. J. Shi, X. L. Wang and C. D. Gu, *J. Power Sources*, 2012, **199**, 413-417.
38. J. Zhong, X. L. Wang, X. H. Xia, C. D. Gu, J. Y. Xiang, J. Zhang and J. P. Tu, *J. Alloy. Compd.*, 2011, **509**, 3889-3893.
39. J. H. Zhu, J. A. Jiang, J. P. Liu, R. M. Ding, H. Ding, Y. M. Feng, G. M. Wei and X. T. Huang, *J. Solid State Chem.*, 2011, **184**, 578-583.
40. A. Pan, H. B. Wu, L. Yu, T. Zhu and X. W. Lou, *ACS Appl. Mater. Interfaces*, 2012, **4**, 3874-3879.
41. Y. Z. Zheng, H. Y. Ding and M. L. Zhang, *Mater. Res. Bull.*, 2009, **44**, 403-407.
42. L. Fan, L. Tang, H. F. Gong, Z. H. Yao and R. Guo, *J. Mater. Chem.*, 2012, **22**, 16376-16381.
43. Y. Q. Zou and Y. Wang, *Nanoscale*, 2011, **3**, 2615-2620.
44. S. B. Ni, T. Li, X. H. Lv, X. L. Yang and L. L. Zhang, *Electrochim. Acta*, 2013, **91**, 267-274.
45. C. H. Luo, W. L. Lu, Y. Li, Y. Y. Feng, W. Feng, Y. H. Zhao and X. Y. Yuan, *Appl. Phys. A-mater.*, 2013, **113**, 683-692.
46. M. M. Liu, J. Chang, J. Sun and L. Gao, *RSC Adv.*, 2013, **3**, 8003-8008.
47. Y. G. Zhu, G. S. Cao, C. Y. Sun, J. Xie, S. Y. Liu, T. J. Zhu, X. B. Zhao and H. Y. Yang, *RSC Adv.*, 2013, **3**, 19409-19415.
48. Q. Li, Y. J. Chen, T. Yang, D. N. Lei, G. H. Zhang, L. Mei, L. B. Chen, Q. H. Li and T. H. Wang, *Electrochim. Acta*, 2013, **90**, 80-89.
49. H. Liu and W. Yang, *Energy Environ. Sci.*, 2011, **4**, 4000.
50. J. M. Ma, J. Q. Yang, L. F. Jiao, Y. H. Mao, T. H. Wang, X. C. Duan, J. B. Lian and W. J. Zheng, *CrystEngComm*, 2012, **14**, 453-459.
51. A. K. Mondal, D. W. Su, Y. Wang, S. Q. Chen, Q. Liu and G. X. Wang, *J. Alloy. Compd.*, 2014, **582**, 522-527.
52. Q. F. Wu, Z. H. Hu and Y. F. Liu, *J. Mater. Eng. Perform.*, 2013, **22**, 2398-2402.
53. Z. H. Zhu, J. Ping, X. P. Huang, J. G. Hu, Q. Y. Chen, X. B. Ji and C. E. Banks, *J. Mater. Sci.*, 2012, **47**, 503-507.
54. D. W. Wang, F. Li and H. M. Cheng, *J. Power Sources*, 2008, **185**, 1563-1568.
55. Q. F. Wu, Y. F. Liu and Z. H. Hu, *J. Solid State Electr.*, 2013, **17**, 1711-1716.
56. Y. G. Li and Y. Y. Wu, *Chem. Mater.*, 2010, **22**, 5537-5542.
57. X. H. Xia, J. P. Tu, J. Y. Xiang, X. H. Huang, X. L. Wang and X. B. Zhao, *J. Power Sources*, 2010, **195**, 2014-2022.
58. D. W. Su, H. S. Kim, W. S. Kim and G. X. Wang, *Chem-eur. J.*, 2012, **18**, 8224-8229.
59. X. H. Wang, L. Qiao, X. L. Sun, X. W. Li, D. K. Hu, Q. Zhang and D. Y. He, *J. Mater. Chem. A*, 2013, **1**, 4173-4176.
60. J. T. Zai, C. Yu, L. Q. Tao, M. Xu, Y. L. Xiao, B. Li, Q. Y. Han, K. X. Wang and X. F. Qian, *CrystEngComm*, 2013, **15**, 6663-6671.
61. Z.-l. Wang, D. Xu, L.-m. Wang and X.-b. Zhang, *ChemPlusChem*, 2012, **77**, 124-128.
62. M. M. Liu, J. Chang, J. Sun and L. Gao, *Electrochim. Acta*, 2013, **107**, 9-15.
63. M. S. Wu and C. H. Yang, *Appl. Phys. Lett.*, 2007, **91**, 033109 - 033109-033103
64. M. S. Wu and Y. P. Lin, *Electrochim. Acta*, 2011, **56**, 2068-2073.
65. M. S. Wu and H. H. Hsieh, *Electrochim. Acta*, 2008, **53**, 3427-3435.
66. M. S. Wu, Y. A. Huang, C. H. Yang and H. H. Jow, *Int. J. Hydrogen. Energ.*, 2007, **32**, 4153-4159.
67. M. S. Wu and M. J. Wang, *Electrochem. Solid St.*, 2010, **13**, A1-A3.
68. M. S. Wu, M. J. Wang and J. J. Jow, *J. Power Sources*, 2010, **195**, 3950-3955.
69. Y. F. Yuan, X. H. Xia, J. B. Wu, J. L. Yang, Y. B. Chen and S. Y. Guo, *Electrochem. Commun.*, 2010, **12**, 890-893.
70. X. H. Wang, Z. B. Yang, X. L. Sun, X. W. Li, D. S. Wang, P. Wang and D. Y. He, *J. Mater. Chem.*, 2011, **21**, 9988-9990.
71. S. G. Hwang, G. O. Kim, S. R. Yun and K. S. Ryu, *Electrochim. Acta*, 2012, **78**, 406-411.
72. K. Liang, X. Z. Tang and W. C. Hu, *J. Mater. Chem.*, 2012, **22**, 11062-11067.

73. M. S. Wu, D. S. Chan, K. H. Lin and J. J. Jow, *Mater. Chem. Phys.*, 2011, **130**, 1239-1245.
74. M. S. Wu, C. Y. Huang and K. H. Lin, *J. Power Sources*, 2009, **186**, 557-564.
75. U. M. Patil, R. R. Salunkhe, K. V. Gurav and C. D. Lokhande, *Appl. Surf. Sci.*, 2008, **255**, 2603-2607.
76. M. W. Xu, S. J. Bao and H. L. Li, *J. Solid State Electr.*, 2007, **11**, 372-377.
77. M. P. Yeager, D. Su, N. S. Marinkovic and X. W. Teng, *J. Electrochem. Soc.*, 2012, **159**, A1598-A1603.
78. F. B. Zhang, Y. K. Zhou and H. L. Li, *Mater. Chem. Phys.*, 2004, **83**, 260-264.
79. L. Yuan, Z. P. Guo, K. Konstantinov, P. Munroe and H. K. Liu, *Electrochem. Solid St*, 2006, **9**, A524-A528.
80. D. D. Han, P. C. Xu, X. Y. Jing, J. Wang, D. L. Song, J. Y. Liu and M. L. Zhang, *J. Solid State Chem.*, 2013, **203**, 60-67.
81. D. D. Han, P. C. Xu, X. Y. Jing, J. Wang, P. P. Yang, Q. H. Shen, J. Y. Liu, D. L. Song, Z. Gao and M. L. Zhang, *J. Power Sources*, 2013, **235**, 45-53.
82. Q. Li, H. F. Ni, Y. Cai, X. Y. Cai, Y. J. Liu, G. Chen, L. Z. Fan and Y. D. Wang, *Mater. Res. Bull.*, 2013, **48**, 3518-3526.
83. C. Z. Yuan, L. R. Hou, Y. L. Feng, S. L. Xiong and X. G. Zhang, *Electrochim. Acta*, 2013, **88**, 507-512.
84. S. M. Abbas, S. T. Hussain, S. Ali, K. S. Munawar, N. Ahmad and N. Ali, *Mater. Lett.*, 2013, **107**, 158-161.
85. L. Q. Tao, J. T. Zai, K. X. Wang, Y. H. Wan, H. J. Zhang, C. Yu, Y. L. Xiao and X. F. Qian, *RSC Adv.*, 2012, **2**, 3410-3415.
86. M. S. Wu and H. W. Chang, *J. Phys. Chem. C*, 2013, **117**, 2590-2599.
87. X. J. Zhu, J. Hu, H. L. Dai, L. Ding and L. Jiang, *Electrochim. Acta*, 2012, **64**, 23-28.
88. A. S. Adekunle, K. I. Ozoemena, B. B. Mamba, B. O. Agboola and O. S. Oluwatobi, *International Journal of Electrochemical Science*, 2011, **6**, 4760-4774.
89. J. Xu, X. F. Gu, J. Y. Cao, W. C. Wang and Z. D. Chen, *J. Solid State Electr.*, 2012, **16**, 2667-2674.
90. X. H. Huang, J. P. Tu, C. Q. Zhang and F. Zhou, *Electrochim. Acta*, 2010, **55**, 8981-8985.
91. S. I. Kim, J. S. Lee, H. J. Ahn, H. K. Song and J. H. Jang, *ACS Appl. Mater. Interfaces*, 2013, **5**, 1596-1603.
92. M. C. Liu, L. B. Kong, C. Lu, X. M. Li, Y. C. Luo and L. Kang, *ACS Appl. Mater. Interfaces*, 2012, **4**, 4631-4636.
93. A. K. Rai, L. T. Anh, C. J. Park and J. Kim, *Ceram. Int.*, 2013, **39**, 6611-6618.
94. N. Behm, D. Brokaw, C. Overson, D. Peloquin and J. C. Poler, *J. Mater. Sci.*, 2013, **48**, 1711-1716.
95. C. Y. Cao, W. Guo, Z. M. Cui, W. G. Song and W. Cai, *J. Mater. Chem.*, 2011, **21**, 3204-3209.
96. Y. Ren and L. A. Gao, *J. Am. Ceram. Soc.*, 2010, **93**, 3560-3564.
97. S. Vijayakumar, S. Nagamuthu and G. Muralidharan, *ACS Appl. Mater. Interfaces*, 2013, **5**, 2188-2196.
98. J. P. Liu, J. Jiang, C. W. Cheng, H. X. Li, J. X. Zhang, H. Gong and H. J. Fan, *Adv. Mater.*, 2011, **23**, 2076-2081.
99. X. H. Xia, J. P. Tu, Y. Q. Zhang, J. Chen, X. L. Wang, C. D. Gu, C. Guan, J. S. Luo and H. J. Fan, *Chem. Mater.*, 2012, **24**, 3793-3799.
100. C. Guan, J. P. Liu, C. W. Cheng, H. X. Li, X. L. Li, W. W. Zhou, H. Zhang and H. J. Fan, *Energy Environ. Sci.*, 2011, **4**, 4496-4499.
101. C. Guan, X. H. Xia, N. Meng, Z. Y. Zeng, X. H. Cao, C. Soci, H. Zhang and H. J. Fan, *Energy Environ. Sci.*, 2012, **5**, 9085-9090.
102. J. Chen, X. H. Xia, J. P. Tu, Q. Q. Xiong, Y. X. Yu, X. L. Wang and C. D. Gu, *J. Mater. Chem.*, 2012, **22**, 15056-15061.
103. X. H. Xia, J. P. Tu, Y. Q. Zhang, Y. J. Mai, X. L. Wang, C. D. Gu and X. B. Zhao, *RSC Adv.*, 2012, **2**, 1835-1841.
104. J. Jiang, J. P. Liu, R. M. Ding, X. X. Ji, Y. Y. Hu, X. Li, A. Z. Hu, F. Wu, Z. H. Zhu and X. T. Huang, *J. Phys. Chem. C*, 2010, **114**, 929-932.
105. X. Y. Xue, S. A. Yuan, L. L. Xing, Z. H. Chen, B. He and Y. J. Chen, *Chem. Commun.*, 2011, **47**, 4718-4720.

106. J. H. Kwak, Y. W. Lee and J. H. Bang, *Mater. Lett.*, 2013, **110**, 237-240.
107. F. D. Wu and Y. Wang, *J. Mater. Chem.*, 2011, **21**, 6636-6641.
108. D. Fang, L. C. Li, W. L. Xu, G. Z. Li, G. Li, N. F. Wang, Z. P. Luo, J. Xu, L. Liu, C. L. Huang, C. W. Liang and Y. S. Ji, *J. Mater. Chem. A*, 2013, **1**, 13203-13208.
109. J. Liu, Y. C. Zhou, C. P. Liu, J. B. Wang, Y. Pan and D. F. Xue, *CrystEngComm*, 2012, **14**, 2669-2674.
110. L. Li, K. H. Seng, Z. X. Chen, Z. P. Guo and H. K. Liu, *Nanoscale*, 2013, **5**, 1922-1928.
111. X. C. Dong, H. Xu, X. W. Wang, Y. X. Huang, M. B. Chan-Park, H. Zhang, L. H. Wang, W. Huang and P. Chen, *ACS Nano*, 2012, **6**, 3206-3213.
112. L. Yang, S. Cheng, Y. Ding, X. B. Zhu, Z. L. Wang and M. L. Liu, *Nano Lett.*, 2012, **12**, 321-325.
113. X. H. Xia, J. P. Tu, Y. J. Mai, X. L. Wang, C. D. Gu and X. B. Zhao, *J. Mater. Chem.*, 2011, **21**, 9319-9325.
114. C. Zhou, Y. W. Zhang, Y. Y. Li and J. P. Liu, *Nano Lett.*, 2013, **13**, 2078-2085.
115. G. M. Wang, X. H. Lu, Y. C. Ling, T. Zhai, H. Y. Wang, Y. X. Tong and Y. Li, *ACS Nano*, 2012, **6**, 10296-10302.
116. K. T. Nam, D. W. Kim, P. J. Yoo, C. Y. Chiang, N. Meethong, P. T. Hammond, Y. M. Chiang and A. M. Belcher, *Science*, 2006, **312**, 885-888.
117. H. Qiao, L. F. Xiao, Z. Zheng, H. W. Liu, F. L. Jia and L. Z. Zhang, *J. Power Sources*, 2008, **185**, 486-491.
118. C. Guan, Z. Zeng, X. Li, X. Cao, Y. Fan, X. Xia, G. Pan, H. Zhang and H. J. Fan, *Small*, 2013, n/a-n/a.
119. J. Xu, Q. F. Wang, X. W. Wang, Q. Y. Xiang, B. Hang, D. Chen and G. Z. Shen, *ACS Nano*, 2013, **7**, 5453-5462.
120. H. N. Zhang, Y. J. Chen, W. W. Wang, G. H. Zhang, M. Zhuo, H. M. Zhang, T. Yang, Q. H. Li and T. H. Wang, *J. Mater. Chem. A*, 2013, **1**, 8593-8600.
121. H. Xia, D. D. Zhu, Z. T. Luo, Y. Yu, X. Q. Shi, G. L. Yuan and J. P. Xie, *Scientific Reports*, 2013, **3**, 2978.
122. G. H. Zhang, T. H. Wang, X. Z. Yu, H. N. Zhang, H. G. Duan and B. A. Lu, *Nano Energy*, 2013, **2**, 586-594.
123. C. H. Tang, X. S. Yin and H. Gong, *ACS Appl. Mater. Interfaces*, 2013, **5**, 10574-10582.
124. Y. J. Fu, X. W. Li, X. L. Sun, X. H. Wang, D. Q. Liu and D. Y. He, *J. Mater. Chem.*, 2012, **22**, 17429-17431.
125. S. L. Xiong, C. Z. Yuan, M. F. Zhang, B. J. Xi and Y. T. Qian, *Chem-eur. J.*, 2009, **15**, 5320-5326.
126. G. X. Wang, X. P. Shen, J. Horvat, B. Wang, H. Liu, D. Wexler and J. Yao, *J. Phys. Chem. C*, 2009, **113**, 4357-4361.
127. H. T. Wang, L. Zhang, X. H. Tan, C. M. B. Holt, B. Zahiri, B. C. Olsen and D. Mitlin, *J. Phys. Chem. C*, 2011, **115**, 17599-17605.
128. H. Pang, F. Gao, Q. Chen, R. M. Liu and Q. Y. Lu, *Dalton T.*, 2012, **41**, 5862-5868.
129. F. Zhang, C. Z. Yuan, X. J. Lu, L. J. Zhang, Q. Che and X. G. Zhang, *J. Power Sources*, 2012, **203**, 250-256.
130. H. Y. Sun, M. Ahmad and J. Zhu, *Electrochim. Acta*, 2013, **89**, 199-205.
131. S. B. Zhou, G. Wang, Y. Z. Xie, H. Wang and J. B. Bai, *J Nanopart. Res.*, 2013, **15**.
132. Y. Liu and X. G. Zhang, *Solid State Ionics*, 2013, **231**, 63-68.
133. S. W. Bian and L. Zhu, *RSC Adv.*, 2013, **3**, 4212-4215.
134. X. W. Wang, S. Q. Liu, H. Y. Wang, F. Y. Tu, D. Fang and Y. H. Li, *J. Solid State Electr.*, 2012, **16**, 3593-3602.
135. X. M. Liu, Q. Long, C. H. Jiang, B. B. Zhan, C. Li, S. J. Liu, Q. Zhao, W. Huang and X. C. Dong, *Nanoscale*, 2013, **5**, 6525-6529.
136. L. J. Xie, K. X. Li, G. H. Sun, Z. A. Hu, C. X. Lv, J. L. Wang and C. M. Zhang, *J. Solid State Electr.*, 2013, **17**, 55-61.
137. S. K. Meher and G. R. Rao, *J. Phys. Chem. C*, 2011, **115**, 15646-15654.
138. B. R. Duan and Q. Cao, *Electrochim. Acta*, 2012, **64**, 154-161.
139. Y. Liu, C. H. Mi, L. H. Su and X. G. Zhang, *Electrochim. Acta*, 2008, **53**, 2507-2513.
140. Y. Wang, H. Xia, L. Lu and J. Y. Lin, *ACS Nano*, 2010, **4**, 1425-1432.
141. W. L. Yao, J. Yang, J. L. Wang and Y. Nuli, *J. Electrochem. Soc.*, 2008, **155**, A903-A908.

142. C. Z. Yuan, L. Yang, L. R. Hou, J. Y. Li, Y. X. Sun, X. G. Zhang, L. F. Shen, X. J. Lu, S. L. Xiong and X. W. Lou, *Adv. Funct. Mater.*, 2012, **22**, 2560-2566.
143. W. W. Yuan, D. Xie, Z. M. Dong, Q. M. Su, J. Zhang, G. H. Du and B. S. Xu, *Mater. Lett.*, 2013, **97**, 129-132.
144. G. M. Zhou, L. Li, Q. Zhang, N. Li and F. Li, *Phys. Chem. Chem. Phys.*, 2013, **15**, 5582-5587.
145. C. C. Li, Q. H. Li, L. B. Chen and T. H. Wang, *J. Mater. Chem.*, 2011, **21**, 11867-11872.
146. A. M. Hashem, A. M. Abdel-Latif, H. M. Abuzeid, H. M. Abbas, H. Ehrenberg, R. S. Farag, A. Mauger and C. M. Julien, *J. Alloy. Compd.*, 2011, **509**, 9669-9674.
147. M. X. Liao, Y. F. Liu, Z. H. Hu and Q. Yu, *J. Alloy. Compd.*, 2013, **562**, 106-110.
148. T. Zhu, J. S. Chen and X. W. Lou, *J. Mater. Chem.*, 2010, **20**, 7015-7020.
149. L. R. Hou, C. Z. Yuan, L. Yang, L. F. Shen, F. Zhang and X. G. Zhang, *RSC Adv.*, 2011, **1**, 1521-1526.
150. Q. Wang, C. Y. Zhang, X. B. Xia, L. L. Xing and X. Y. Xue, *Mater. Lett.*, 2013, **112**, 162-164.
151. L. H. Zhuo, Y. Q. Wu, J. Ming, L. Y. Wang, Y. C. Yu, X. B. Zhang and F. Y. Zhao, *J. Mater. Chem. A*, 2013, **1**, 1141-1147.
152. G. X. Wang, X. P. Shen, J. N. Yao, D. Wexler and J. Ahn, *Electrochem. Commun.*, 2009, **11**, 546-549.
153. Y. H. Xiao, S. J. Liu, F. Li, A. Q. Zhang, J. H. Zhao, S. M. Fang and D. Z. Jia, *Adv. Funct. Mater.*, 2012, **22**, 4052-4059.
154. D. H. Zhang and W. B. Zou, *Curr. Appl. Phys.*, 2013, **13**, 1796-1800.
155. K. Deori, S. K. Ujjain, R. K. Sharma and S. Deka, *ACS Appl. Mater. Interfaces*, 2013, **5**, 10665-10672.
156. J. Liu, H. Xia, L. Lu and D. F. Xue, *J. Mater. Chem.*, 2010, **20**, 1506-1510.
157. L. Q. Tao, J. T. Zai, K. X. Wang, H. J. Zhang, M. Xu, J. Shen, Y. Z. Su and X. F. Qian, *J. Power Sources*, 2012, **202**, 230-235.
158. Y. Wang, F. Yan, S. W. Liu, A. Y. S. Tan, H. H. Song, X. W. Sun and H. Y. Yang, *J. Mater. Chem. A*, 2013, **1**, 5212-5216.
159. Z. G. Wen, F. Zheng, Z. R. Jiang, M. X. Li and Y. X. Luo, *J. Mater. Sci.*, 2013, **48**, 342-347.
160. N. Du, H. Zhang, B. Chen, J. B. Wu, X. Y. Ma, Z. H. Liu, Y. Q. Zhang, D. Yang, X. H. Huang and J. P. Tu, *Adv. Mater.*, 2007, **19**, 4505-4509.
161. L. Y. Pan, H. B. Zhao, W. C. Shen, X. W. Dong and J. Q. Xu, *J. Mater. Chem. A*, 2013, **1**, 7159-7166.
162. X. W. Lou, D. Deng, J. Y. Lee, J. Feng and L. A. Archer, *Adv. Mater.*, 2008, **20**, 258-262.
163. H. W. Shim, A. H. Lim, J. C. Kim, E. Jang, S. D. Seo, G. H. Lee, T. D. Kim and D. W. Kim, *Scientific Reports*, 2013, **3**, 2325.
164. X. Zhu, G. Q. Ning, X. L. Ma, Z. J. Fan, C. G. Xu, J. S. Gao, C. M. Xu and F. Wei, *J. Mater. Chem. A*, 2013, **1**, 14023-14030.
165. J. Sun, H. M. Liu, X. Chen, D. G. Evans and W. S. Yang, *Nanoscale*, 2013, **5**, 7564-7571.
166. S. Vijayanand, R. Kannan, H. S. Potdar, V. K. Pillai and P. A. Joy, *J. Appl. Electrochem.*, 2013, **43**, 995-1003.
167. R. Xu, J. W. Wang, Q. Y. Li, G. Y. Sun, E. B. Wang, S. H. Li, J. M. Gu and M. L. Ju, *J. Solid State Chem.*, 2009, **182**, 3177-3182.
168. Y. M. Sun, X. L. Hu, W. Luo and Y. H. Huang, *J. Mater. Chem.*, 2012, **22**, 13826-13831.
169. C. H. Chen, B. J. Hwang, J. S. Do, J. H. Weng, M. Venkateswarlu, M. Y. Cheng, R. Santhanam, K. Ragavendran, J. F. Lee, J. M. Chen and D. G. Liu, *Electrochem. Commun.*, 2010, **12**, 496-498.
170. J. Zhi, S. Deng, Y. X. Zhang, Y. F. Wang and A. G. Hu, *J. Mater. Chem. A*, 2013, **1**, 3171-3176.
171. W. Du, R. M. Liu, Y. W. Jiang, Q. Y. Lu, Y. Z. Fan and F. Gao, *J. Power Sources*, 2013, **227**, 101-105.
172. S. G. Kandalkar, C. D. Lokhande, R. S. Mane and S. H. Han, *Appl. Surf. Sci.*, 2007, **253**, 3952-3956.
173. S. G. Kandalkar, J. L. Gunjekar and C. D. Lokhande, *Appl. Surf. Sci.*, 2008, **254**, 5540-5544.
174. B. J. Li, H. Q. Cao, J. Shao, G. Q. Li, M. Z. Qu and G. Yin, *Inorg. Chem.*, 2011, **50**, 1628-1632.
175. G. L. Wang, J. C. Liu, S. Tang, H. Y. Li and D. X. Cao, *J. Solid State Electr.*, 2011, **15**, 2587-2592.

176. Y. F. Wang and L. J. Zhang, *J. Power Sources*, 2012, **209**, 20-29.
177. M. Zhang, M. Q. Jia, Y. H. Jin and X. R. Shi, *Appl. Surf. Sci.*, 2012, **263**, 573-578.
178. W. W. Zhou, J. P. Liu, T. Chen, K. S. Tan, X. T. Jia, Z. Q. Luo, C. X. Cong, H. P. Yang, C. M. Li and T. Yu, *Phys. Chem. Chem. Phys.*, 2011, **13**, 14462-14465.
179. J. Zhang, J. P. Tu, X. H. Xia, X. L. Wang and C. D. Gu, *J. Mater. Chem.*, 2011, **21**, 5492-5498.
180. H. C. Liu and S. K. Yen, *J. Power Sources*, 2007, **166**, 478-484.
181. S. L. Chou, J. Z. Wang, H. K. Liu and S. X. Dou, *J. Power Sources*, 2008, **182**, 359-364.
182. G. P. Kim, I. Nam, N. D. Kim, J. Park, S. Park and J. Yi, *Electrochem. Commun.*, 2012, **22**, 93-96.
183. V. Srinivasan and J. W. Weidner, *J. Power Sources*, 2002, **108**, 15-20.
184. C. Z. Yuan, L. Yang, L. R. Hou, L. F. Shen, X. G. Zhang and X. W. Lou, *Energy Environ. Sci.*, 2012, **5**, 7883-7887.
185. Y. F. Yuan, X. H. Xia, J. B. Wu, X. H. Huang, Y. B. Pei, J. L. Yang and S. Y. Guo, *Electrochem. Commun.*, 2011, **13**, 1123-1126.
186. X. H. Xia, J. P. Tu, X. L. Wang, C. D. Gu and X. B. Zhao, *Chem. Commun.*, 2011, **47**, 5786-5788.
187. J. B. Wu, Y. Lin, X. H. Xia, J. Y. Xu and Q. Y. Shi, *Electrochim. Acta*, 2011, **56**, 7163-7170.
188. C. W. Kung, H. W. Chen, C. Y. Lin, R. Vittal and K. C. Ho, *J. Power Sources*, 2012, **214**, 91-99.
189. J. H. Zhong, A. L. Wang, G. R. Li, J. W. Wang, Y. N. Ou and Y. X. Tong, *J. Mater. Chem.*, 2012, **22**, 5656-5665.
190. N. A. Kyeremateng, C. Lebouin, P. Knauth and T. Djenizian, *Electrochim. Acta*, 2013, **88**, 814-820.
191. C. Wang, D. L. Wang, Q. M. Wang and L. Wang, *Electrochim. Acta*, 2010, **55**, 6420-6425.
192. C. Lin, J. A. Ritter and B. N. Popov, *J. Electrochem. Soc.*, 1998, **145**, 4097-4103.
193. B. Guo, C. S. Li and Z. Y. Yuan, *J. Phys. Chem. C*, 2010, **114**, 12805-12817.
194. W. L. Yao, J. Q. Chen and H. W. Cheng, *J. Solid State Electr.*, 2011, **15**, 183-188.
195. Y. X. Gu, F. F. Jian and X. Wang, *Thin Solid Films*, 2008, **517**, 652-655.
196. Y. H. Ding, P. Zhang, Z. L. Long, Y. Jiang, J. N. Huang, W. J. Yan and G. Liu, *Mater. Lett.*, 2008, **62**, 3410-3412.
197. J. Park, W. G. Moon, G. P. Kim, I. Nam, S. Park, Y. Kim and J. Yi, *Electrochim. Acta*, 2013, **105**, 110-114.
198. G. Chen, E. G. Fu, M. Zhou, Y. Xu, L. Fei, S. G. Deng, V. Chaitanya, Y. Q. Wang and H. M. Luo, *J. Alloy. Compd.*, 2013, **578**, 349-354.
199. Y. Lu, Y. Wang, Y. Q. Zou, Z. Jiao, B. Zhao, Y. Q. He and M. H. Wu, *Electrochem. Commun.*, 2010, **12**, 101-105.
200. J. Q. Wang, B. Niu, G. D. Du, R. Zeng, Z. X. Chen, Z. P. Guo and S. X. Dou, *Mater. Chem. Phys.*, 2011, **126**, 747-754.
201. S. Q. Chen and Y. Wang, *J. Mater. Chem.*, 2010, **20**, 9735-9739.
202. J. Q. Wang, G. D. Du, R. Zeng, B. Niu, Z. X. Chen, Z. P. Guo and S. X. Dou, *Electrochim. Acta*, 2010, **55**, 4805-4811.
203. C. T. Hsieh, J. S. Lin, Y. F. Chen and H. S. Teng, *J. Phys. Chem. C*, 2012, **116**, 15251-15258.
204. S. Vijayakumar, A. K. Ponnalagi, S. Nagamuthu and G. Muralidharan, *Electrochim. Acta*, 2013, **106**, 500-505.
205. L. Cui, J. Li and X. G. Zhang, *J. Appl. Electrochem.*, 2009, **39**, 1871-1876.
206. J. Yan, T. Wei, W. M. Qiao, B. Shao, Q. K. Zhao, L. J. Zhang and Z. J. Fan, *Electrochim. Acta*, 2010, **55**, 6973-6978.
207. Y. G. Li, B. Tan and Y. Y. Wu, *J. Am. Chem. Soc.*, 2006, **128**, 14258-14259.
208. Y. G. Li, B. Tan and Y. Y. Wu, *Nano Lett.*, 2008, **8**, 265-270.
209. Y. Y. Gao, S. L. Chen, D. X. Cao, G. L. Wang and J. L. Yin, *J. Power Sources*, 2010, **195**, 1757-1760.
210. G. Filipic and U. Cvelbar, *Nanotechnology*, 2012, **23**.
211. J. C. Park, J. Kim, H. Kwon and H. Song, *Adv. Mater.*, 2009, **21**, 803-807.
212. B. Wang, X.-L. Wu, C.-Y. Shu, Y.-G. Guo and C.-R. Wang, *J. Mater. Chem.*, 2010, **20**, 10661-10664.

213. X. Zhang, W. Shi, J. Zhu, D. J. Kharistal, W. Zhao, B. S. Lalia, H. H. Hng and Q. Yan, *ACS Nano*, 2011, **5**, 2013-2019.
214. J. Xiang, J. Tu, Y. Yuan, X. Huang, Y. Zhou and L. Zhang, *Electrochem. Commun.*, 2009, **11**, 262-265.
215. J. Xiang, J. Tu, L. Zhang, Y. Zhou, X. Wang and S. Shi, *J. Power Sources*, 2010, **195**, 313-319.
216. B. Heng, C. Qing, D. Sun, B. Wang, H. Wang and Y. Tang, *RSC Adv.*, 2013, **3**, 15719-15726.
217. J. Xiang, J. Tu, X. Huang and Y. Yang, *J. Solid State Electr.*, 2008, **12**, 941-945.
218. J. Xiang, J. Tu, J. Zhang, J. Zhong, D. Zhang and J. Cheng, *Electrochem. Commun.*, 2010, **12**, 1103-1107.
219. J. Xiang, J. Tu, L. Zhang, Y. Zhou, X. Wang and S. Shi, *Electrochim. Acta*, 2010, **55**, 1820-1824.
220. Y. J. Mai, X. L. Wang, J. Y. Xiang, Y. Q. Qiao, D. Zhang, C. D. Gu and J. P. Tu, *Electrochim. Acta*, 2011, **56**, 2306-2311.
221. S. Ko, J. I. Lee, H. S. Yang, S. Park and U. Jeong, *Adv. Mater.*, 2012, **24**, 4451-4456.
222. J. Y. Lin, J. H. Liao and S. W. Chou, *Electrochim. Acta*, 2011, **56**, 8818-8826.
223. B. Zhao, P. Liu, H. Zhuang, Z. Jiao, T. Fang, W. Xu, B. Lu and Y. Jiang, *J. Mater. Chem. A*, 2013, **1**, 367-373.
224. X. Y. Shen, S. Chen, D. B. Mu, B. R. Wu and F. Wu, *J. Power Sources*, 2013, **238**, 173-179.
225. Z. Wang, F. Su, S. Madhavi and X. W. Lou, *Nanoscale*, 2011, **3**, 1618-1623.
226. J. Xiang, J. Tu, Y. Yuan, X. Wang, X. Huang and Z. Zeng, *Electrochim. Acta*, 2009, **54**, 1160-1165.
227. L. Yu, Y. Jin, L. Li, J. Ma, G. Wang, B. Geng and X. Zhang, *CrystEngComm*, 2013, **15**, 7657-7662.
228. A. Banerjee, U. Singh, V. Aravindan, M. Srinivasan and S. Ogale, *Nano Energy*, 2013, **2**, 1158-1163.
229. S. Gao, S. Yang, J. Shu, S. Zhang, Z. Li and K. Jiang, *J. Phys. Chem. C*, 2008, **112**, 19324-19328.
230. G. S. Gund, D. P. Dubal, D. S. Dhawale, S. S. Shinde and C. D. Lokhande, *RSC Adv.*, 2013, **3**, 24099-24107.
231. W. X. Zhang, X. G. Wen and S. H. Yang, *Inorg. Chem.*, 2003, **42**, 5005-5014.
232. Y. Lee, I. Leu, C. Liao, S. Chang, M. Wu, J. Yen and K. Fung, *Electrochem. Solid St.*, 2006, **9**, A207-A210.
233. X. M. Liu and Y. C. Zhou, *Appl. Phys. A-mater.*, 2005, **81**, 685-689.
234. J. Xiang, X. Wang, X. Xia, L. Zhang, Y. Zhou, S. Shi and J. Tu, *Electrochim. Acta*, 2010, **55**, 4921-4925.
235. A. Goyal, A. L. M. Reddy and P. M. Ajayan, *Small*, 2011, **7**, 1709-1713.
236. M. J. Deng, C. Z. Song, P. J. Ho, C. C. Wang, J. M. Chen and K. T. Lu, *Phys. Chem. Chem. Phys.*, 2013, **15**, 7479-7483.
237. W. F. Wei, X. W. Cui, W. X. Chen and D. G. Ivey, *Chem. Soc. Rev.*, 2011, **40**, 1697-1721.
238. J. L. Liu, L. Z. Fan and X. H. Qu, *Electrochim. Acta*, 2012, **66**, 302-305.
239. Y. Liu, D. Yan, R. F. Zhuo, S. K. Li, Z. G. Wu, J. Wang, P. Y. Ren, P. X. Yan and Z. R. Geng, *J. Power Sources*, 2013, **242**, 78-85.
240. Y. S. Luo, D. Z. Kong, J. S. Luo, S. Chen, D. Y. Zhang, K. W. Qiu, X. Y. Qi, H. Zhang, C. M. Li and T. Yu, *RSC Adv.*, 2013, **3**, 14413-14422.
241. H. Xia, M. O. Lai and L. Lu, *J. Mater. Chem.*, 2010, **20**, 6896-6902.
242. S. W. Bian, Y. P. Zhao and C. Y. Xian, *Mater. Lett.*, 2013, **111**, 75-77.
243. J. X. Zhu, W. H. Shi, N. Xiao, X. H. Rui, H. T. Tan, X. H. Lu, H. H. Hng, J. Ma and Q. Y. Yan, *ACS Appl. Mater. Interfaces*, 2012, **4**, 2769-2774.
244. Z. C. Yang, C. H. Tang, H. Gong, X. Li and J. Wang, *J. Power Sources*, 2013, **240**, 713-720.
245. Y. Wang, Z. J. Han, S. F. Yu, R. R. Song, H. H. Song, K. Ostrikov and H. Y. Yang, *Carbon*, 2013, **64**, 230-236.
246. M. Xu, L. Kong, W. Zhou and H. Li, *J. Phys. Chem. C*, 2007, **111**, 19141-19147.
247. Y. Huang, Y. Y. Li, Z. Q. Hu, G. M. Wei, J. L. Guo and J. P. Liu, *J. Mater. Chem. A*, 2013, **1**, 9809-9813.
248. X. D. Liu, C. Z. Chen, Y. Y. Zhao and B. Jia, *J. Nanomater.*, 2013.

249. V. Subramanian, H. W. Zhu, R. Vajtai, P. M. Ajayan and B. Q. Wei, *J. Phys. Chem. B*, 2005, **109**, 20207-20214.
250. B. Ming, J. Li, F. Kang, G. Pang, Y. Zhang, L. Chen, J. Xu and X. Wang, *J. Power Sources*, 2012, **198**, 428-431.
251. A. Bahloul, B. Nessark, E. Briot, H. Groult, A. Mauger, K. Zaghib and C. M. Julien, *J. Power Sources*, 2013, **240**, 267-272.
252. A. Sumboja, C. Y. Foo, J. Yan, C. Y. Yan, R. K. Gupta and P. S. Lee, *J. Mater. Chem.*, 2012, **22**, 23921-23928.
253. W. Tang, Y. Y. Hou, X. J. Wang, Y. Bai, Y. S. Zhu, H. Sun, Y. B. Yue, Y. P. Wu, K. Zhu and R. Holze, *J. Power Sources*, 2012, **197**, 330-333.
254. X. Wang and Y. D. Li, *J. Am. Chem. Soc.*, 2002, **124**, 2880-2881.
255. P. Yu, X. Zhang, D. L. Wang, L. Wang and Y. W. Ma, *Crst. Growth. Des.*, 2009, **9**, 528-533.
256. Z. J. Sun, H. Y. Chen, D. Shu, C. He, S. Q. Tang and J. Zhang, *J. Power Sources*, 2012, **203**, 233-242.
257. R. S. Kalubarme, H. S. Jadhav and C. J. Park, *Electrochim. Acta*, 2013, **87**, 457-465.
258. D. L. Yan, Z. L. Guo, G. S. Zhu, Z. Z. Yu, H. R. Xu and A. B. Yu, *J. Power Sources*, 2012, **199**, 409-412.
259. X. Zhang, P. Yu, H. T. Zhang, D. C. Zhang, X. Z. Sun and Y. W. Ma, *Electrochim. Acta*, 2013, **89**, 523-529.
260. X. M. Feng, Z. Z. Yan, N. N. Chen, Y. Zhang, Y. W. Ma, X. F. Liu, Q. L. Fan, L. H. Wang and W. Huang, *J. Mater. Chem. A*, 2013, **1**, 12818-12825.
261. Y. Zhao, P. Jiang and S. S. Xie, *J. Power Sources*, 2013, **239**, 393-398.
262. W. Yao, H. Zhou and Y. Lu, *J. Power Sources*, 2013, **241**, 359-366.
263. C. Z. Yuan, L. R. Hou, L. Yang, D. K. Li, L. F. Shen, F. Zhang and X. G. Zhang, *J. Mater. Chem.*, 2011, **21**, 16035-16041.
264. N. A. Tang, X. K. Tian, C. Yang and Z. B. Pi, *Mater. Res. Bull.*, 2009, **44**, 2062-2067.
265. W. Y. Li, Q. Liu, Y. G. Sun, J. Q. Sun, R. J. Zou, G. Li, X. H. Hu, G. S. Song, G. X. Ma, J. M. Yang, Z. G. Chen and J. Q. Hu, *J. Mater. Chem.*, 2012, **22**, 14864-14867.
266. Y. X. Zhang, F. Li and M. Huang, *Mater. Lett.*, 2013, **112**, 203-206.
267. B. J. Zhang, W. Y. Li, J. Q. Sun, G. J. He, R. J. Zou, J. Q. Hu and Z. G. Chen, *Mater. Lett.*, 2014, **114**, 40-43.
268. L. Yu, G. Q. Zhang, C. Z. Yuan and X. W. Lou, *Chem. Commun.*, 2013, **49**, 137-139.
269. W. M. Chen, L. Qie, Q. G. Shao, L. X. Yuan, W. X. Zhang and Y. H. Huang, *ACS Appl. Mater. Interfaces*, 2012, **4**, 3047-3053.
270. J. Jiang, J. H. Zhu, Y. M. Feng, J. P. Liu and X. T. Huang, *Chem. Commun.*, 2012, **48**, 7471-7473.
271. J. Wang, J. Liu, Y. C. Zhou, P. Hodgson and Y. C. Li, *RSC Adv.*, 2013, **3**, 25937-25943.
272. F. Y. Cheng, J. Z. Zhao, W. Song, C. S. Li, H. Ma, J. Chen and P. W. Shen, *Inorg. Chem.*, 2006, **45**, 2038-2044.
273. X. Y. Lang, A. Hirata, T. Fujita and M. W. Chen, *Nat. Nanotech.*, 2011, **6**, 232-236.
274. H. J. Wang, C. Peng, J. D. Zheng, F. Peng and H. Yu, *Mater. Res. Bull.*, 2013, **48**, 3389-3393.
275. Y. F. Yan, Q. L. Cheng, V. Pavlinek, P. Saha and C. Z. Li, *Electrochim. Acta*, 2012, **71**, 27-32.
276. Z. X. Song, W. Liu, M. Zhao, Y. J. Zhang, G. C. Liu, C. Yu and J. S. Qiu, *J. Alloy. Compd.*, 2013, **560**, 151-155.
277. H. J. Huang and X. Wang, *Nanoscale*, 2011, **3**, 3185-3191.
278. Z. S. Wu, W. C. Ren, D. W. Wang, F. Li, B. L. Liu and H. M. Cheng, *ACS Nano*, 2010, **4**, 5835-5842.
279. X. Zhao, L. L. Zhang, S. Murali, M. D. Stoller, Q. H. Zhang, Y. W. Zhu and R. S. Ruoff, *ACS Nano*, 2012, **6**, 5404-5412.
280. X. Y. Xie, C. Zhang, M. B. Wu, Y. Tao, W. Lv and Q. H. Yang, *Chem. Commun.*, 2013, **49**, 11092-11094.
281. V. Subramanian, H. W. Zhu and B. Q. Wei, *Electrochem. Commun.*, 2006, **8**, 827-832.
282. S. J. He, C. X. Hu, H. Q. Hou and W. Chen, *J. Power Sources*, 2014, **246**, 754-761.
283. H. Lai, J. X. Li, Z. G. Chen and Z. G. Huang, *ACS Appl. Mater. Interfaces*, 2012, **4**, 2325-2328.

284. J. X. Li, Y. Zhao, N. Wang, Y. H. Ding and L. H. Guan, *J. Mater. Chem.*, 2012, **22**, 13002-13004.
285. J. Y. Liao, D. Higgins, G. Lui, V. Chabot, X. C. Xiao and Z. W. Chen, *Nano Lett.*, 2013, **13**, 5467-5473.
286. H. Pang, S. M. Wang, G. C. Li, Y. H. Ma, J. Li, X. X. Li, L. Zhang, J. S. Zhang and H. H. Zheng, *J. Mater. Chem. A*, 2013, **1**, 5053-5060.
287. Q. X. Chu, J. Du, W. B. Lu, G. H. Chang, Z. C. Xing, H. Y. Li, C. J. Ge, L. Wang, Y. L. Luo, A. M. Asiri, A. O. Al-Youbi and X. P. Sun, *Chempluschem*, 2012, **77**, 872-876.
288. L. L. Peng, X. Peng, B. R. Liu, C. Z. Wu, Y. Xie and G. H. Yu, *Nano Lett.*, 2013, **13**, 2151-2157.
289. Y. Hou, Y. W. Cheng, T. Hobson and J. Liu, *Nano Lett.*, 2010, **10**, 2727-2733.
290. Q. T. Qu, P. Zhang, B. Wang, Y. H. Chen, S. Tian, Y. P. Wu and R. Holze, *J. Phys. Chem. C*, 2009, **113**, 14020-14027.
291. B. You, N. Li, H. Y. Zhu, X. L. Zhu and J. Yang, *Chemosuschem*, 2013, **6**, 474-480.
292. S. Chen, J. W. Zhu, X. D. Wu, Q. F. Han and X. Wang, *ACS Nano*, 2010, **4**, 2822-2830.
293. M. Kim, Y. Hwang and J. Kim, *J. Power Sources*, 2013, **239**, 225-233.
294. H. J. Zheng, J. X. Wang, Y. Jia and C. A. Ma, *J. Power Sources*, 2012, **216**, 508-514.
295. A. Sumboja, C. Y. Foo, X. Wang and P. S. Lee, *Adv. Mater.*, 2013, **25**, 2809-2815.
296. T. Brousse, P. L. Taberna, O. Crosnier, R. Dugas, P. Guillemet, Y. Scudeller, Y. Zhou, F. Favier, D. Belanger and P. Simon, *J. Power Sources*, 2007, **173**, 633-641.
297. S. Devaraj, G. S. Gabriel, S. R. Gajjela and P. Balaya, *Electrochem. Solid St*, 2012, **15**, A57-A59.
298. C. Y. Wan, M. Cheng, Q. S. Zhang and N. Q. Jia, *Powder Technol.*, 2013, **235**, 706-711.
299. S. Chen, J. W. Zhu, Q. F. Han, Z. J. Zheng, Y. Yang and X. Wang, *Crst. Growth. Des.*, 2009, **9**, 4356-4361.
300. A. M. Hashem, H. M. Abuzeid, A. E. Abdel-Ghany, A. Mauger, K. Zaghbi and C. M. Julien, *J. Power Sources*, 2012, **202**, 291-298.
301. Q. Li, J. M. Anderson, Y. Q. Chen and L. Zhai, *Electrochim. Acta*, 2012, **59**, 548-557.
302. L. Chen, Z. X. Song, G. C. Liu, J. S. Qiu, C. Yu, J. W. Qin, L. Ma, F. Q. Tian and W. Liu, *J. Phys. Chem. Solids*, 2013, **74**, 360-365.
303. B. X. Li, G. X. Rong, Y. Xie, L. F. Huang and C. Q. Feng, *Inorg. Chem.*, 2006, **45**, 6404-6410.
304. X. L. Li, H. F. Song, H. Wang, Y. L. Zhang, K. Du, H. Y. Li and J. M. Huang, *J. Appl. Electrochem.*, 2012, **42**, 1065-1070.
305. L. H. Bao, J. F. Zang and X. D. Li, *Nano Lett.*, 2011, **11**, 1215-1220.
306. J. W. Zhao, Z. Z. Lu, M. F. Shao, D. P. Yan, M. Wei, D. G. Evans and X. Duan, *RSC Adv.*, 2013, **3**, 1045-1049.
307. D. Sarkar, G. G. Khan, A. K. Singh and K. Mandal, *J. Phys. Chem. C*, 2013, **117**, 15523-15531.
308. J. F. Zang and X. D. Li, *J. Mater. Chem.*, 2011, **21**, 10965-10969.
309. A. J. Roberts, A. F. D. de Namor and R. C. T. Slade, *Phys. Chem. Chem. Phys.*, 2013, **15**, 3518-3526.
310. M. Kim, Y. Hwang and J. Kim, *J. Mater. Sci.*, 2013, **48**, 7652-7663.
311. M. P. He, Y. Y. Zheng and Q. F. Du, *Mater. Lett.*, 2013, **104**, 48-52.
312. L. L. Xing, C. X. Cui, C. H. Ma and X. Y. Xue, *Mater. Lett.*, 2011, **65**, 2104-2106.
313. C. X. Guo, M. Wang, T. Chen, X. W. Lou and C. M. Li, *Adv. Energy. Mater.*, 2011, **1**, 736-741.
314. A. Pan, D. Liu, X. Zhou, B. B. Garcia, S. Liang, J. Liu and G. Cao, *J. Power Sources*, 2010, **195**, 3893-3899.
315. J. L. Kang, A. Hirata, L. J. Kang, X. M. Zhang, Y. Hou, L. Y. Chen, C. Li, T. Fujita, K. Akagi and M. W. Chen, *Angew. Chem. Int. Edit.*, 2013, **52**, 1664-1667.
316. X. H. Lu, T. Zhai, X. H. Zhang, Y. Q. Shen, L. Y. Yuan, B. Hu, L. Gong, J. Chen, Y. H. Gao, J. Zhou, Y. X. Tong and Z. L. Wang, *Adv. Mater.*, 2012, **24**, 938-944.
317. L. Y. Chen, J. L. Kang, Y. Hou, P. Liu, T. Fujita, A. Hirata and M. W. Chen, *J. Mater. Chem. A*, 2013, **1**, 9202-9207.
318. D. D. Zhao, Y. Q. Zhao, X. Zhang, C. L. Xu, Y. Peng, H. L. Li and Z. Yang, *Mater. Lett.*, 2013, **107**, 115-118.

319. Z. J. Su, C. Yang, C. J. Xu, H. Y. Wu, Z. X. Zhang, T. Liu, C. Zhang, Q. H. Yang, B. H. Li and F. Y. Kang, *J. Mater. Chem. A*, 2013, **1**, 12432-12440.
320. M. Kundu and L. F. Liu, *J. Power Sources*, 2013, **243**, 676-681.
321. J. W. Xiao, S. X. Yang, L. Wan, F. Xiao and S. Wang, *J. Power Sources*, 2014, **245**, 1027-1034.
322. X. H. Lu, D. Z. Zheng, T. Zhai, Z. Q. Liu, Y. Y. Huang, S. L. Xie and Y. X. Tong, *Energy Environ. Sci.*, 2011, **4**, 2915-2921.
323. X. Zhang, D. D. Zhao, Y. Q. Zhao, P. Y. Tang, Y. L. Shen, C. L. Xu, H. L. Li and Y. Xiao, *J. Mater. Chem. A*, 2013, **1**, 3706-3712.
324. J. S. Luo, X. H. Xia, Y. S. Luo, C. Guan, J. L. Liu, X. Y. Qi, C. F. Ng, T. Yu, H. Zhang and H. J. Fan, *Adv. Energy Mater.*, 2013, **3**, 737-743.
325. H. C. Gao, F. Xiao, C. B. Ching and H. W. Duan, *ACS Appl. Mater. Interfaces*, 2012, **4**, 2801-2810.
326. J. W. Liu, J. Essner and J. Li, *Chem. Mater.*, 2010, **22**, 5022-5030.
327. M. H. Yu, T. Zhai, X. H. Lu, X. J. Chen, S. L. Xie, W. Li, C. L. Liang, W. X. Zhao, L. P. Zhang and Y. X. Tong, *J. Power Sources*, 2013, **239**, 64-71.
328. C. L. Xu, Y. Q. Zhao, G. W. Yang, F. S. Li and H. L. Li, *Chem. Commun.*, 2009, 7575-7577.
329. P. Y. Tang, Y. Q. Zhao, Y. M. Wang and C. L. Xu, *Nanoscale*, 2013, **5**, 8156-8163.
330. R. Liu and S. B. Lee, *J. Am. Chem. Soc.*, 2008, **130**, 2942-2943.
331. S. M. Dong, X. Chen, L. Gu, X. H. Zhou, L. F. Li, Z. H. Liu, P. X. Han, H. X. Xu, J. H. Yao, H. B. Wang, X. Y. Zhang, C. Q. Shang, G. L. Cui and L. Q. Chen, *Energy Environ. Sci.*, 2011, **4**, 3502-3508.
332. J. Duay, S. A. Sherrill, Z. Gui, E. Gillette and S. B. Lee, *ACS Nano*, 2013, **7**, 1200-1214.
333. M. S. Wu and P. C. J. Chiang, *Electrochem. Commun.*, 2006, **8**, 383-388.
334. S. L. Chou, Y. X. Wang, J. T. Xu, J. Z. Wang, H. K. Liu and S. X. Dou, *Electrochem. Commun.*, 2013, **31**, 35-38.
335. M. Kundu, C. C. A. Ng, D. Y. Petrovykh and L. F. Liu, *Chem. Commun.*, 2013, **49**, 8459-8461.
336. M. S. Wu, P. C. J. Chiang, J. T. Lee and J. C. Lin, *J. Phys. Chem. B*, 2005, **109**, 23279-23284.
337. W. F. Wei, X. W. Cui, W. X. Chen and D. G. Ivey, *J. Power Sources*, 2009, **186**, 543-550.
338. S. L. Chou, J. Z. Wang, S. Y. Chew, H. K. Liu and S. X. Dou, *Electrochem. Commun.*, 2008, **10**, 1724-1727.
339. Y. M. He, W. J. Chen, X. D. Li, Z. X. Zhang, J. C. Fu, C. H. Zhao and E. Q. Xie, *ACS Nano*, 2013, **7**, 174-182.
340. Y. Jin, H. Y. Chen, M. H. Chen, N. Liu and Q. W. Li, *ACS Appl. Mater. Interfaces*, 2013, **5**, 3408-3416.
341. Z. P. Sun, S. Firdoz, E. Y. X. Yap, L. Li and X. M. Lu, *Nanoscale*, 2013, **5**, 4379-4387.
342. S. Park, I. Nam, G. P. Kim, J. W. Han and J. Yi, *ACS Appl. Mater. Interfaces*, 2013, **5**, 9908-9912.
343. H. Xia, J. K. Feng, H. L. Wang, M. O. Lai and L. Lu, *J. Power Sources*, 2010, **195**, 4410-4413.
344. Y. L. Chen, P. C. Chen, T. L. Chen, C. Y. Lee and H. T. Chiu, *J. Mater. Chem. A*, 2013, **1**, 13301-13307.
345. Z. G. Ye, G. W. Liu, G. B. Huang, K. Wang and G. J. Qiao, *ECS Electrochem. Lett.*, 2013, **2**, A118-A120.
346. J. Y. Tao, N. S. Liu, W. Z. Ma, L. W. Ding, L. Y. Li, J. Su and Y. H. Gao, *Scientific Reports*, 2013, **3**, 2286.
347. J. C. Chou, Y. L. Chen, M. H. Yang, Y. Z. Chen, C. C. Lai, H. T. Chiu, C. Y. Lee, Y. L. Chueh and J. Y. Gan, *J. Mater. Chem. A*, 2013, **1**, 8753-8758.
348. W. F. Wei, X. W. Cui, W. X. Chen and D. G. Ivey, *J. Phys. Chem. C*, 2008, **112**, 15075-15083.
349. M. S. Wu and Y. H. Fu, *Carbon*, 2013, **60**, 236-245.
350. G. R. Li, Z. P. Feng, Y. N. Ou, D. C. Wu, R. W. Fu and Y. X. Tong, *Langmuir*, 2010, **26**, 2209-2213.
351. Y. B. He, G. R. Li, Z. L. Wang, C. Y. Su and Y. X. Tong, *Energy Environ. Sci.*, 2011, **4**, 1288-1292.
352. W. Xiao, H. Xia, J. Y. H. Fuh and L. Lu, *J. Electrochem. Soc.*, 2009, **156**, A627-A633.

353. D. W. Liu, Q. F. Zhang, P. Xiao, B. B. Garcia, Q. Guo, R. Champion and G. Z. Cao, *Chem. Mater.*, 2008, **20**, 1376-1380.
354. H. Zhao, G. Y. Han, Y. Z. Chang, M. Y. Li and Y. P. Li, *Electrochim. Acta*, 2013, **91**, 50-57.
355. D. D. Zhao, Z. Yang, L. Y. Zhang, X. L. Feng and Y. F. Zhang, *Electrochem. Solid St*, 2011, **14**, A93-A96.
356. K. Sivula, F. Le Formal and M. Gratzel, *Chemsuschem*, 2011, **4**, 432-449.
357. C. Ban, Z. Wu, D. T. Gillaspie, L. Chen, Y. Yan, J. L. Blackburn and A. C. Dillon, *Adv. Mater.*, 2010, **22**, E145-E149.
358. Q. Xiong, Y. Lu, X. Wang, C. Gu, Y. Qiao and J. Tu, *J. Alloy. Compd.*, 2012, **536**, 219-225.
359. W. Zhang, X. Wang, H. Zhou, J. Chen and X. Zhang, *J. Alloy. Compd.*, 2012, **521**, 39-44.
360. Y. Zhao, J. Li, Y. Ding and L. Guan, *Chem. Commun.*, 2011, **47**, 7416-7418.
361. B. Wang, J. S. Chen, H. B. Wu, Z. Wang and X. W. Lou, *J. Am. Chem. Soc.*, 2011, **133**, 17146-17148.
362. S. Jin, H. Deng, D. Long, X. Liu, L. Zhan, X. Liang, W. Qiao and L. Ling, *J. Power Sources*, 2011, **196**, 3887-3893.
363. D. Chen, G. Ji, Y. Ma, J. Y. Lee and J. Lu, *ACS Appl. Mater. Interfaces*, 2011, **3**, 3078-3083.
364. Y. Lu, J. P. Tu, C. D. Gu, X. L. Wang and S. X. Mao, *J. Mater. Chem.*, 2011, **21**, 17988-17997.
365. Q. Q. Xiong, J. P. Tu, Y. Lu, J. Chen, Y. X. Yu, Y. Q. Qiao, X. L. Wang and C. D. Gu, *J. Phys. Chem. C*, 2012, **116**, 6495-6502.
366. S. Wang, J. Zhang and C. Chen, *J. Power Sources*, 2010, **195**, 5379-5381.
367. W. M. Zhang, X. L. Wu, J. S. Hu, Y. G. Guo and L. J. Wan, *Adv. Funct. Mater.*, 2008, **18**, 3941-3946.
368. W. Shi, J. Zhu, D. H. Sim, Y. Y. Tay, Z. Lu, X. Zhang, Y. Sharma, M. Srinivasan, H. Zhang and H. H. Hng, *J. Mater. Chem.*, 2011, **21**, 3422-3427.
369. Y. Ma, G. Ji and J. Y. Lee, *J. Mater. Chem.*, 2011, **21**, 13009-13014.
370. L. Wang, H. Ji, S. Wang, L. Kong, X. Jiang and G. Yang, *Nanoscale*, 2013, **5**, 3793-3799.
371. Y. Chen, H. Xia, L. Lu and J. Xue, *J. Mater. Chem.*, 2012, **22**, 5006-5012.
372. P. M. Hallam, M. Gómez-Mingot, D. K. Kampouris and C. E. Banks, *RSC Adv.*, 2012, **2**, 6672-6679.
373. S.-Y. Wang, K.-C. Ho, S.-L. Kuo and N.-L. Wu, *J. Electrochem. Soc.*, 2006, **153**, A75-A80.
374. X. Zhao, C. Johnston and P. S. Grant, *J. Mater. Chem.*, 2009, **19**, 8755-8760.
375. S. Zeng, K. Tang, T. Li, Z. Liang, D. Wang, Y. Wang, Y. Qi and W. Zhou, *J. Phys. Chem. C*, 2008, **112**, 4836-4843.
376. M. S. Wu and R. H. Lee, *J. Electrochem. Soc.*, 2009, **156**, A737-A743.
377. G. F. Ortiz, I. Hanzu, P. Lavela, J. L. Tirado, P. Knauth and T. Djenizian, *J. Mater. Chem.*, 2010, **20**, 4041-4046.
378. M. S. Wu, Y. H. Ou and Y. P. Lin, *Electrochim. Acta*, 2010, **55**, 3240-3244.
379. Q. Q. Xiong, J. P. Tu, Y. Lu, J. Chen, Y. X. Yu, X. L. Wang and C. D. Gu, *J. Mater. Chem.*, 2012, **22**, 18639-18645.
380. S. Mitra, P. Poizot, A. Finke and J. M. Tarascon, *Adv. Funct. Mater.*, 2006, **16**, 2281-2287.
381. L. Taberna, S. Mitra, P. Poizot, P. Simon and J. M. Tarascon, *Nat. Mater.*, 2006, **5**, 567-573.
382. H. Duan, J. Gnanaraj and J. Y. Liang, *J. Power Sources*, 2011, **196**, 4779-4784.
383. K. Y. Xie, Z. G. Lu, H. T. Huang, W. Lu, Y. Q. Lai, J. Li, L. M. Zhou and Y. X. Liu, *J. Mater. Chem.*, 2012, **22**, 5560-5567.
384. J. P. Liu, Y. Y. Li, H. J. Fan, Z. H. Zhu, J. Jiang, R. M. Ding, Y. Y. Hu and X. T. Huang, *Chem. Mater.*, 2009, **22**, 212-217.
385. J. S. Luo, J. L. Liu, Z. Y. Zeng, C. F. Ng, L. J. Ma, H. Zhang, J. Y. Lin, Z. X. Shen and H. J. Fan, *Nano Lett.*, 2013, **13**, 6136-6143.
386. Y. S. Luo, J. S. Luo, J. Jiang, W. W. Zhou, H. P. Yang, X. Y. Qi, H. Zhang, H. J. Fan, D. Y. W. Yu, C. M. Li and T. Yu, *Energy Environ. Sci.*, 2012, **5**, 6559-6566.
387. Y. Wang, J. L. Cao, S. R. Wang, X. Z. Guo, J. Zhang, H. J. Xia, S. M. Zhang and S. H. Wu, *J. Phys. Chem. C*, 2008, **112**, 17804-17808.
388. Y. He, L. Huang, J. S. Cai, X. M. Zheng and S. G. Sun, *Electrochim. Acta*, 2010, **55**, 1140-1144.
389. P. Tartaj and J. M. Amarilla, *J. Power Sources*, 2011, **196**, 2164-2170.

390. J. Z. Wang, C. Zhong, D. Wexler, N. H. Idris, Z. X. Wang, L. Q. Chen and H. K. Liu, *Chem-eur. J.*, 2011, **17**, 661-667.
391. J. Y. Zhong, C. B. Cao, Y. Y. Liu, Y. A. Li and W. S. Khan, *Chem. Commun.*, 2010, **46**, 3869-3871.
392. B. J. Li, H. Q. Cao, J. Shao, M. Z. Qu and J. H. Warner, *J. Mater. Chem.*, 2011, **21**, 5069-5075.
393. A. Q. Pan, H. B. Wu, L. Zhang and X. W. Lou, *Energy Environ. Sci.*, 2013, **6**, 1476.
394. J. W. Lee, S. Y. Lim, H. M. Jeong, T. H. Hwang, J. K. Kang and J. W. Choi, *Energy Environ. Sci.*, 2012, **5**, 9889.
395. J. Zhu, L. Cao, Y. Wu, Y. Gong, Z. Liu, H. E. Hoster, Y. Zhang, S. Zhang, S. Yang, Q. Yan, P. M. Ajayan and R. Vajtai, *Nano Lett.*, 2013, **13**, 5408-5413.
396. A. Pan, H. B. Wu, L. Yu and X. W. D. Lou, *Angewandte Chemie*, 2013, **125**, 2282-2286.
397. J. Xie, C. Wu, S. Hu, J. Dai, N. Zhang, J. Feng, J. Yang and Y. Xie, *Phys. Chem. Chem. Phys.*, 2012, **14**, 4810-4816.
398. M. Jayalakshmi, M. M. Rao, N. Venugopal and K. B. Kim, *J. Power Sources*, 2007, **166**, 578-583.
399. S. D. Perera, A. D. Liyanage, N. Nijem, J. P. Ferraris, Y. J. Chabal and K. J. Balkus, *J. Power Sources*, 2013, **230**, 130-137.
400. S. D. Perera, B. Patel, N. Nijem, K. Roodenko, O. Seitz, J. P. Ferraris, Y. J. Chabal and K. J. Balkus, *Adv. Energy. Mater.*, 2011, **1**, 936-945.
401. Q. T. Qu, Y. S. Zhu, X. W. Gao and Y. P. Wu, *Adv. Energy. Mater.*, 2012, **2**, 950-955.
402. J. Shao, X. Y. Li, Q. T. Qu and H. H. Zheng, *J. Power Sources*, 2012, **219**, 253-257.
403. Y. Y. Liu, M. Clark, Q. F. Zhang, D. M. Yu, D. W. Liu, J. Liu and G. Z. Cao, *Adv. Energy. Mater.*, 2011, **1**, 194-202.
404. G. Du, K. H. Seng, Z. Guo, J. Liu, W. Li, D. Jia, C. Cook, Z. Liu and H. Liu, *RSC Adv.*, 2011, **1**, 690.
405. X. Rui, J. Zhu, W. Liu, H. Tan, D. Sim, C. Xu, H. Zhang, J. Ma, H. H. Hng, T. M. Lim and Q. Yan, *RSC Adv.*, 2011, **1**, 117.
406. S. Yang, Y. Gong, Z. Liu, L. Zhan, D. P. Hashim, L. Ma, R. Vajtai and P. M. Ajayan, *Nano Lett.*, 2013, **13**, 1596-1601.
407. X. H. Rui, D. H. Sim, C. Xu, W. L. Liu, H. T. Tan, K. M. Wong, H. H. Hng, T. M. Lim and Q. Y. Yan, *RSC Adv.*, 2012, **2**, 1174-1180.
408. C. J. Fontenot, J. W. Wiench, M. Pruski and G. L. Schrader, *J. Phys. Chem. B*, 2000, **104**, 11622-11631.
409. M. L. Li, G. Y. Sun, P. P. Yin, C. P. Ruan and K. L. Ai, *ACS Appl. Mater. Interfaces*, 2013, **5**, 11462-11470.
410. J. Yang, T. B. Lan, J. D. Liu, Y. F. Song and M. D. Wei, *Electrochim. Acta*, 2013, **105**, 489-495.
411. Y. L. Cheah, V. Aravindan and S. Madhavi, *ACS Appl. Mater. Interfaces*, 2013, **5**, 3475-3480.
412. X. H. Rui, J. X. Zhu, D. Sim, C. Xu, Y. Zeng, H. H. Hng, T. M. Lim and Q. Y. Yan, *Nanoscale*, 2011, **3**, 4752-4758.
413. B. Saravanakumar, K. K. Purushothaman and G. Muralidharan, *ACS Appl. Mater. Interfaces*, 2012, **4**, 4484-4490.
414. H. Yamada, K. Tagawa, M. Komatsu, I. Moriguchi and T. Kudo, *J. Phys. Chem. C*, 2007, **111**, 8397-8402.
415. N. A. Galiote, M. N. Camargo, R. M. Iost, F. Crespilho and F. Huguenin, *Langmuir.*, 2011, **27**, 12209-12217.
416. M. Sathiya, A. S. Prakash, K. Ramesha, J. M. Tarascon and A. K. Shukla, *J. Am. Chem. Soc.*, 2011, **133**, 16291-16299.
417. T. Kudo, Y. Ikeda, T. Watanabe, M. Hibino, M. Miyayama, H. Abe and K. Kajita, *Solid State Ionics*, 2002, **152**, 833-841.
418. J. S. Bonso, A. Rahy, S. D. Perera, N. Nour, O. Seitz, Y. J. Chabal, K. J. Balkus, J. P. Ferraris and D. J. Yang, *J. Power Sources*, 2012, **203**, 227-232.
419. A. Kuwahara, S. Suzuki and M. Miyayama, *Solid State Ionics*, 2008, **179**, 1890-1896.
420. W. Y. Zhang, Y. Zeng, N. Xiao, H. H. Hng and Q. Y. Yan, *J. Mater. Chem.*, 2012, **22**, 8455-8461.
421. A. M. Engstrom and F. M. Doyle, *J. Power Sources*, 2013, **228**, 120-131.

422. C. C. Hu, C. M. Huang and K. H. Chang, *J. Power Sources*, 2008, **185**, 1594-1597.
423. I. H. Kim, J. H. Kim, B. W. Cho, Y. H. Lee and K. B. Kim, *J. Electrochem. Soc.*, 2006, **153**, A989-A996.
424. K. I. Park, H. M. Song, Y. Kim, S. I. Mho, W. I. Cho and I. H. Yeo, *Electrochim. Acta*, 2010, **55**, 8023-8029.
425. Q. H. Wang, L. F. Jiao, H. M. Du, J. Q. Yang, Q. N. Huan, W. X. Peng, Y. C. Si, Y. J. Wang and H. T. Yuan, *CrystEngComm*, 2011, **13**, 6960-6963.
426. G. F. Cai, X. L. Wang, D. Zhou, J. H. Zhang, Q. Q. Xiong, C. D. Gu and J. P. Tu, *RSC Adv.*, 2013, **3**, 6896-6905.
427. G. F. Cai, D. Zhou, Q. Q. Xiong, J. H. Zhang, X. L. Wang, C. D. Gu and J. P. Tu, *Sol. Energ. Mat. Sol. C.*, 2013, **117**, 231-238.
428. J. Zhang, J. P. Tu, G. H. Du, Z. M. Dong, Q. M. Su, D. Xie and X. L. Wang, *Electrochim. Acta*, 2013, **88**, 107-111.
429. J. Zhang, J. P. Tu, G. H. Du, Z. M. Dong, Y. S. Wu, L. Chang, D. Xie, G. F. Cai and X. L. Wang, *Sol. Energ. Mat. Sol. C.*, 2013, **114**, 31-37.
430. J. Zhang, J. P. Tu, X. H. Xia, Y. Qiao and Y. Lu, *Sol. Energ. Mat. Sol. C.*, 2009, **93**, 1840-1845.
431. J. Zhang, X. L. Wang, Y. Lu, Y. Qiao, X. H. Xia and J. P. Tu, *J. Solid State Electr.*, 2011, **15**, 2213-2219.
432. J. Zhang, X. L. Wang, X. H. Xia, C. D. Gu and J. P. Tu, *Sol. Energ. Mat. Sol. C.*, 2011, **95**, 2107-2112.
433. J. Zhang, X. L. Wang, X. H. Xia, C. D. Gu, Z. J. Zhao and J. P. Tu, *Electrochim. Acta*, 2010, **55**, 6953-6958.
434. X. X. Li, G. Y. Zhang, F. Y. Cheng, B. Guo and J. Chen, *J. Electrochem. Soc.*, 2006, **153**, H133-H137.
435. L. N. Gao, X. F. Wang, Z. Xie, W. F. Song, L. J. Wang, X. Wu, F. Y. Qu, D. Chen and G. Z. Shen, *J. Mater. Chem. A*, 2013, **1**, 7167-7173.
436. Y. C. Qiu, G. L. Xu, Q. Kuang, S. G. Sun and S. H. Yang, *Nano Research*, 2012, **5**, 826-832.
437. X. Y. Xue, B. He, S. Yuan, L. L. Xing, Z. H. Chen and C. H. Ma, *Nanotechnology*, 2011, **22**.
438. J. Q. Yang, L. F. Jiao, Q. Q. Zhao, Q. H. Wang, H. Y. Gao, Q. N. Huan, W. J. Zheng, Y. J. Wang and H. T. Yuan, *J. Mater. Chem.*, 2012, **22**, 3699-3701.
439. M. P. Yu, H. T. Sun, X. Sun, F. Y. Lu, T. Hu, G. K. Wang, H. Qiu and J. Lian, *Mater. Lett.*, 2013, **108**, 29-32.
440. B. Dunn, H. Kamath and J. M. Tarascon, *Science*, 2011, **334**, 928-935.
441. C. Y. Kim, M. Lee, S. H. Huh and E. K. Kim, *J. Sol-gel. Sci. Techn.*, 2010, **53**, 176-183.
442. K. Huang and Q. Zhang, *Nano Energy*, 2012, **1**, 172-175.
443. K. Huang, Q. Pan, F. Yang, S. Ni, X. Wei and D. He, *J. Phys. D. Appl. Phys.*, 2008, **41**.
444. B. X. Zou, Y. Liang, X. X. Liu, D. Diamond and K. T. Lau, *J. Power Sources*, 2011, **196**, 4842-4848.
445. C. A. Cai, D. S. Guan and Y. Wang, *J. Alloy. Compd.*, 2011, **509**, 909-915.
446. Y. U. Jeong and A. Manthiram, *J. Electrochem. Soc.*, 2001, **148**, A189-A193.
447. K. H. Chang, C. C. Hu, C. M. Huang, Y. L. Liu and C. I. Chang, *J. Power Sources*, 2011, **196**, 2387-2392.
448. X. B. Ren, H. Y. Lu, H. B. Lin, Y. N. Liu and Y. Xing, *Russ. J. Electrochem.*, 2010, **46**, 77-80.
449. Z. P. Chen, W. C. Ren, L. B. Gao, B. L. Liu, S. F. Pei and H. M. Cheng, *Nat. Mater.*, 2011, **10**, 424-428.
450. C. Guan, X. L. Li, Z. L. Wang, X. H. Cao, C. Soci, H. Zhang and H. J. Fan, *Adv. Mater.*, 2012, **24**, 4186-4190.